WASHINGTON UNIVERSITY

School of Engineering and Applied Science

Department of Energy, Environmental, & Chemical Engineering

Dissertation Examination Committee:
Pratim Biswas, Chair
Richard L. Axelbaum
Da-Ren Chen
Chenyang Lu
Jay R. Turner
Brent J. Williams

Miniaturization of Electrical Ultrafine Particle Sizers

by

Siqin He

A dissertation presented to the
Graduate School of Arts and Sciences
of Washington University in
partial fulfillment of the
requirements for the degree
of Doctor of Philosophy

May 2014

Saint Louis, Missouri

ProQuest LLC.
789 East Eisenhower Parkway
P.O. Box 1346
Ann Arbor, MI 48106 - 1346

Table of Contents

List of Figures ..... **vi**

List of Tables ..... **xi**

Acknowledgments ..... **xii**

Abstract ..... **xv**

Chapter 1 : Introduction and Overview **1**

1.1. Introduction 2

1.1.1. What are ultrafine particles? 2

1.1.2. Why should we care about ultrafine particles? 3

1.1.3. Assessment methodology 4

1.1.4. Review of miniature particle sizers 6

1.2. Motivation 12

1.3. Objectives and approach 13

1.4. Dissertation outline 15

1.5. Reference 16

Chapter 2 : Hardware design and component calibration of the precipitator-type electrical ultrafine particle sizer **19**

2.1. Introduction 20

2.2. Hardware design and configuration 23

2.2.1. Previous calibration work 25

2.2.2. Hardware component modifications 30

2.3. Experimental setups for component calibration 31

2.3.1. Calibration of the mini-charger 31
2.3.2. Evaluation of humidity effect 35
2.3.3. Calibration of the mini-disk precipitator 38
2.3.4. Calibration of P-Trak counting efficiency 39
2.4. Experimental results for component calibration 40
2.4.1. Calibration curves of the mini-charger 40
2.4.2. Evaluation of the humidity effect 42
2.4.3. Calibration curves of the mini-disk precipitator 44
2.4.4. Calibration curves of the particle count detector 46
2.5. Conclusions 48
2.6. References 49
Chapter 3 : Data inversion scheme and performance evaluation of the precipitator-type electrical ultrafine particle sizer 53
3.1. Introduction 54
3.2. Data inversion scheme 56
3.2.1. Presumed log-normal scheme 57
3.2.2. Constrained least square scheme 58
3.3. Laboratory evaluation of the p-type EUPS performance 62
3.3.1. Steady stream aerosol measurements 62
3.3.2. Unsteady stream aerosol measurements 67
3.4. Field evaluation of the p-type EUPS performance 73
3.5. Conclusions 76
3.6. References 76

Chapter 4 : A high efficiency, miniature unipolar charger for the electrical ultrafine particle sizer 78

4.1. Introduction 79

4.2. Hardware design 81

4.3. Numerical modeling of the charger performance 84

4.3.1. Flow and electrical field modeling 84

4.3.2. Modeling of particle penetration through the charger 88

4.4. Experimental evaluation of the unipolar charger 91

4.4.1. Experimental Setup for miniature unipolar charger evaluation 93

4.4.2. Calibration results of the miniature unipolar charger 96

4.5. Conclusions 100

4.6. References 101

Chapter 5 : A miniature dumbbell electrostatic aerosol classifier (Dumbbell EAC) for the electrical ultrafine particle sizer 104

5.1. Introduction 105

5.2. Hardware design 109

5.2.1. Why Dumbbell EAC? 109

5.2.2. Optimization of design parameters 111

5.2.3. Design of the Dumbbell EAC 119

5.3. Numerical modeling of the Dumbbell EAC performance 121

5.3.1. Flow and electrical field modeling 122

5.3.2. Particle Trajectory Modeling 124

5.4. Experimental evaluation of the Dumbbell EAC 127

5.4.1. Experimental setup for the Dumbbell EAC evaluation 127

5.4.2. Results of the Dumbbell EAC performance evaluation 131

5.5. Conclusions 135

5.6. References 136

Chapter 6 : Dissertation Accomplishments and Recommendations for Future Work 139

6.1. Summary of accomplishments 140

6.1.1. The precipitator-type electrical ultrafine particle sizer 140

6.1.2. Component development and evaluation for the next generation electrical ultrafine particle sizer 142

6.2. Recommendations for Future Work 144

List of Figures

Figure 1-1. Schematic diagram illustrating nanoparticles in the environment [5] 3

Figure 1-2. The personal respirable particulate sampler (PRPS) [23] 7

Figure 1-3. Schematic diagram of the Respicon™ [24] 8

Figure 1-4. Exploded diagram and photograph of the prototype thermophoretic aerosol sampler [25] 9

Figure 1-5. The miniature DiSC, front (left), and opened back (right) [27] 11

Figure 1-6. Schematic of the miniature DiSC, D = diffusion stage, F = filter stage [27] .. 11

Figure 2-1. Schematic diagram of prototype mini-disk precipitator [2] 23

Figure 2-2. Schematic diagram of the mini-charger [14] 24

Figure 2-3. Intrinsic charging efficiency of the prototype mini-charger [14] 26

Figure 2-4. Penetration of neutral and singly charged particles in the mini-disk precipitator [2] 27

Figure 2-5. Particle cutoff curves of the mini-disk precipitator, Q = 0.3 lpm [2] 27

Figure 2-6. $P^{1/2}$ vs. applied voltage for experimental results from the dual chamber precipitation operation, Q=0.3 lpm 29

Figure 2-7. The assembled package of the first generation EUPS 30

Figure 2-8. Experimental setup for the particle generation and characterization system 31

Figure 2-9. Experimental setup for the mini-charger calibration 33

Figure 2-10. Variation of ion mobility with relative humidity at different applied voltages, ... 36

Figure 2-11. Schematic of the humidification chamber design 37

Figure 2-12. Experimental setup for humidity effect evaluation of the mini-charger 38

Figure 2-13. Experimental setup for mini-disk precipitator calibration 38

Figure 2-14. Calibration curves of charging efficiencies for the mini-charger operated at 0.7 lpm 40

Figure 2-15. Calibration curve of average charges for the mini-charger operated at 0.7 lpm 41

Figure 2-16. Intrinsic charging efficiencies measured with NaCl and K_2SO_4 particles under different relative humidity conditions 42

Figure 2-17. Extrinsic charging efficiencies measured with NaCl and K_2SO_4 particles under different relative humidity conditions 43

Figure 2-18. Average charge measured with NaCl and K_2SO_4 particles under different relative humidity conditions 43

Figure 2-19. Penetration as a function of $Z_p \cdot V$ for the mini-disk precipitator operated at 0.7 lpm 45

Figure 2-20. Square root of penetration as a function of $Zp \cdot V$ for the mini-disk precipitator operated at 0.7 lpm 45

Figure 2-21. Calibration of P-Trak counting efficiency, with UCPC as a reference 47

Figure 2-22. Calibration of CPC 3010 counting efficiency, with UCPC as a reference . 47

Figure 3-1. Experimental setup for lab evaluation of steady aerosol measurement 64

Figure 3-2. Comparison of unimodal size distribution measurements for steady stream aerosols 65

Figure 3-3. Comparison of bimodal size distribution measurements for steady stream aerosols 67

Figure 3-4. Experimental setup for evaluation of dynamic aerosol measurement 69

Figure 3-5. Dilution flow profile for the dynamic aerosol dilutor 69

Figure 3-6. Comparison of dynamic aerosol measurements between EEPS (left) and EUPS 70

Figure 3-7. Experimental setup for verifying the dynamic identification mode..... 71

Figure 3-8. Evaluation of the dynamic identification mode measurement 72

Figure 3-9. Experimental setup for field evaluation of ambient aerosol measurement ... 73

Figure 3-10. Comparison of the outdoor aerosol measurement..... 74

Figure 3-11. Field evaluation of dynamic identification mode..... 75

Figure 4-1. Schematic of the new miniaturized charger design..... 83

Figure 4-2. Electrical field in the charger, tubular case at 20 V, and aerosol flow inlet grounded. 87

Figure 4-3. Flow field in the charger, aerosol flow at 1.5 lpm, corona sheath flow at 0.3 lpm 88

Figure 4-4. Particle trajectory modeling results for the miniature unipolar charger 90

Figure 4-5. Experimental setup for the particle generation and particle size characterization 94

Figure 4-6. Experimental setup for the miniature unipolar charger calibration 95

Figure 4-7. Intrinsic charging efficiency of the new miniature unipolar charger, compared with the previous mini-charger 97

Figure 4-8. Extrinsic charging efficiency of the new miniature unipolar charger, compared with the previous mini-charger 98

Figure 4-9. Average number of elementary charges per charged particle for the new miniature unipolar charger, compared with the previous mini-charger 99

Figure 5-1. Schematics and transfer functions of the three generations of electrical mobility classifiers: (a) precipitator, (b) electrical aerosol analyzer, and (c) differential mobility analyzer [11] 107

Figure 5-2. Schematic diagram of the mini-disk EAC [17] 109

Figure 5-3. Overall and cutoff view of the Dumbbell EAC design 110

Figure 5-4. Computational domain for Dumbbell EAC flow field modeling 111

Figure 5-5. Modeling of the aerosol slit channel angle: (a) α = 60°, (b) α = 45°, and (c) α = 30°. 114

Figure 5-6. Modeling of the aerosol and sheath flowrats: (a) Qa = 0.5 lpm, Qs = 1 lpm,(b) Qa = 0.5 lpm, Qs = 2 lpm, (c) Qa = 0.5 lpm, Qs = 3 lpm, (d) Qa = 1 lpm, Qs = 3 lpm, and (e) Qa = 0.5 lpm, Qs = 4 lpm 117

Figure 5-7. Modeling of the classification channel spacing 118

Figure 5-8. Schematic diagram of the Dumbbell EAC 119

Figure 5-9. Electrical field modeling of the Dumbbell EAC: (a) electrical potential (V), and (b) streamline of the electric field 123

Figure 5-10. Particle trajectory modeling results for six different operational voltages 126

Figure 5-11. Experimental setup for particle generation and particle size characterization 127

Figure 5-12. Experimental setup for Dumbbell EAC performance evaluation 129

Figure 5-13. Particle transmission efficiency through the Dumbbell EAC 131

Figure 5-14. Cutoff curves of the Dumbbell EAC 133

Figure 5-15. Same aerosol to sheath flowrate ratio cutoff curves for the Dumbbell EAC 134

Figure 5-16. Comparison of modeled and experimental cutoff curves 135

List of Tables

Table 3-1. Identification table for V_1 = 0 V and V_2 = 50 V..... 61

Table 4-1. Comparison of different unipolar chargers..... 82

Acknowledgments

I wish to express my greatest appreciation to my advisor, Professor Pratim Biswas, for all his guidance, advice and support that made my five years being an EECE student so memorable and enjoyable, and for him sharing his wisdom in career life that I will always benefit from. I am also thankful to Dr. Chen, for introducing me into this fantastic world of aerosol instrumentation. I also would like to acknowledge all the other members in my dissertation committee, Dr. Richard L. Axelbaum, Dr. Jay R. Turner, Dr. Chenyang Lu, and Dr. Brent J. Williams, I am very thankful to them for taking interests in my research, examining my dissertation, and providing useful comments and great advice to make this dissertation work more interesting and meaningful. Thanks to all of them for continuously helping me wrap up my work at Washington University, and proceed to the dissertation defense examination.

I would like to thank all my friends and colleagues in the Aerosol Cluster for constantly providing an intellectually challenging and collaborating environment. In particular, I would like to thank Dr. Anna Leavey, for her kindness, patience and company during my hard times, for her sunshine-like warmness that always encourages me to always be positive when facing difficulties. I also want to thank my biomass group member Sameer Patel, thank him for making our cook stove experiment such an enjoyable experience. And I would like to acknowledge all other AAQRL colleagues for numerous discussions and cooperation. Last but not least, I would particularly like to thank my officemate Cheryl Immethun, and my former colleague Marit Meyer, for their kindness and sincere advice always.

I would like to thank Dean Quatrano and Dean Pope, for them so kindly encouraging me and helping me gain back faith and confidence in this dissertation work.

I am thankful to all the administrative assistants in the Department of Energy, Environmental and Chemical Engineering. Many thanks go to Rose Baxter, Lesley Smith, Kim Coleman, Beth Mehringer, Trisha Sutton, and Lynn Zaltsman for their consistent assistance and help that made all administrative processes so smooth to all students. I also want to thank Tim McHugh for his professional IT support through my study at EECE.

I would also like to thank the funding support from USEPA and TSI Incorporated.

Finally, my genuine gratitude goes to my parents, and my boyfriend, Qisheng Ou, without their constant encouragement and support during my study and research at Washington University, this dissertation could not have been completed.

Siqin He

Washington University in St. Louis

May 2014

Dedicated to my parents, Shouhong Xie and Chengjun He,

and my boyfriend, Qisheng Ou

ABSTRACT OF THE DISSERTATION

Miniaturization of Electrical Ultrafine Particle Sizers

by

Siqin He

Doctor of Philosophy in Energy, Environmental & Chemical Engineering

Washington University in St. Louis, 2014

Professor Pratim Biswas, Chair

Nanoparticles, or ultrafine particles, have potential risks for human health, and the adverse health effects caused by ultrafine particles have been proven to be size-related. To meet the increasing demanding for personal exposure monitoring and spatial distribution measurements of ultrafine particles, this dissertation studied the development and miniaturization of electrical ultrafine particle sizers (EUPS). There are three essential components for developing a EUPS unit: a charger to electrically charge the sample particles, an electrical mobility classifier to classify the charged particles, and a downstream particle count detector to measure the number concentrations. Two generations of EUPS were developed in this dissertation.

The first generation was a precipitator-type EUPS, which was assembled with a miniature corona-discharge unipolar charger, a miniature disk-type precipitator, and a portable condensation particle counter. All three components were calibrated under the optimized operation conditions. By combining the component calibration results, a data inversion scheme was developed to retrieve particle size distribution from measured signals. Size distribution measurement performance of the precipitator-type (p-type)

EUPS prototype was then evaluated with both laboratory generated aerosols and field ambient aerosols. Evaluation results solidly verified the size distribution measurement reliability and flexibility of the p-type EUPS.

Several possible improvements were implied, for a more precise EUPS size distribution measurement, based on the p-type EUPS development. These improvements were realized in the second part of this dissertation, as the component development and evaluation for a second generation EUPS. A new corona-discharge based, miniature unipolar aerosol charger was developed and evaluated. The new charger design made significant improvements in both intrinsic and extrinsic charging efficiencies, and it also maintained a more stable charging performance as compared to the previous mini-charger.

To improve the electrical mobility classification resolution, a miniature electrostatic aerosol classifier (EAC) prototype, named the Dumbbell EAC, was designed as an improved replacement of the mini-disk precipitator for the next generation EUPS. It had a novel axial-symmetric dumbbell-shaped curved classification channel design, to achieve an extended classification length within the compact overall device size. The Dumbbell EAC classification performance was evaluated both numerically and experimentally. According to both evaluation results, this palm size device, with its higher aerosol to sheath flow ratio as up to 1:5, and extended detectable size range from 10 to 850 nm, provided an improved solution for more precise portable size distribution measurements by the next generation EUPS.

Chapter 1 : Introduction and Overview

1.1. Introduction

1.1.1. What are ultrafine particles?

Ultrafine particles (UFPs), or alternatively, ultrafine aerosols (UFAs) is widely used in aerosol research to categorize particles with diameters less than 0.1 μm. In particular, the term UFP was first adopted by aerosol scientists in a workshop in the year of 1979 [1]. Later in the 1990s, with the fast development of nanotechnology, the term "nanoparticles" had become more popular [2]. The prefix "nano" comes from the Greek language, with the original meaning of "dwarf", and now denotes a factor of 1×10^{-9} in the metric system. Although the definition of nanoparticles differs greatly among different materials, fields, and application areas, in aerosol research, nanoparticles, or "ultrafine particles" are used interchangeably, and refer to particulate matter that has at least one dimension smaller than 100 nanometers [3]. Ultrafine particles, or nanoparticles, because of their nanoscale sizes, can have different physical and chemical properties than bulk-sized particles of the same material [4]. Benefiting from these distinctively different "nano" properties, various industries and people all over the world have produced and used nano-sized particles for thousands of years [5]. Arising from both natural sources and anthropogenic emissions, ultrafine particles are ubiquitous and widespread in the environment, as shown in Figure 1-1 [5]. They have been reported in the exhausts of combustion sources [6], chemical processes, and aerosol reactors [7], as well in exhaust streams from waste incinerators, welding systems, cook ovens, smelters, nuclear reactor accidents, and utility boilers [8]. Nowadays, as a result of the automobile's global popularity, the primary emission sources for ultrafine particles are traffic-related, and automobile engines are now the most significant ultrafine particle emitters [9].

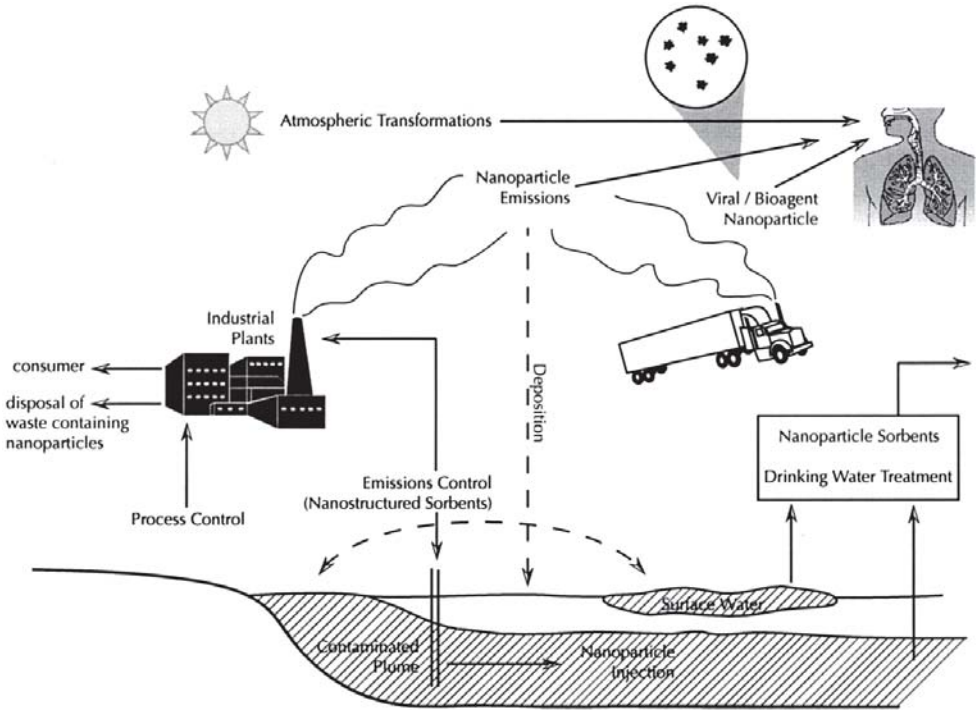

Figure 1-1. Schematic diagram illustrating nanoparticles in the environment [5]

1.1.2. Why should we care about ultrafine particles?

Air is essential for the survival of living organisms. There are multitudinous liquid and solid particles suspended in the ambient air, which are known as ambient aerosols [10]. The size ranges of ambient aerosols can vary as much as the variety of their materials. To categorize the size ranges, Whitby and Sverdrup proposed three terms in 1980, including nucleation mode, accumulation mode, and coarse mode, representing aerosols with diameters less than 0.1 μm, between 0.08 to 1 μm, and larger than 1.3 μm respectively [11]. Particle emissions from natural sources, such as wind-blown dust, are mostly found in the coarse mode, while anthropogenic processes make the major contributions to the nucleation and accumulation mode aerosols [12].

Although nanotechnology has tremendously promoted the development of modern technology, it has also caused increased exposures to ultrafine particles in recent years. Nano-sized ultrafine particles in the ambient environment are considered environmental pollution and are increasingly raising health concerns [8]. Among all the ambient aerosols, ultrafine particles constitute the least fraction of the overall mass, but they have the greatest surface area and highest number concentration [13]. More recent studies show that exposure to ultrafine particles may be particularly relevant to pulmonary and cardiovascular diseases, cancer, and mortality. These adverse health effects are indicated by pulmonary toxicity studies in rats, which demonstrate that ultrafine particles produce greater adverse inflammatory responses than do larger particles of identical composition at equivalent mass concentrations [14]. Epidemiological studies have also evidenced that increased asthma prevalence, including the number of patients diagnosed with the disease as well as asthma-related hospital visits, is closely associated with ultrafine particle levels in the ambient air, the regional motor vehicle traffic density, and residential proximity to freeways [15, 16]. Studies show that inhaled ultrafine particles have a highly size-specific deposition in the respiratory system, so the size and concentration of ultrafine particles are thus postulated as the two most significant factors in influencing the development of nanoparticle-related lung toxicity [17].

1.1.3. Assessment methodology

Thus, given the size-and-concentration-dependent adverse health effects from ultrafine particle exposure, a characterization of ultrafine particle sizes and concentrations, or the ultrafine particle size distribution as it is called in aerosol research, is vitally needed for personal ultrafine particle exposure assessment.

An "exposure" to a pollutant is defined by Ott as "occurrence of the event that a pollutant (at a particular concentration) comes into contact with the physical boundary of the individual", and it is measured by the concentration of the pollutant at the particular instant of time when that person is exposed to [18]. There are two approaches to performing personal exposure measurements: the indirect approach characterizes the responsible emission sources with stationary measurement results and human exposure models, and the direct approach statistically measures a given pollutant directly [19]. The personal ultrafine particle exposure measurement discussed here is an example of a direct approach.

The direct approach normally includes two measurement methods, quantifying the biological markers for known specific exposures by comparing air and body concentration of the markers, and the personal sampling method [12]. Further, there is integrated personal sampling, which measures the average exposure within a period of time with one-stage samplers, and also continuous personal monitoring, which provides time-varying exposure with real-time personal monitors [20].

For suspended aerosols, spatial heterogeneity can be significantly affected by physical processes such as sedimentation and coagulation [10]. It is observed that ultrafine particle concentrations dramatically decay within a few hundred meters from emission sources [21]. This spatial variability reveals that it will not be proper or accurate to monitor ultrafine particle exposures using an integrated sampling method, or by using continuous measurements with only a small number of community or central monitoring stations. Instead, strategically distributed measurements must be carried out for monitoring the spatial and temporal variations of ambient ultrafine particles [22]. Therefore, to better

monitor personal ultrafine particle exposure distribution, a dispersed real-time monitoring method is needed. To implement this method, a large number of ultrafine particle sizing instruments are required, with simple, miniaturized, and low-cost designs preferred.

1.1.4. Review of miniature particle sizers

Numerous designs of portable samplers have been employed to classify particle size distribution on a personal scale. The most popular designs use impaction or filtration to collect the particles in different size ranges, and then characterize the particle concentration of each sample range by an offline measurement.

In 2006, Lee, Demokritou et al. developed a personal respirable particulate sampler (PRPS) based on inertial impaction of particles [23]. This sampling system utilizes polyurethane foam (PUF) as the particle collection medium, which has been shown to be a nearly perfect impaction substrate that can minimize particle bounce-off and re-entrainment from the substrate, and as well avoiding using adhesives to preserve particle chemical and physical characteristics for subsequent toxicological, biological, and chemical characterizations. The PRPS is operated at 5 lpm flowrate, and its components are shown in Figure 1-2, including (1) five independently selectable impaction stages, with cut-off sizes of 10, 4.5, 2.5, 1.0, and 0.5 μm respectively, (2) two passive diffusion samplers to collect gaseous pollutants, such as O_3, NO_2, and SO_2, which are typically of the highest interest, and (3) a Teflon membrane backup filter to capture the particles that exit the final impaction stage.

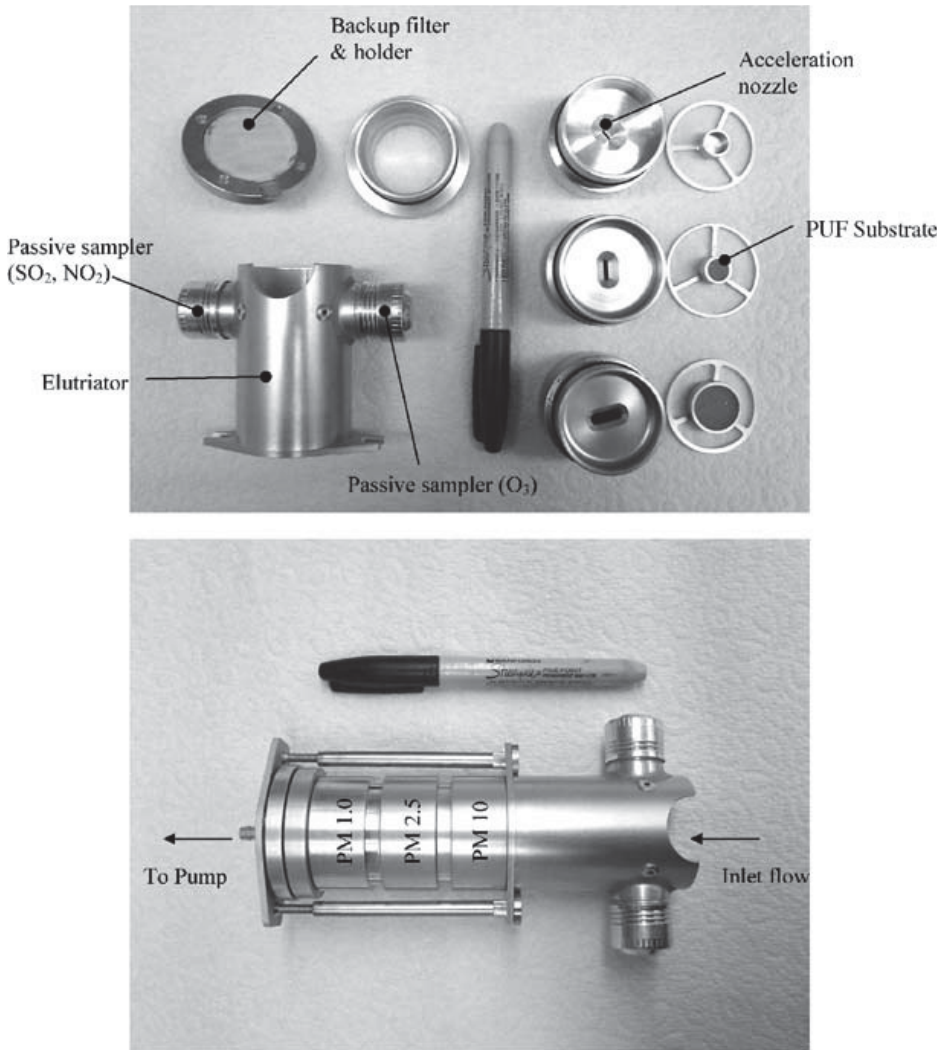

Figure 1-2. The personal respirable particulate sampler (PRPS) [23]

Both laboratory and field evaluations have been made for this PRPS system. Two real-time measurement instruments, the Scanning Mobility Particle Sizer (SMPS™) spectrometer (TSI Inc., Shoreview, MN) and the Aerodynamic Particle Sizer® (APS™, TSI Inc., Shoreview, MN), were referenced for the laboratory measurements, and the Harvard personal environmental monitor (PEM), Harvard impactor (HI), and USEPA $PM_{2.5}$ WINS impactor were referenced for the field measurements. Good agreements have been achieved for both evaluations, which indicate the PRPS sampler can be used to provide comparable particle size distribution measurements for personal exposure studies.

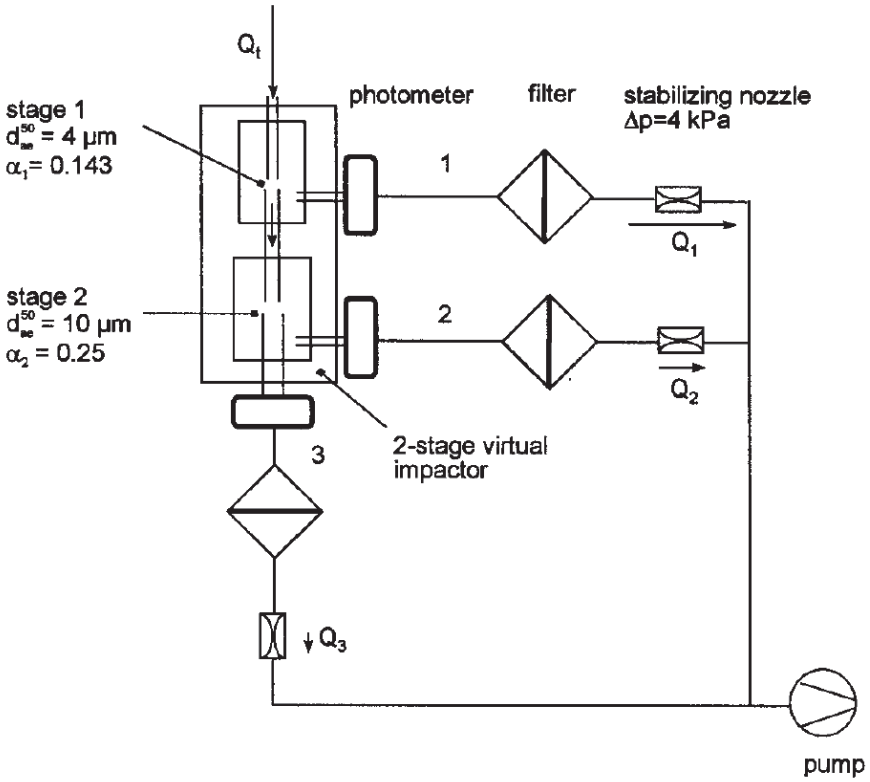

Figure 1-3. Schematic diagram of the Respicon™ [24]

However, to get a particle size distribution profile, inertial separation based technology always requires offline mass characterization for each impaction substrate, making it difficult to use as a real-time personal nanoparticle monitor. The Respicon™, developed by Koch, Dunkhorst et al. [24], solves this problem by first using virtual impactors to size-select the particles into three stages, and then measuring their concentrations via three light scattering photometers, as shown in Figure 1-3. Nevertheless, inertial separation technology is still not the best choice for a personal nanoparticle sizer, although it can work well for classifying particles with more obvious inertial effect in the larger submicron or even supermicron size ranges, it always requires high vacuum for effective performance in classifying smaller particles [25]. Thus, the

inertial separation technology would be impractical for measuring inhaled nanoparticles in the sizes of interest.

Besides inertial separation, thermophoretic precipitation has also been utilized for measuring personal exposure to airborne nanoparticles. One such personal thermophoretic sampler was developed by Thayer, Koehler et al. [26]. As shown in Figure 1-4, it operates at a maximum 20 ml/min flowrate and has a measurable particle size range from 15 to 240 nm.

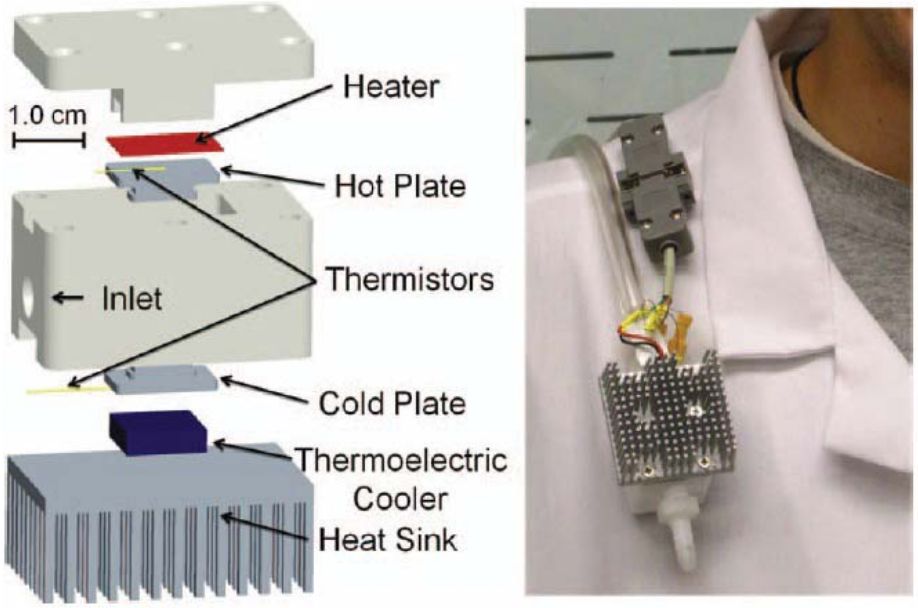

Figure 1-4. Exploded diagram and photograph of the prototype thermophoretic aerosol sampler [26]

By creating a temperature gradient orthogonal to the aerosol flow between the hot and cold plates inside, this aerosol sampler uses thermophoretic force to separate particles from a moving air stream. The thermophoretic velocity V_{th} is estimated as

$$V_{th} = \frac{-0.55\eta\nabla T}{\rho_g T} \quad (1\text{-}1)$$

for particles with diameters smaller than the gas mean free path, and it is independent of particle size. In the equation, η is the gas viscosity, ρ_g is the gas density, T is the local temperature, and ∇T is the temperature gradient [27].

Thus the thermophoretic sampler has a much more favorable detectable size range than that of impactors for monitoring personal exposure to nanoparticles. Unfortunately, this technique has a major drawback, in that it is not direct reading and requires a time-integrated sample and subsequent laboratory analysis after every sampling period. The precipitation plate has to be systematically imaged using a field-emission scanning electron microscope (SEM), and the image must be processed with software to get the deposited particle concentration for three selected diameter ranges [26].

To overcome the problems and inconvenience of the above techniques, in 2011 Fierz, Houle et al. develped and miniaturized an instrument called diffusion size classifier (DiSC), which is capable of measuring nanoparticles online. As labeled in **Figure 1-5**, its internal components are (A) an inlet, (B) a high voltage module, (C) a unipolar charger, (D) a filter stage, (E) a battery, and (F) a pump [28].

The operating principle of the miniature DiSC is the unipolar charging of nanoparticles. As shown in Figure 1-6, sampled aerosols are charged in a unipolar corona charger, excess ions are removed by an ion trap, and the current carried by the charged aerosols is measured in two successive electrometer stages, a diffusion stage and a filter stage. Due to Brownian diffusion, smaller particles with larger Brownian motion are mostly captured in the diffusion stage, while all the remaining particles flow into and get captured at the filter stage, which is equipped with a HEPA filter.

Figure 1-5. The miniature DiSC, front (left), and opened back (right) [28]

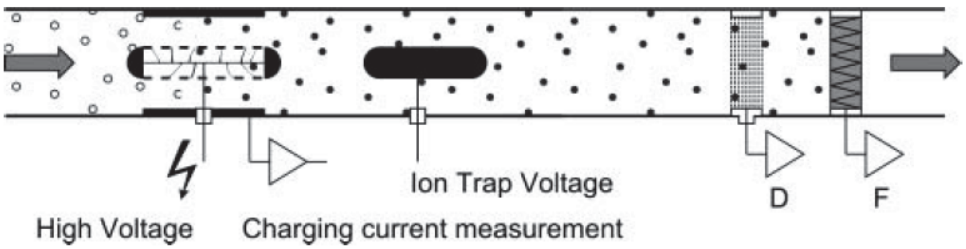

Figure 1-6. Schematic of the miniature DiSC, D = diffusion stage, F = filter stage [28]

This instrument has been shown to have a good correspondence (within 20% variation) to a reference SMPS measurement. However, for a precise measurement, we

must know the predefined geometrical standard deviation σ_g to find a median diameter, and we cannot distinguish between narrow and broad particle size distributions.

1.2. Motivation

Considering the difficulties and disadvantages of applying the inertial, gravitational, optical, and diffusional techniques for ultrafine particle measuring, the electrical mobility based classification method, with its higher resolution and higher efficiency for ultrafine particle and submicron particle detection, becomes the primary choice for sizing ultrafine particles [29].

Electrical mobility is the ability of charged particles to move through a medium in response to an electric field that is pulling them; it is therefore a function of both particle size and particle charge status. The electrical mobility for a charged particle can be calculated as its migration velocity per unit of applied electrical field strength, or

$$Z = \frac{neC_c}{3\pi\mu d_p}, \tag{1-2}$$

in which n is the number of elementary charges $e = 1.6\times10^{-19}$ C, C_c is the slip correction factor, μ is the gas viscosity, and d_p is the particle size in diameter, assuming a spherical shape [10]. The electrical mobility method for submicron particle size characterization is thus based on the relationship between electrical mobility Z and the particle size d_p as shown in equation (1-2).

Several commercial electrical mobility classifiers commercially can measure particles in the sub-micrometer and nanometer size ranges [30]. The most widely employed model is the scanning mobility particle sizer (SMPS) (Wang, 1990), which is

primarily designed for scientific studies and provides good particle size resolution and sensitive particle concentration detection. However, this instrument is too large and expensive for personal use [31]. Also, the long residence time of particles in the classification region of the differential mobility analyzer (DMA) makes this instrument too slow for many applications other than laboratory calibration studies. Thus, in addition to these scientific instruments, to monitor personal exposure or make spatially distributed measurements, we still need to develop a miniaturized, low cost, ultrafine particle and submicron aerosol classifier based on electrical mobility [21]. This kind of particle sizer normally consists of three essential components: a particle charger to electrically charge sampled particles to a known charge distribution, a particle-electrical-mobility-based classifier to size particles, and an aerosol counter to measure the concentration of sized particles.

1.3. Objectives and approach

The four research objectives for the miniaturization of the electrical ultrafine particle sizer (EUPS) were the design and evaluation of the miniaturized hardware components for the EUPS, hardware assembly, laboratory evaluation of the particle size distribution measurement by EUPS, and finally a field evaluation to validate the EUPS' measurement ability of real ambient aerosols.

Three key components were designed and calibrated to build the electrical ultrafine particle sizer: a charger to electrically charge the sample particles, an electrical mobility classifier to classify the charged particles, and a downstream particle count detector to measure the number concentrations.

All the three components were designed to

- be low-cost and miniaturized
- be simple to construct and operate
- have minimal loss of nanoparticles
- achieve high detection efficiency

After the hardware construction, laboratory calibrations were carried out separately for each component, yielding the intrinsic and extrinsic charging efficiencies and the average number of charges on charged particles for charger performance, transfer functions for the electrical mobility classifier, and the counting efficiency of the particle counter as a function of particle size.

The calibrated components were be assembled and packaged into a complete EUPS working unit. A data inversion scheme was derived by summarizing the component performance parameters to retrieve the original size distribution information from the instrument's response to the sampled aerosols. With the help of the inversion scheme, the EUPS unit was then be evaluated for measuring the particle size distribution of laboratory generated particles.

The performance of the EUPS in measuring real ambient aerosols was also validated by taking particle size distribution measurements in the field. The response of the instrument to both steady and dynamic measurements was evaluated to verify the unit's working ability as a particle sizer for personal and spatial measurements.

1.4. Dissertation outline

To achieve the research objectives, two generationss of EUPS were developed in this dissertation work, as described in the following seven chapters. Each chapter may stand alone as a description of a research project, with its own list of references. Some references are cited in multiple chapters and therefore appear in multiple reference sections.

The first generation EUPS was a precipitator-type EUPS, which uses a mini-disk precipitator as the electrical mobility classifier, and also includes a miniature aerosol charger and a portable condensation particle counter P-Trak® (Model 8525, TSI Inc., Shoreview, MN) as the other two key components. There are three chapters discussing the precipitator-type EUPS work. Chapter 2 focuses on the hardware designs and performance calibrations for the three key components. Chapter 3 presents the fast-mode data inversion scheme developed for the precipitator-type EUPS, as well the performance evaluation results of the EUPS as used for aerosol size distribution measurements.

The second generation was an EAC-type EUPS, which uses an electrostatic aerosol classifier (EAC) as the electrical mobility classifier, and with improvements made for all the key components.

To get higher charging efficiency for sample particles, a new miniature charger was also designed and evaluated for the electrical ultrafine particle sizer, as described in chapter 4. This high efficiency charger designed was a corona-discharge based parallel flow unipolar charger, which introduces a gentle corona sheath flow into the corona discharge chamber. Necessary modifications to the flow field and electric field

configurations were also made to get a higher penetration of charged particles. Chapter 4 also gives the charging performance calibration results, which include three indices, extrinsic and intrinsic charging efficiencies, and the average number of charges a single particle carries.

Chapter 5 introduces a novel design of EAC, named the Dumbbell EAC as it has a dumbbell-shaped classification region. With the extended classification length, the Dumbbell EAC can thus achieve a high classification resolution and a larger detection range, while keeping a compact overall size for the ultrafine particle size classification.

In the last chapter, chapter 6, the major accomplishments of this dissertation work are summarized, and the challenges that deserve future research efforts are also addressed.

1.5. Reference

1. Liu, B.*, et al.* (1982) Intercomparison of different "absolute" instruments for measurement of aerosol number concentration. *Journal of Aerosol Science* 13(5):429-450.

2. Hosokawa, M., Nogi, K., Naito, M., & Yokoyama, T. (2007) *Nanoparticle technology handbook* (Elsevier).

3. Warheit, D. B., Sayes, C. M., Reed, K. L., & Swain, K. A. (2008) Health effects related to nanoparticle exposures: Environmental, health and safety considerations for assessing hazards and risks. *Pharmacology & Therapeutics* 120(1):35-42.

4. Pui, D. Y. H. & Chen, D.-R. (1997) Nanometer particles: A new frontier for multidisciplinary research. *Journal of Aerosol Science* 28(4):539-544.

5. Biswas, P. & Wu, C.-Y. (2005) Nanoparticles and the environment. *Journal of the Air & Waste Management Association* 55(6):708-746.

6. Hasler, P. & Nussbaumer, T. (1998) Particle size distribution of the fly ash from biomass combustion. *Proceedings of the 10th European Conference and Technology Exhibition*, pp 8-11.

7. Kauppinen, E. I. & Pakkanen, T. A. (1990) Coal combustion aerosols: a field study. *Environmental Science & Technology* 24(12):1811-1818.

8. Stone, V., Johnston, H., & Clift, M. J. D. (2007) Air pollution, ultrafine and nanoparticle toxicology: cellular and molecular interactions. *NanoBioscience, IEEE Transactions on* 6(4):331-340.

9. Kittelson, D. B.*, et al.* (2006) On-road evaluation of two diesel exhaust aftertreatment devices. *Journal of Aerosol Science* 37(9):1140-1151.

10. Hinds, W. C. (1999) *Aerosol technology: properties, behavior, and measurment of airborne paticles* (Wiley) 2nd edition Ed.

11. Whitby, K. & Sverdrup, G. (1980) California aerosols-their physical and chemical characteristics. *Adv. Environ. Sci. Technol.;(United States)* 9.

12. Monn, C. (2001) Exposure assessment of air pollutants: a review on spatial heterogeneity and indoor/outdoor/personal exposure to suspended particulate matter, nitrogen dioxide and ozone. *Atmospheric Environment* 35(1):1-32.

13. Donaldson, K., Stone, V., Clouter, A., Renwick, L., & MacNee, W. (2001) Ultrafine particles. *Occupational and Environmental Medicine* 58(3):211-216.

14. Warheit, D. B. (2004) Nanoparticles: health impacts? *Materials today* 7(2):32-35.

15. Zhu, Y., Hinds, W. C., Kim, S., & Sioutas, C. (2002) Concentration and size distribution of ultrafine particles near a major highway. *Journal of the Air & Waste Management Association* 52(9):1032-1042.

16. Utell, M. J. & Frampton, M. W. (2000) Acute health effects of ambient air pollution: the ultrafine particle hypothesis. *Journal of aerosol medicine* 13(4):355-359.

17. Peters, A., Wichmann, H. E., Tuch, T., Heinrich, J., & Heyder, J. (1997) Respiratory effects are associated with the number of ultrafine particles. *American Journal of Respiratory and Critical Care Medicine* 155(4):1376-1383.

18. Ott, W. R. (1982) Concepts of human exposure to air pollution. *Environment International* 7(3):179-196.

19. Ott, W. R. (1985) Total human exposure. *Environmental Science & Technology* 19(10):880-886.

20. Duan, N. (1982) Models for human exposure to air pollution. *Environment International* 8(1–6):305-309.

21. Flagan, R. (2004) Opposed migration aerosol classifier (OMAC). *Aerosol Science and Technology* 38(9):890-899.

22. Junker, M., *et al.* (2000) Airborne particle number profiles, particle mass distributions and particle-bound PAH concentrations within the city environment of Basel: an assessment as part of the BRISKA Project. *Atmospheric Environment* 34(19):3171-3181.

23. Lee, S. J., Demokritou, P., Koutrakis, P., & Delgado-Saborit, J. M. (2006) Development and evaluation of personal respirable particulate sampler (PRPS). *Atmospheric Environment* 40(2):212-224.

24. Koch, W., Dunkhorst, W., & Lodding, H. (1999) Design and performance of a new personal aerosol monitor. *Aerosol Science and Technology* 31(2-3):231-246.

25. Sioutas, C. & Koutrakis, P. (1996) Inertial separation of ultrafine particles using a condensational growth/virtual impaction system. *Aerosol Science and Technology* 25(4):424-436.

26. Thayer, D., Koehler, K. A., Marchese, A., & Volckens, J. (2011) A personal, thermophoretic sampler for airborne nanoparticles. *Aerosol Science and Technology* 45(6):744-750.

27. Waldmann, L. & Schmitt, K. (1966) Thermophoresis and diffusiophoresis of aerosols. *Aerosol science*:137-162.

28. Fierz, M., Houle, C., Steigmeier, P., & Burtscher, H. (2011) Design, calibration, and field performance of a miniature diffusion size classifier. *Aerosol Science and Technology* 45(1):1-10.

29. Flagan, R. C. (2011) Electrical Mobility methods for submicrometer particle characterization. *Aerosol Measurement*, (John Wiley & Sons, Inc.): 339-364.

30. Qi, C., Chen, D.-R., & Greenberg, P. (2008) Performance study of a unipolar aerosol mini-charger for a personal nanoparticle sizer. *Journal of Aerosol Science* 39(5):450-459.

31. Li, L., Chen, D.-R., Qi, C., & Kulkarni, P. S. (2009) A miniature disk electrostatic aerosol classifier (mini-disk EAC) for personal nanoparticle sizers. *Journal of Aerosol Science* 40(11):982-992.

Chapter 2 : Hardware design and component calibration of the precipitator-type electrical ultrafine particle sizer

2.1. Introduction

Numerous techniques have been employed for the design of portable samplers to classify particle size distribution on a personal scale. The most popular design uses impaction or filtration to collect particles in different size ranges, and then characterizes the particle concentration of each sample range by an offline measurement. However, there are inherent difficulties and disadvantages in applying inertial, gravitational, optical, and diffusional techniques for ultrafine particle monitoring or measuring. Thus, the electrical mobility based classification method, with its higher resolution and higher efficiency for ultrafine and submicron particle detection, becomes the primary choice for characterizing ultrafine particle size distributions [1].

Several commercial electrical mobility classifiers can measure particles in the sub-micrometer and nanometer size ranges (Qi, Chen et al. 2008) [2]. The most widely employed type is the scanning electrical mobility spectrometer [3], or commercially called a Scanning Mobility Particle Sizer spectrometer (SMPS™, TSI Inc., Shoreview, MN). The SMPS™ is primarily designed for scientific studies, where it provides good resolution in particle size classification and sensitive particle concentration detection. However, this instrument is too large and expensive for personal use (Li, Chen et al. 2009) [4]. Besides, for most of these spectrometers, radioactive materials are used as the charging sources, and these are strictly regulated and impractical to use for routine field monitoring measurements [5]. Also, the long residence time of particles in the classification region of the differential mobility analyzer (DMA) makes this instrument too slow for many applications other than laboratory calibration studies. Thus, to monitor personal exposure or make spatially distributed measurements, there is a demand for a

miniaturized, low cost, ultrafine and submicron aerosol classifier based on electrical mobility classification [6]. This type of particle sizer normally consists of three essential components: a particle charger to electrically charge sampled particles to a known charge distribution, a particle-electrical-mobility-based classifier to size the particles, and an aerosol counter to measure the concentration of sized particles.

To meet the increasing market demand, considerable efforts have been devoted to the development of portable solutions for real time and spatial nanoparticle size distribution measurements. Two models came on the market in the last year. One is the Portable Aerosol Mobility Spectrometer (PAMS) developed by KANOMAX USA Inc. (Andover, NJ), and the other is the NanoScan SMPS provided by TSI Inc. (Shoreview, MN).

The PAMS is an electrical mobility size spectrometer designed for portable, mobile, or handheld aerosol sampling applications. The unit provides number-weighted aerosol size distributions over almost the entire submicrometer range (10 to 863 nm) in one scan. A non-radioactive bipolar charger is used to charge the incoming aerosols to avoid radioactive safety concern, while reducing measurement uncertainty of larger sizes. The charged aerosols are then classified by a following miniature, cylindrical DMA, which is operated at the low flow rate of 0.05 l/min to cover the wide size range in a single geometry. Finally, particle counts of each classified group are given by a small condensation particle counter (CPC). There are two measurement modes: a single diameter count mode to get a total count within a narrow size range, and a size distribution mode to measure size distributions over a desired size range or size resolution. This stand-alone, battery-operated instrument weighs only 4.5 kg and measures 23×23×15 cm, compact and portable enough for personal and spatial

measurements [5]. But to cover the size range of 10 to 863 nm, the low flow rate required for PAMS operation brings a potential problem of diffusional loss inside, thus making the size distribution measurement unrepresentative, especially for the lower size range. Besides, isopropyl alcohol is used as the working fluid of the CPC, and it may also interfere with the measurement environment.

The NanoScan SMPS (model 3910, TSI Inc, Shoreview, MN) has two key features that enable portable measurement [7]. One is a non-radioactive opposed flow unipolar diffusion charger developed and patented by Medved, Dorman et al. [8]. The other is the radial Differential Mobility Analyzer (rDMA) incorporated as the electrical mobility classifer in the instrument, a technology first introduced by Pourprix [9], and further developed by Zhang, Akutsu et al. [10] and Fissan, Pöcher et al. [11]. Different from the conventional cylindrical DMA design devised by Knutson and Whitby in 1975 [12], in this radial DMA design, the sheath and sample air are introduced radially inwards between two parallel and flat electrodes. The classified flow exits from the classification region through a monodisperse outlet port in the center of the bottom plate, and the excess flow exits through a top center port. The NanoScan SMPS also has two operation modes. The size distribution measurement mode requires 60 s sampling time, with a 45 s up-scan and a 15 s down-scan. The single mode continuously monitors the particle concentration at a single electrical mobility diameter with a resolution of 1 s [7]. However, the NanoScan SMPS can cover only the size range of 10 to 420 nm, with 13 size channels, which is not enough to present the whole size distribution spectrum of submicrometer particles. Besides, because it uses an isopropanol-based CPC as the particle counter, working fluid is always required, and there is an upper limit of 1×10^6 #/cm^3 for total concentration

detection. The dimensions of 45×23×39 cm and weight of 8 to 9 kg also make the NanoScan SMPS not suitably compact and lightweight for personal exposure assessment.

2.2. Hardware design and configuration

In this study, an electrical ultrafine particle sizer (EUPS) was designed for the personal and spatial measurement. For the development of this first generation electrical ultrafine particle sizer, low cost and miniaturization were the two most pressing requirements. Therefore, every component was designed as a simple and small structure.

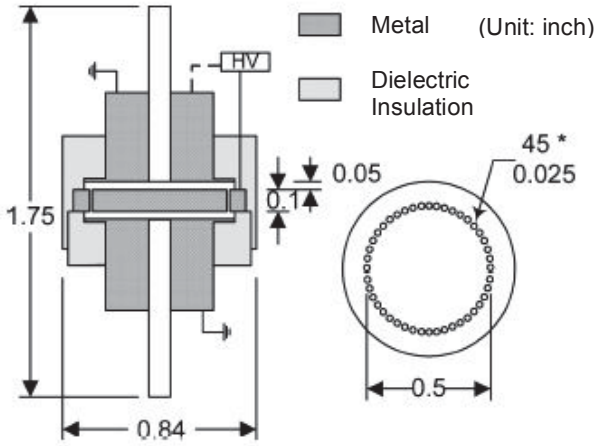

Figure 2-1. Schematic diagram of prototype mini-disk precipitator (unit in inches) [2]

In designing electrical mobility classifiers, there are three classifying mechanisms to choose from: precipitation as the zero-th order, electrical aerosol classification as the first order, and differential mobility classification as the second order. Among the three orders of classifying mechanisms, only the precipitation method, with the electrical precipitator as the classifier, does not require a sheath flow to be introduced into the classification region. To simplify the classifier design, the precipitation mechanism was chosen for the first generation electrical ultrafine particle sizer, because of its greatest simplicity and

cost-efficiency among all three mechanisms. Following the design criteria for a miniature precipitator, in 2008, Qi et al. developed a low cost, miniaturized electrical mobility particle classifier, which is a mini-disk dual-chamber precipitator shown in Figure 2-1. This miniature precipitator was designed by modifying the disk-type single-chamber precipitator of Hurd and Mullins [13]. To make the overall size more compact than the single-chamber design, while maintaining a particle size detection limit up to 500 nm, high voltage is applied to both the top and bottom flow chambers to form a dual-chamber precipitator, and to geometrically maximize the region for electrical mobility classification [2].

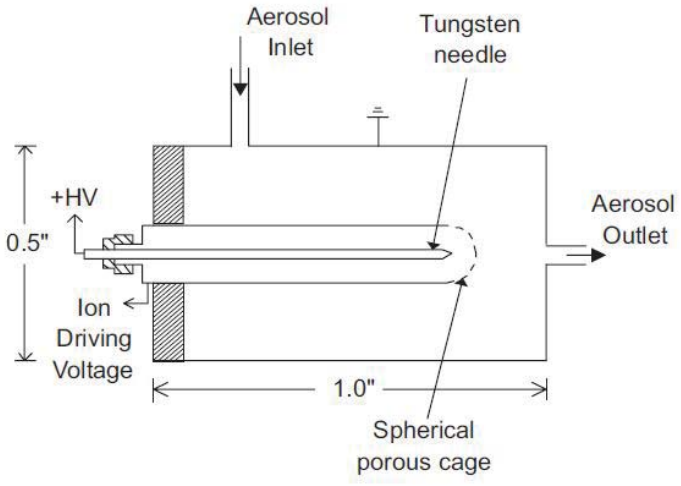

Figure 2-2. Schematic diagram of the mini-charger [14]

In the same year, Qi, Chen et al. also designed a miniaturized corona-discharge-based unipolar aerosol charger for electrically charging the sampled ultrafine and submicron particles [14]. As shown in Figure 2-2, the prototype mini-charger is simply constructed with a tubular metal case, with the aerosol inlet connected at 90° and the aerosol outlet at the downstream end. The tungsten corona discharge tip is inserted into

and electrically insulated from the case. High voltage is applied on the tip to initiate the corona discharge process for generating ions. The ion driving voltage is applied to a perforated spherical dome with a 74% open area. This small voltage helps drive the generated ions out of the corona case through the perforated dome, and at the same time establishes a small electrical potential difference between the dome and the grounded charger case. The difference helps drive the ions to mix with the incoming particles in the particle charging zone, and also reduces particle loss inside the charger case by quickly driving charged particles to exit the charger once they get electrically charged.

Combining the achievements of these two hardware component designs, this study presents the development of an electrical ultrafine particle sizer (EUPS). The assembly of this first edition EUPS includes a modified mini-charger, a modified disk-type dual-chamber precipitator, and a P-Trak (model 8525, TSI Inc., Shoreview, MN) as the particle number concentration detector. The EUPS design enables the easy portability and fast response measurement ability of an electrical mobility classification based particle sizer, which can be used for both personal and spatial aerosol size distribution monitoring.

2.2.1. Previous calibration work

After the components were manufactured, Qi, Chen et al. made preliminary performance calibrations for both the mini-charger and mini-disk aerosol precipitator prototypes.

First, optimized operational settings were determined for maximizing the charging performance of the aerosol mini-charger. Both extrinsic and intrinsic charging efficiencies of 20 nm monodisperse particles were measured under different operation

conditions, i.e., different aerosol flowrates, corona currents and ion driving voltages. According to the experimental results, the optimized operational conditions of this prototype were set as a corona current of 1 μA and an ion driving voltage of 40 V for a 0.3 lpm aerosol flowrate, and a corona current of 2 μA and an ion driving voltage of 120 V for a 1.5 lpm aerosol flowrate. Operating under these optimal conditions, the intrinsic charging efficiency of the prototype mini-charger was measured as a function of particle size. As shown in Figure 2-3, with error bars representing replicate runs, the intrinsic charging efficiency could reach up to 100% for sizes larger than 30 nm when operated at a 0.3 lpm aerosol flowrate, or 50 nm at a 1.5 lpm aerosol flowrate.

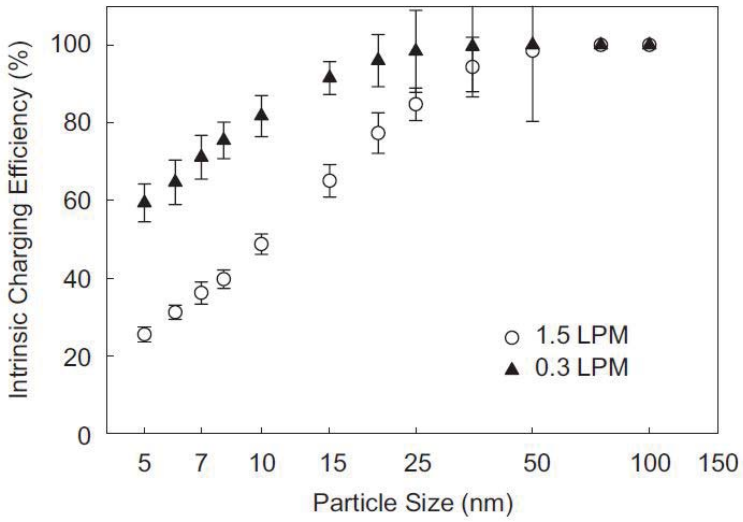

Figure 2-3. Intrinsic charging efficiency of the prototype mini-charger [14]

The prototype mini-disk aerosol precipitator was also evaluated by both penetration and precipitation measurements. The penetration measurement was motivated by concern about particle loss inside this compact aerosol classifier, and as well the computational requirements of data inversion process for further recovering the particle size distributions.

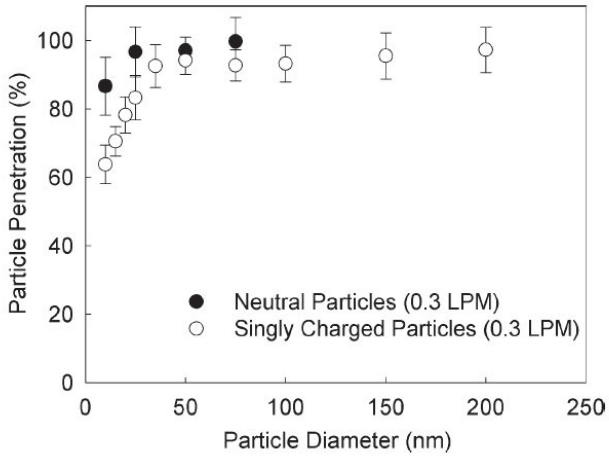

Figure 2-4. Penetration of neutral and singly charged particles in the mini-disk precipitator [2]

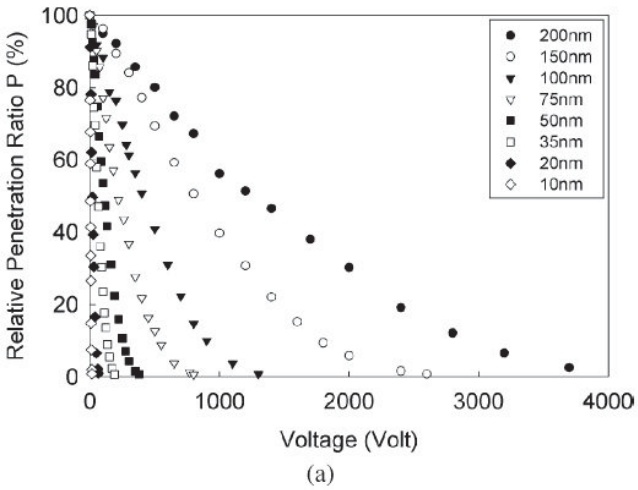

Figure 2-5. Particle cutoff curves of the mini-disk precipitator, Q = 0.3 lpm [2]

The precipitation measurement was performed to get the characteristic particle cut-off curve (or transfer function) of the mini-disk precipitator at a fixed operational flowrate, i.e., 0.3 lpm for Qi's experiment, and it measured the penetration of DMA classified monodisperse particles at various voltages applied to the middle disk. The results are shown in Figure 2-4 and Figure 2-5, with both showing that the relative penetration ratio increases as particle size increases, and decreases when the applied high voltage increases.

A semi-empirical model was also developed and experimentally verified by Qi [2] for the dual chamber precipitation process in this prototype mini-disk precipitator. The model could be used to predict the particle cutoff curves, and as well as to develop the data inversion scheme to retrieve the sampled particle size distributions from penetration measurements of the precipitator. As concluded in Qi's study, the penetration of charged particles through a single chamber disk precipitation zone can be described by

$$P = (1 - K_1 V), \tag{2-1}$$

where K_1 is the characteristic slope of the particle precipitation cutoff curves. The slope can be determined from the input particle electrical mobility Z_p, inlet flowrate Q, and the precipitator geometry that

$$K_1 = \frac{\pi r_0^2}{2bQ\alpha_1} Z_p, \tag{2-2}$$

with α_1 as an empirical coefficient which accounts for the discrepancy between the real flow conditions and the ideal conditions (steady, axisymmetric laminar flow and no radial component to the electrical field).

For the dual-chamber mini-disk precipitator, we can get the charged particle penetration by multiplying the penetrations through the two precipitation zones:

$$P = (1 - K_2 V)^2, \tag{2-3}$$

which is based on the assumption that particles get remixed into a uniform particle distribution in the small orifices of the perforated plate between the upper and lower flow chambers. Similarly, we can obtain the characteristic slope of the particle precipitation cutoff curves represented by K_2. Also, with the empirical coefficient α_2 included, K_2 is defined as

$$K_2 = \frac{\pi r_0^2}{2bQ\alpha_2} Z_p. \tag{2-4}$$

This linear relationship between the square root of particle penetration $P^{1/2}$ and the operation voltage V was also evidenced by the correlation of the experimental results under a 0.3 lpm aerosol flow operation, which is shown in Figure 2-6.

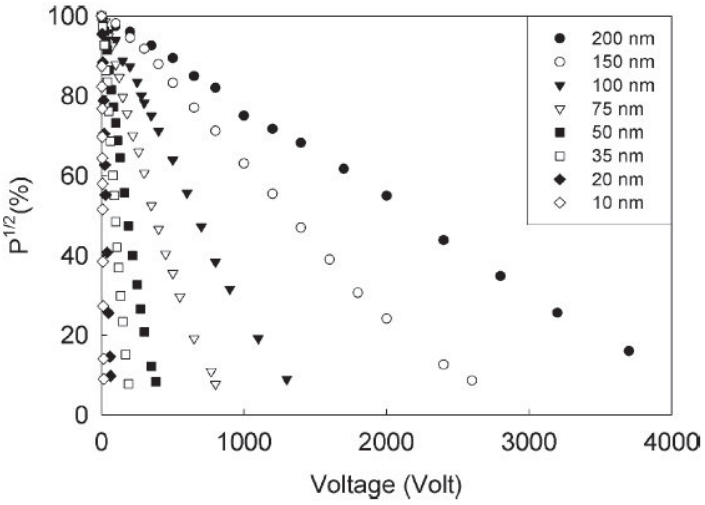

Figure 2-6. $P^{1/2}$ vs. applied voltage for experimental results from the dual chamber precipitation operation, Q=0.3 lpm

2.2.2. Hardware component modifications

Based on Qi's early designs of the mini-charger and the mini-disk precipitator, in this work, a prototype precipitator-type electrical ultrafine particle sizer (p-type EUPS) was assembled, with both the mini-charger and mini-disk precipitator redesigned by TSI Inc.. Additionally, the sizer unit used an ultrafine particle counter P-Trak® (Model 8525, TSI Inc., Shoreview, MN) attached as the downstream particle number concentration detector. Figure 2-7 shows the P-Trak, classifier assembly, and the assembled prototype of the p-type EUPS from left to right successively.

P-Trak (TSI 8525) Classifier assembly Assembled prototype

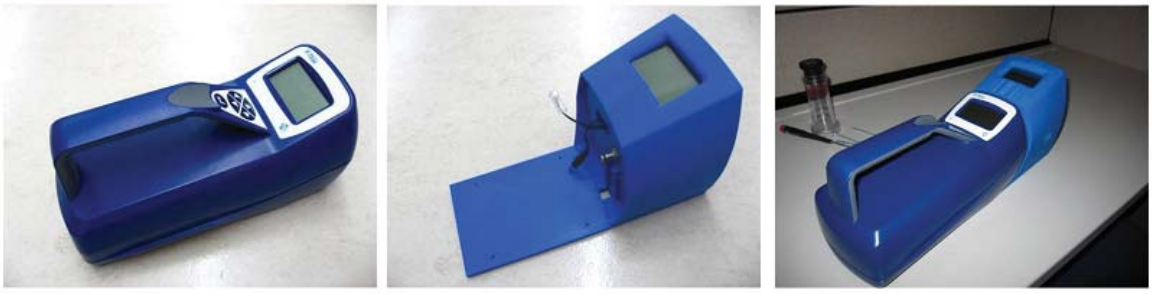

Figure 2-7. The assembled package of the first generation EUPS

All of the components were manufactured by TSI Inc., with necessary modifications to meet both long-term durability and mass-manufacturing cost requirements. Also, the operating aerosol flowrate was set at 0.7 lpm to coordinate with the P-Trak's sampling flowrate of 0.7 lpm. Therefore, all the performance curves had to be recalibrated separately to verify the working ability of individual components, and further to be more representative of the performance of this redesigned prototype package.

2.3. Experimental setups for component calibration

2.3.1. Calibration of the mini-charger

With high voltage applied, the mini-charger was maintained at a stable working current of 2.0 μA. With the ion driving voltage applied to the screen, we calibrated the charger's performance as a function of the charged particle size. The test aerosols were monodisperse sodium chloride (NaCl) particles selected by a Differential Mobility Analyzer (DMA, model 3081 and 3085, TSI Inc., Shoreview, MN), with sizes ranging from 20 nm to 500 nm (the lower size limit of 20 nm was determined by the detection limit of the P-Trak condensation particle counter). Figure 2-8 is a schematic diagram of the experimental setup used for monodisperse sodium chloride particle generation.

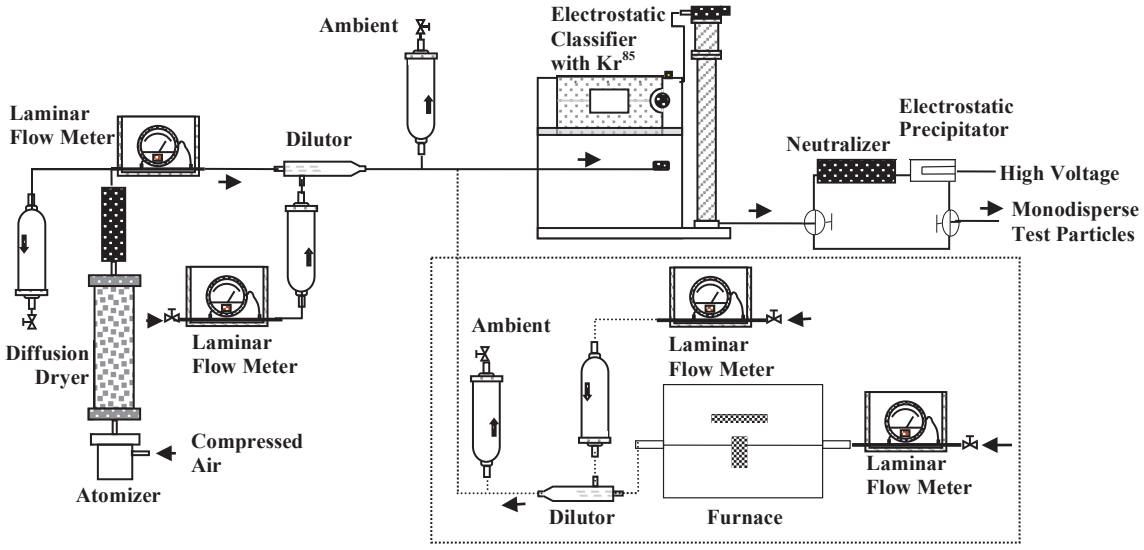

Figure 2-8. Experimental setup for the particle generation and characterization system

Two different systems were used for generating polydisperse sodium chloride particles. For particles with mean diameters smaller than 50 nm, a furnace generated

particles via the evaporation-condensation process described by Hussin [15]. A combustion boat loaded with sodium chloride powder was placed in a ceramic tube passing through a tube furnace. When the furnace was heated to a required high temperature, the sodium chloride powder evaporated to form a rich vapor in the ceramic tube. A stream of inert gas passed through the furnace tube, carrying the vapor-rich stream to the dilutor, where the hot vapor-rich stream was quenched by another stream of particle-free inert gas at room temperature. Polydisperse nanoparticles were formed during this quenching process, and sent to the Nano-Differential Mobility Analyzer (Nano-DMA, model 3085, TSI Inc., Shoreview, MN) system downstream, where they were classified and the monodisperse nanoparticles needed for the following evaluation experiment were obtained.

For polydisperse particles in larger sizes, which in our study were particles with mean diameters ranging from 50 to 500 nm, the generator system was a homemade Collison mechanical atomizer, shown on the left in Figure 2-8. Compressed air atomized a water solution with the test particle material as the only solute. The droplets were then thoroughly dried by two diffusion dryers filled with silicon desiccant and connected in series. The final yield was dry polydisperse sodium chloride particles at the outlet of the second diffusion dryer. Downstream, a standard long DMA (model 3081, TSI Inc., Shoreview, MN) classified monodisperse particles with diameters larger than 50 nm. Since DMA classification is based on particle electrical mobility, all the classified monodisperse particles exiting from the DMA systems were electrically charged. To get the monodisperse neutral particles needed for the charger evaluation experiment, both a Po^{210} neutralizer and a high voltage electrostatic precipitator (charged particle remover)

were used downstream of the DMAs. To get monodisperse singly charged particles for the penetration measurement, there was also an optional bypass flow route parallel to the charge-removing route.

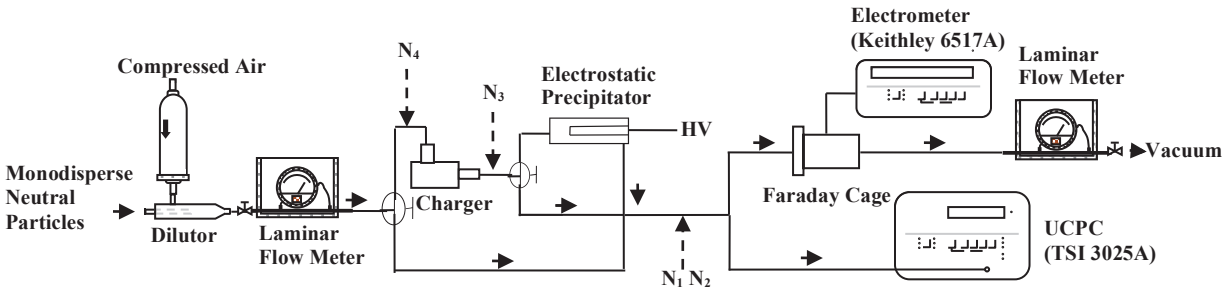

Figure 2-9. Experimental setup for the mini-charger calibration

Using monodisperse neutral test particles, we calibrated the mini-charger for extrinsic charging efficiency, intrinsic charging efficiency, and average charge of the charged particles, using the experimental setup shown in Figure 2-9. To conduct the charging efficiency measurement, another electrostatic precipitator was added downstream of the mini-charger. With sufficient high voltage applied to its central electrode, this electrostatic precipitator removed the charged fraction of particles from the passing aerosol flow, letting only neutral particles penetrate. As before, the second particle remover could also be bypassed to get the number concentration of all the particles, charged and neutral, exiting from the mini-charger. An ultrafine condensation particle counter (UCPC, model 3025A, TSI Inc., Shoreview, MN) was then used to measure all the particle number concentrations needed to investigate the neutral or charged fractions in the aerosol flow passing through the mini-charger.

In this evaluation, two kinds of charging efficiencies were measured, known as the extrinsic charging efficiency and the intrinsic charging efficiency. The measurements of

the two charging efficiencies are quite different. The extrinsic charging efficiency η_{ex}, as described by Chen and Pui [16], is defined as

$$\eta_{ex} = \frac{N_3 - N_1/P_{cpr}}{N_4}, \tag{2-5}$$

where N_1 is the number concentration of particles measured downstream of the second charged particle remover, with the operating voltages for corona discharge module and the second charged particle remover both switched on. N_3 is the number concentration of particles exiting the mini-charger, N_4 is the total number concentration of particles entering the mini-charger, and P_{cpr} is the penetration of neutral particles through the second charged particle remover as a function of particle size. P_{cpr} was evaluated separately for the second charged particle remover before it was installed into the mini-charger evaluation setup.

Different from the consideration of particle loss during the charging and transportation processes in measuring the extrinsic charging efficiency, the measurement of intrinsic charging efficiency directly counted all the particles lost before exiting the second particle remover as charged particles. The charged fraction, i.e., the intrinsic charging efficiency η_{in}, was obtained by subtracting the neutral fraction of particles exiting the second particle remover, as defined by Adachi, Romay et al. [17]:

$$\eta_{in} = 1 - \frac{N_1}{N_2}, \tag{2-6}$$

in which N_1 is the same number concentration that appeared in the extrinsic charging efficiency measurement, and N_2 was measured similarly to N_1, but with the voltages for the corona discharge module and the second charged particle remover turned off.

Besides the number concentration measurement route, there was a second flow route with a Faraday cage and an electrometer installed, for measuring the current carried by the charged particles. The measured current could then be used along with the particle number concentration of the aerosol flow for calculating the average number of charges on the charged particles, using the equation

$$n = \frac{I}{V \cdot C \cdot e}. \tag{2-7}$$

Here n is the average number of charges, I is the current captured by the Faraday cage and measured by the electrometer, V is the total volume of air passing through the Faraday cage during the current sampling time, C is the concentration measured by UCPC, and e is the elementary charge of 1.6×10^{-19} C.

During all these experimental measurements, the aerosol flowrate through the mini-charger was kept exactly at 0.7 lpm, the same flowrate as the aerosol flowrate for the P-Trak in the packaged working unit.

2.3.2. Evaluation of humidity effect

Considering that the ultimate aim of the miniature p-type electrical ultrafine particle sizers is personal monitoring or spatial distribution particle measurement, it is necessary to investigate how this working unit will perform when sizing real ambient aerosols. In real conditions, the measuring environment and the measured particles are both quite different from the laboratory generated dry particles that we used for the hardware calibration. Conditions of both the measuring environment and the measured particles can vary a lot in humidity, temperature, materials, and other chemical properties. The most variable factor would be the environmental relative humidity, which can range from 0%

as the absolute dry condition to 100% for a humid rainy day. So one question is whether the calibrated performance curves can still be representative of the real world performance of this precipitator-type electrical ultrafine particle sizer unit, when it is used under different relative humidity conditions.

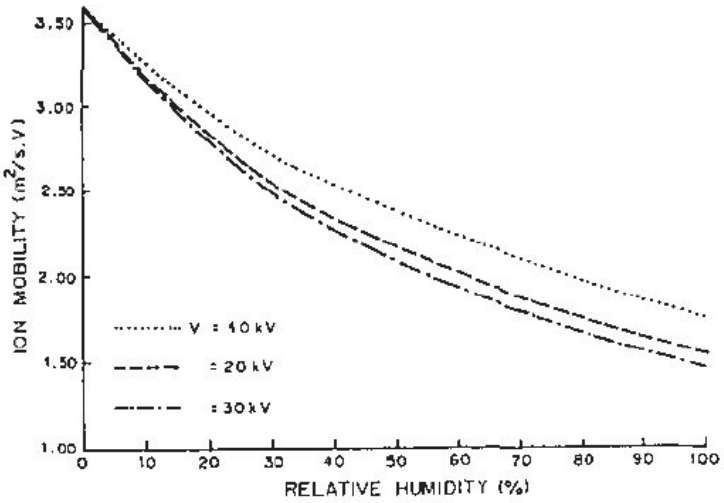

Figure 2-10. Variation of ion mobility with relative humidity at different applied voltages, temperature = 200 °C, pressure = 1 atm. [18]

As demonstrated by Abdel-Salam and shown in Figure 2-10, the mobility of ions decreases with an increase of relative humidity, which is caused by the increasing ion combination efficiency with polar water molecules as the humidity increases [18]. While ion mobility and ion attachment efficiency are the two parameters that can most affect the charging efficiency of the diffusion charging process in the mini-charger, the humidity effect on charging efficiency would be the most critical factor for evaluating the p-type EUPS performance in real field environments.

Therefore, a humidification chamber was designed for conditioning the aerosol stream to a specific relative humidity level while maintaining high particle penetration efficiency. Monodisperse test particles were sent through a porous, seamless, sintered stainless steel tube, with an outer diameter was 0.25 inch, inner diameter of 0.125 inch, and a media grade of 0.2. The tube was tightly wrapped with water saturated foam, and was centered in a cylindrical PVC chamber with an inner diameter of 2.0 inches. Air flow was humidified when passing through a Nafion® tube connected to a digital refrigerated water bath heater/chiller (Isotemp 3013D, Thermo Fisher Scientific, Waltham, MA). A schematic of the chamber design is shown in Figure 2-11.

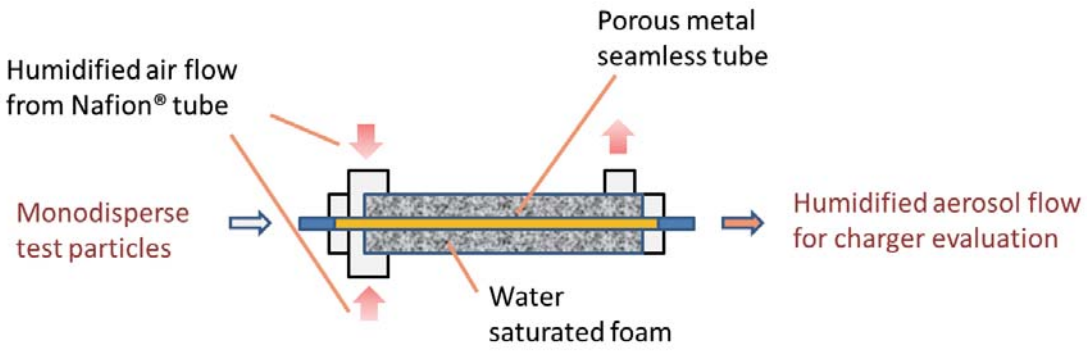

Figure 2-11. Schematic of the humidification chamber design

Thus, the humidified environment of the charging process of the mini-charger was simulated. As shown in Figure 2-12, other than the added humidification chamber, the experimental setup remained the same as in Figure 2-9. Using humidified aerosols, the three performance parameters of the mini-charger were then evaluated and compared to performance under the normal laboratory operation condition (10% RH as measured by a humidity probe).

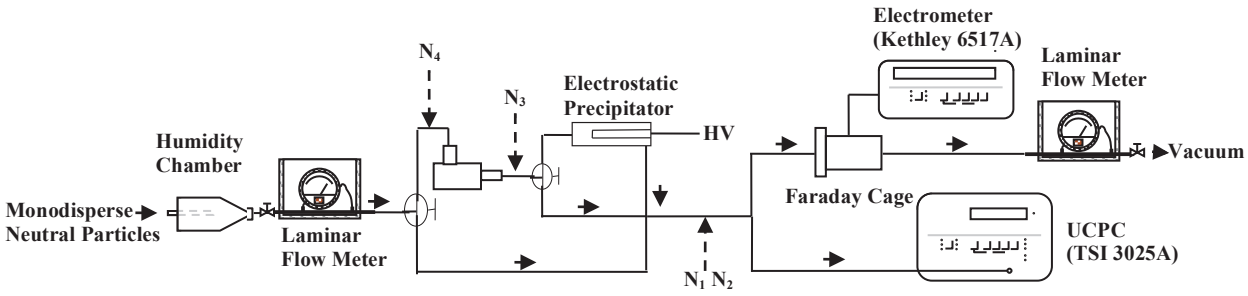

Figure 2-12. Experimental setup for humidity effect evaluation of the mini-charger

2.3.3. Calibration of the mini-disk precipitator

According to Qi's semi-empirical model for dual chamber precipitation as,

$$P^{1/2} = 1 - \frac{\pi r_0^2}{2bQ\alpha_2} \cdot (Z_p \cdot V) \,. \tag{2-8}$$

Here P is the theoretical penetration of charged particles through this dual chamber mini-disk precipitator, and the square root $P^{1/2}$ should be linearly correlated with the product of the applied voltage V and the particle electrical mobility Z_p. To establish the linear relationship between $P^{1/2}$ and Z_p, the mini-disk precipitator was then calibrated at the flowrate of 0.7 lpm by measuring the charged particle penetration of monodisperse particles with diameters ranging from 20 to 500 nm under different operating voltages.

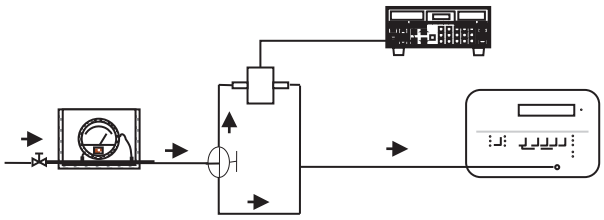

Figure 2-13. Experimental setup for mini-disk precipitator calibration

The test aerosols used for the mini-disk precipitator evaluation were also monodisperse sodium chloride particles generated by the generation and classification

system previously shown in Figure 2-8. However, rather than the neutral particles as used for charger evaluation, singly charged particles, obtained by bypassing the first charged particle remover at the exit of DMA system, were used for determining the penetration curves for the mini-disk precipitator. The experimental setup for the mini-disk precipitator calibration is shown in Figure 2-13. The voltage applied on the mini-disk precipitator was provided by a power supply, operated from 0 to 2500 V for each particle size.

2.3.4. Calibration of P-Trak counting efficiency

Similar to the UCPC (model 3025A, TSI Inc., Shoreview, MN), the P-Trak ultrafine particle counter (model 8525, TSI Inc., Shoreview, MN) used as the downstream particle number concentration detector for the p-type electrical ultrafine particle sizer also counts particles based on condensation particle counting technology. The highest particle number concentration that can be measured by the P-Trak is 5×10^5 particles/cm^3, and the detectable particle size range is from 20 to 1000 nm. The total flowrate at the aerosol inlet was 0.7 lpm, with only 0.1 lpm diverted for particle concentration sampling as the aerosol flow. To achieve more precise measurements with this prototype, it was also very important to calibrate the counting efficiency of the P-Trak as a function of particle size. The calibration reference was the UCPC (model 3025A, TSI Inc., Shoreview, MN), and the counting efficiency is represented in the following equation as

$$\eta = \frac{N_{P-Trak}}{N_{UCPC}}. \tag{2-9}$$

In the equation, $N_{\text{P-Trak}}$ is the concentration reading of the P-Trak, and N_{UCPC} is that of the UCPC's simultaneous measurement of the same aerosol stream. The test particles were monodisperse sodium chloride particles with sizes from 20 to 500 nm.

2.4. Experimental results for component calibration

2.4.1. Calibration curves of the mini-charger

With the experimental setup shown in Figure 2-9, the mini-charger was calibrated for extrinsic and intrinsic charging efficiencies. Both charging efficiencies followed an "exponential growth to a maximum" trend, as shown in Figure 2-14. With error bars representing replicate runs, the intrinsic charging efficiency starts from 80% at 20 nm and increases to 100% for sizes larger than 60 nm. The extrinsic charging efficiency grows from 37% at a particle size of 20 nm and reaches 80% for particle sizes larger than 80 nm.

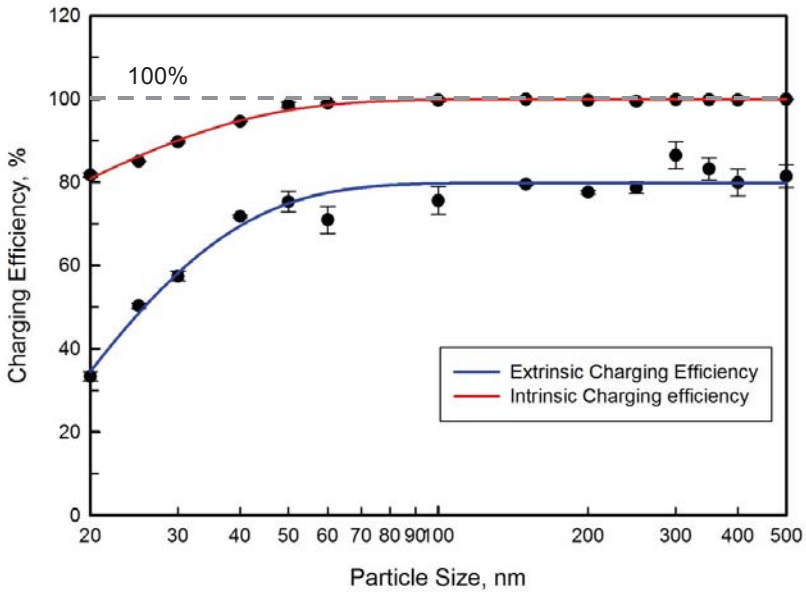

Figure 2-14. Calibration curves of charging efficiencies for the mini-charger operated at 0.7 lpm

Different from the exponential growth profile, Figure 2-15 indicates the average number of charges has an approximately linear relationship with the particle size in nm. The minimum value is one elementary charge per particle because the averaging is

applied only for charged particles, and the number will increase to 24 as the highest value in the evaluated size range, for 500 nm particles.

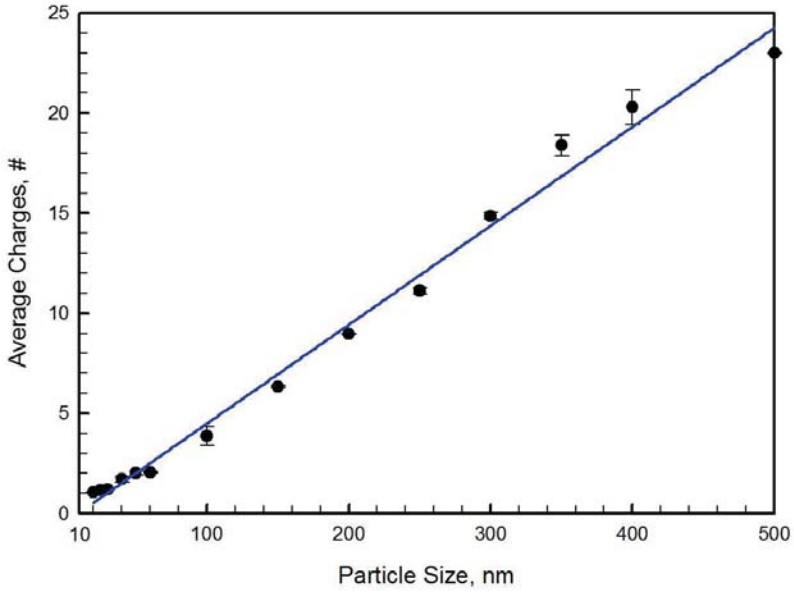

Figure 2-15. Calibration curve of average charges for the mini-charger operated at 0.7 lpm

For the sake of obtaining more precise regression equations of these calibration curves to be used in the data inversion scheme, all the calibration results were further processed with a curve-fitting software, Table Curve 2D®. The software has an extensive equation pool with various functions to closely follow trends of the data. With x representing the particle size in nm, the fitted regression equation for the extrinsic charging efficiency E_{ex} is

$$E_{ex} = 3993.78 - 0.42x + 98.36\,(\ln x)^2 - 1163.47\ln x - 6035.60x^{-0.5}, \quad (2\text{-}10)$$

the intrinsic charging efficiency E_{in} is

$$E_{in} = -182.03 + 14.11x - 1.35xlnx - 39.98x^{0.5}lnx + 133.58x^{0.5}, \quad (2\text{-}11)$$

and the average number of charges on charged particles y is expressed as

$$\sqrt{y} = 0.59 + 0.02x - 9.89\times10^{-5}x^2 + 4.18\times10^{-7}x^3 - 8.16\times10^{-10}x^4 + 5.60\times10^{-13}x^5, \quad (2\text{-}12)$$

with $x \in (20, 500)$ for all three equations.

2.4.2. Evaluation of the humidity effect

In this part of the evaluation, we utilized two particle materials. The sodium chloride particles had a deliquescence point at 75% RH, and the potassium sulfate particles had a deliquescence point at 95%RH.

As shown in the following figures, clearly the intrinsic charging efficiency of sodium chloride particles was more influenced by a change of relative humidity, exhibiting an obvious decreasing trend as the relative humidity increased. While for the measurements with potassium sulfate particles, there was only a slight decrease for particles with sizes under 60 nm.

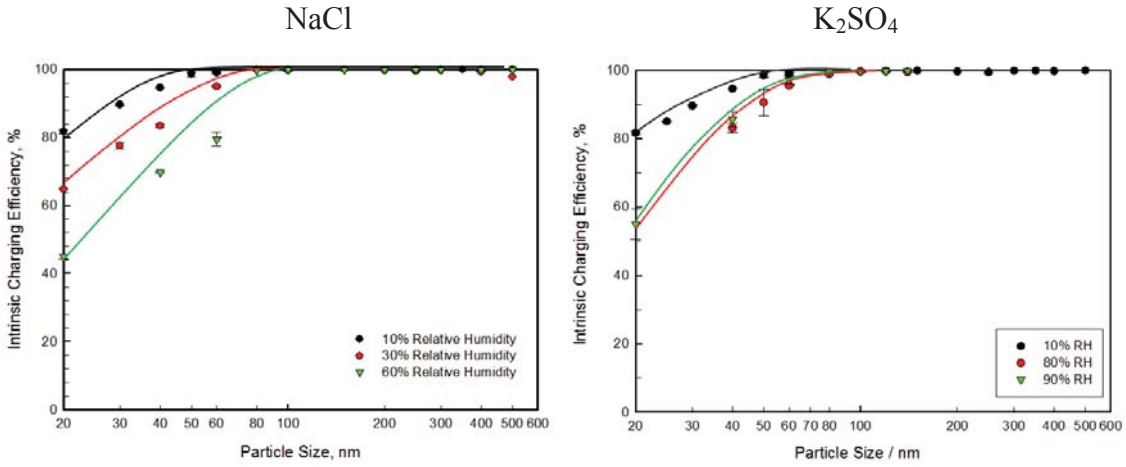

Figure 2-16. Intrinsic charging efficiencies measured with NaCl and K_2SO_4 particles under different relative humidity conditions

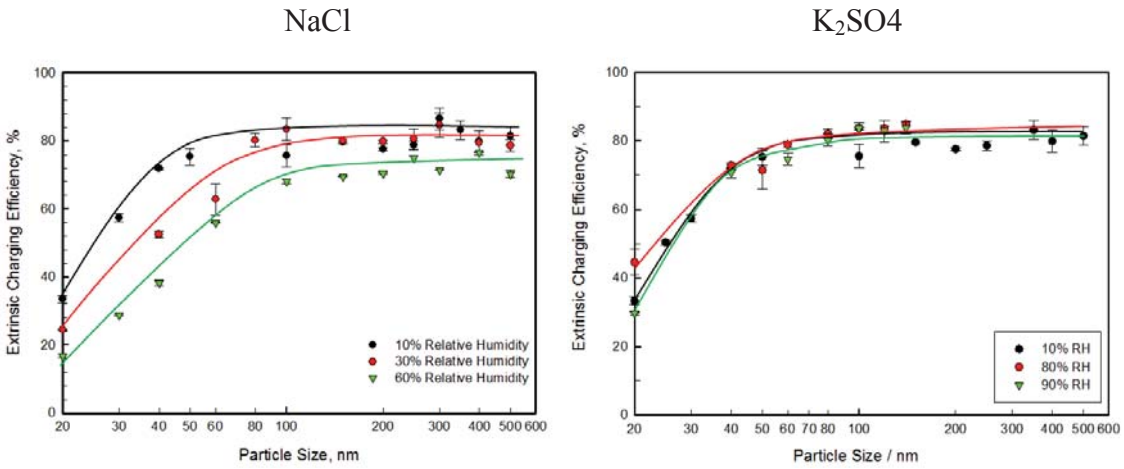

Figure 2-17. Extrinsic charging efficiencies measured with NaCl and K_2SO_4 particles under different relative humidity conditions

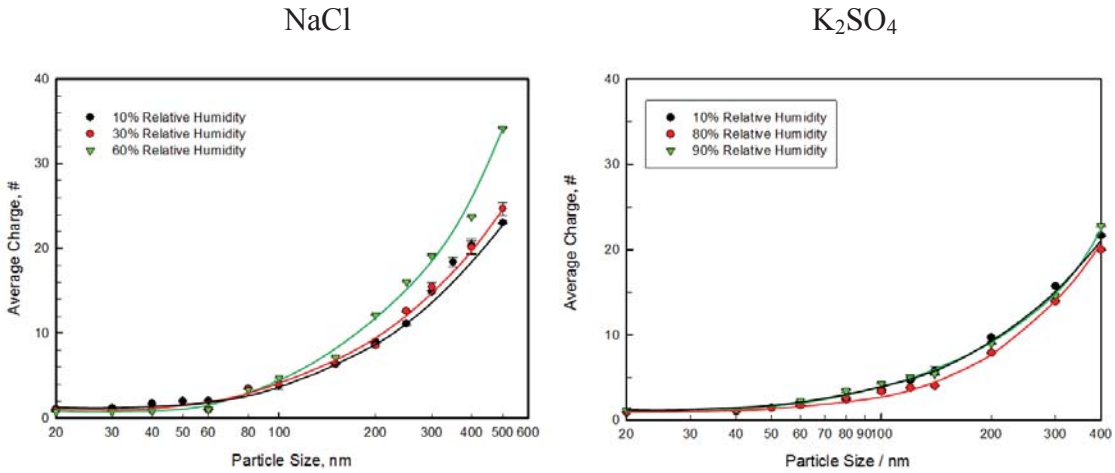

Figure 2-18. Average charge measured with NaCl and K_2SO_4 particles under different relative humidity conditions

The extrinsic charging efficiency measurement is the more important parameter to indicate the mini-charger working condition for this study, as the extrinsic charging efficiency represents the fraction of charged particles exiting the charger, which are the only particles that can be effectively classified in the following mini-disk precipitator. As seen, when the relative humidity increased, the extrinsic charging efficiency measured with sodium chloride particles decreased similarly to the intrinsic charging efficiency.

But for potassium sulfate particles, there was nearly no significant difference between the charging efficiencies measured under different humidity conditions.

Similar to the charging efficiency measurements, the average charge of sodium chloride particles was also more influenced by the relative humidity conditions than that of potassium sulfate particles. As shown in Figure 2-18, as the relative humidity increased, the number of charges on charged sodium chloride particles increased greatly compared to the constant results of potassium sulfate measurement. And the changes under different humidity conditions observed in sodium chloride measurement were primarily caused by the deliquescence effect, which induced a particle size increase of the sodium chloride particles, as reported by Bruzewicz, Checco et al. [19].

Thus, the K_2SO_4 measurements are the superior measurements in this evaluation of humidity effect, from which it can be concluded that the charger performance was not sensitively affected by the relative humidity conditions of both the sampled particles and measurement surroundings.

2.4.3. Calibration curves of the mini-disk precipitator

The mini-disk precipitator was calibrated for its penetration curves of DMA classified monodisperse sodium chloride particles in the size range from 20 to 500 nm, and the operating high voltage applied to the perforated plate in the mini-disk precipitator was varied between 0 and 2500 V for each particle size. To present the final results, all the penetrations were normalized and plotted in one graph as a function of the multiplication of the particle electrical mobility Z_p in $m^2/V{\cdot}s$, and the operation voltage V in volts, as shown in Figure 2-19.

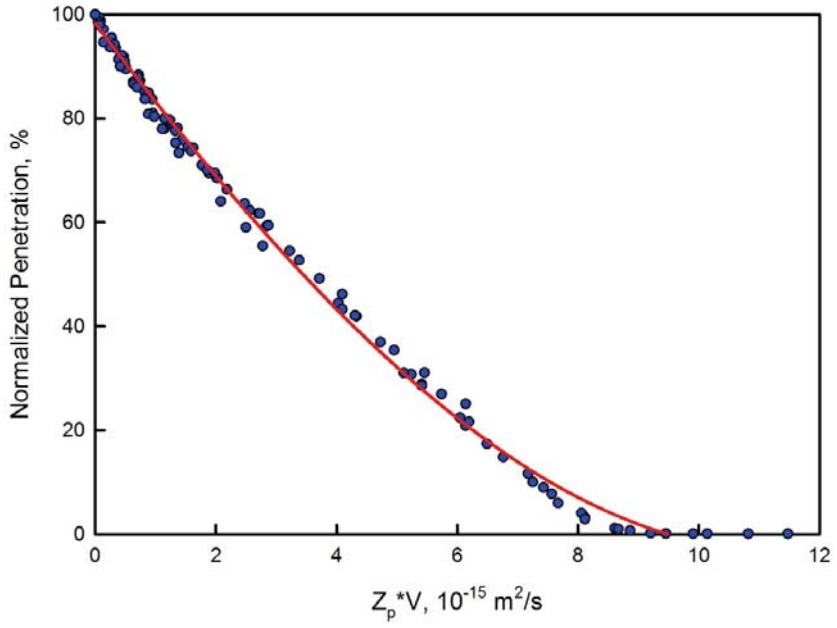

Figure 2-19. Penetration as a function of $Z_p \cdot V$ for the mini-disk precipitator operated at 0.7 lpm

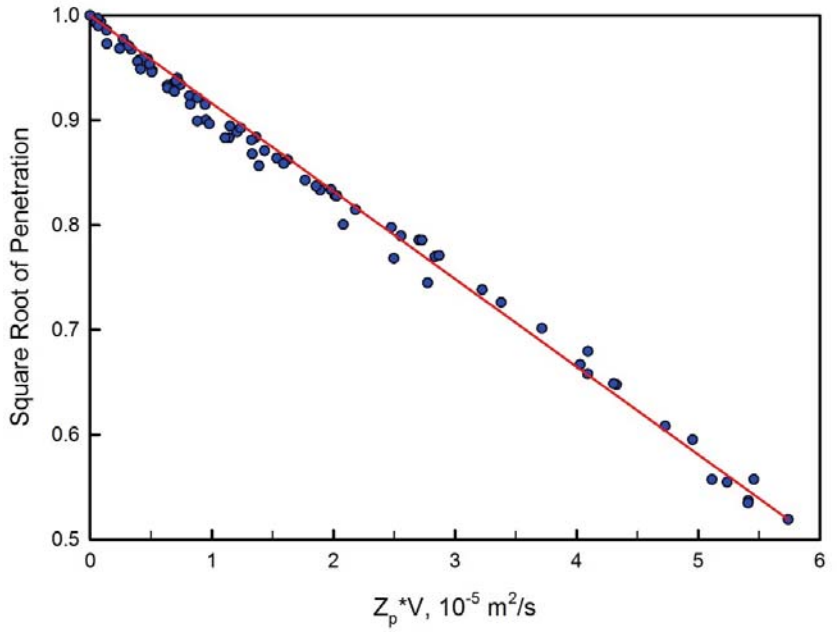

Figure 2-20. Square root of penetration as a function of $Zp \cdot V$ for the mini-disk precipitator operated at 0.7 lpm

To verify the agreement of this modified mini-disk precipitator's performance with the semi-empirical model developed by Qi, Chen et al. [2] for dual chamber precipitation,

the penetration curve was also plotted with the square root of normalized penetration as a function of the product $Z_p \cdot V$, as shown in Figure 2-20.

The calibration curve shown in Figure 2-20 demonstrates an explicit linear relationship between the square root of penetration $P^{1/2}$ and the product of particle electrical mobility and operation voltage ($Z_p \cdot V$). This linear relationship proves the predictable and stable performance of the modified mini-disk precipitator for electrical mobility classification in the particle size range from 20 to 500 nm. The calibration curve was then regressed for further data inversion, yielding the equation

$$P = 0.9985 - 1.5\times10^{4} \cdot x + 3.41\times10^{7} \cdot x^{2} + 2.08\times10^{11} \cdot x^{3}, \qquad (2\text{-}13)$$

where x represents the $Z_p \cdot V$ value, and P is the normalized penetration of the corresponding particle size.

2.4.4. Calibration curves of the particle count detector

Two particle count detectors were used for the first generation (p-type) electrical ultrafine particle sizer evaluation experiment: the P-Trak® ultrafine particle counter (model 8525, TSI Inc., Shoreview, MN) and the CPC (model 3010, TSI Inc., Shoreview, MN). The P-Trak was reported to have a lower detectable size limit of 20 nm, and an upper concentration limit of 5×10^{5} #/cm^3 [20], while the CPC 3010 has a lower detectable size limit of 10 nm, and an upper concentration limit of 1×10^{4} #/cm^3 [21]. Both were calibrated for their counting efficiencies as a function of detected particle size, with the UCPC (model 3025A, TSI Inc., Shoreview, MN) as a reference. The counting efficiency η was calculated as

$$\eta = \frac{C}{C_{UCPC}} \times 100\% , \qquad (2\text{-}14)$$

Where C (#/cm^3) was the number concentration measured by the two EUPS particle detectors, and C_{UCPC} (#/cm^3) was the number concentration measured by the UCPC.

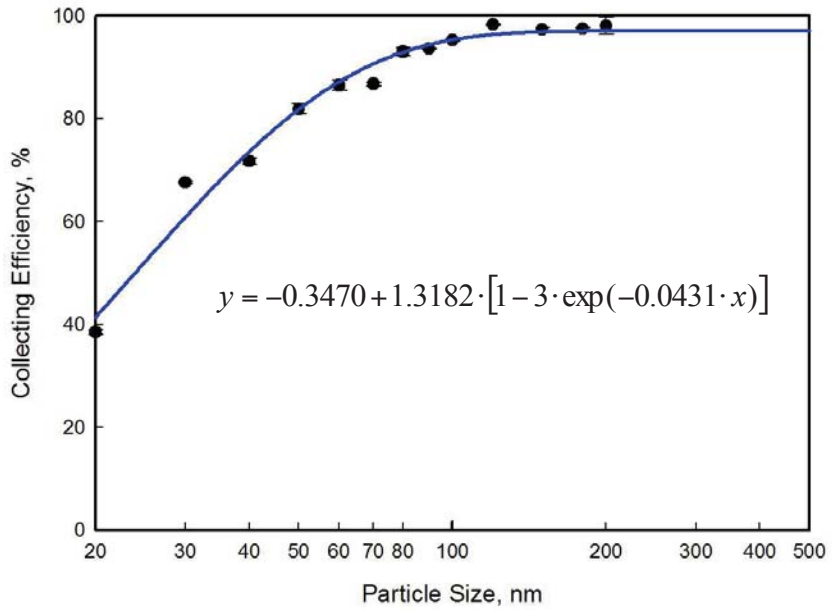

Figure 2-21. Calibration of P-Trak counting efficiency, with UCPC as a reference

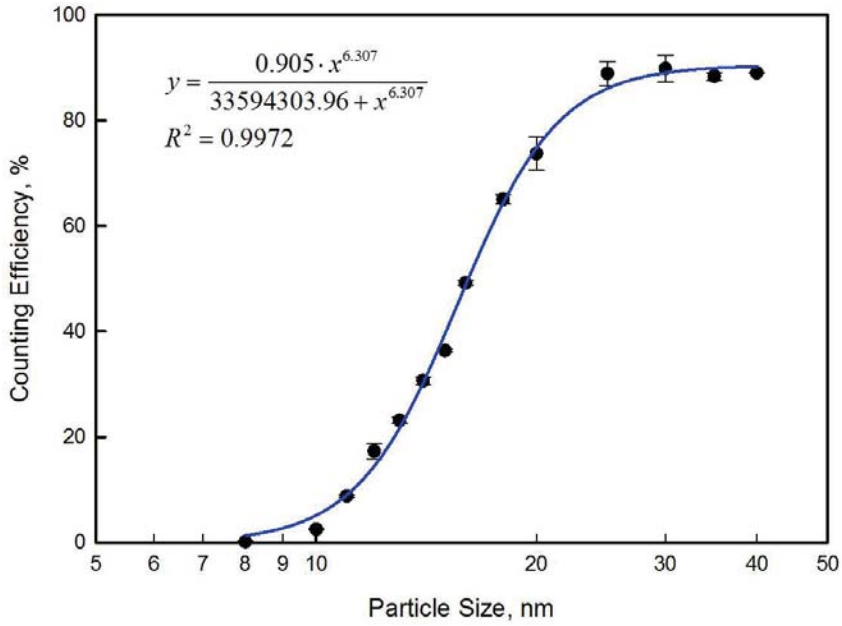

Figure 2-22. Calibration of CPC 3010 counting efficiency, with UCPC as a reference

The results and regression equations are shown in Figure 2-21 and Figure 2-22. The counting efficiencies of the particle count detectors were also needed for inclusion in the data inversion scheme to better recover the original particle size distribution of the measured aerosols.

2.5. Conclusions

In this study, we calibrated and evaluated the three key components for a precipitator-type electrical ultrafine particle sizer assembly, under both normal and humidified conditions. The three components include a miniature corona-discharge unipolar charger, a miniature disk-type precipitator, and a portable condensation particle counter, and all were calibrated using monodisperse particles with sizes ranging from 20 to 500 nm.

The miniature charger was operated at a constant corona-discharge current of 2 μA and an aerosol flowrate of 0.7 lpm. Three parameters were investigated for the miniature charger calibration: intrinsic charging efficiency, extrinsic charging efficiency, and average number of charges on charged particles. According to the calibration results, both charging efficiencies followed an "exponential growth to a maximum" trend, with the intrinsic charging efficiency increasing from 80% at 20 nm to 100% for sizes larger than 60 nm, and the extrinsic charging efficiency from 37% at 20 nm to 80% for particle sizes larger than 80 nm. The humidity effect on charging performance was also evaluated for the miniature charger, and the results showed that it was not sensitively affected by relative humidity conditions. However, for particles of certain hydrophilic materials, the

deliquescence effect induced a particle size increase in a humidified condition which caused some sizing difference, compared to the original or freshly generated particles.

The calibration curve for the mini-disk precipitator was demonstrated as a function of the square root of penetration $P^{1/2}$ and the product of particle electrical mobility and operation voltage ($Z_p \cdot V$). The results showed an explicit linear relationship between the two, which fitted well with the semi-empirical model for dual chamber precipitation. This consistency also proved the predictable and stable performance of the modified mini-disk precipitator for electrical mobility classification in the particle size range from 20 to 500 nm.

Counting efficiencies of the particle number concentration detectors were calibrated by monodisperse particles from 20 to 500 nm, with a UCPC as the reference. Both detectors have increasing counting efficiencies as particle size increases.

Throughout the calibration processes, operation conditions were optimized, and performance was calibrated for all three components. All the calibration results were also regressed into algebra equations to be further included in the data inversion scheme for retrieving the particle size distributions from the measurement signals.

2.6. References

1. Flagan, R. C. (2011) Electrical mobility methods for submicrometer particle characterization. *Aerosol Measurement*, (John Wiley & Sons, Inc.): 339-364.

2. Qi, C., Chen, D.-R., & Greenberg, P. (2008) Fundamental study of a miniaturized disk-type electrostatic aerosol precipitator for a personal nanoparticle sizer. *Aerosol Science and Technology* 42(7):505 - 512.

3. Wang, S. C. & Flagan, R. C. (1990) Scanning electrical mobility spectrometer. *Aerosol Science and Technology* 13(2):230-240.

4. Li, L., Chen, D.-R., Qi, C., & Kulkarni, P. S. (2009) A miniature disk electrostatic aerosol classifier (mini-disk EAC) for personal nanoparticle sizers. *Journal of Aerosol Science* 40(11):982-992.

5. Kulkarni, P., Qi, C., Kato, T., & Fukushima, N. (2011) Development of portable aerosol electrical mobility spectrometer for aerosol exposure measurement. *Proceedings of the 30th AAAR Annual Conference.*

6. Flagan, R. (2004) Opposed migration aerosol classifier (OMAC). *Aerosol Science and Technology* 38(9):890-899.

7. Torsten, T., *et al.* (2013) NanoScan SMPS – A novel, portable nanoparticle sizing and counting instrument. *Journal of Physics: Conference Series* 429(1):012061.

8. Medved, A., Dorman, F., Kaufman, S. L., & Pöcher, A. (2000) A new corona-based charger for aerosol particles. *Journal of Aerosol Science* 31, Supplement 1(0):616-617.

9. Pourprix, M. (1990) Electrostatic precipitation of aerosol on wafers, a new mobility spectrometer. *Proceedings of the 6th International Conference* 2:797.

10. Zhang, S.-H., Akutsu, Y., Russell, L. M., Flagan, R. C., & Seinfeld, J. H. (1995) Radial differential mobility analyzer. *Aerosol Science and Technology* 23(3):357-372.

11. Fissan, H., Pöcher, A., Neumann, S., Boulaud, D., & Pourprix, M. (1998) Analytical and empirical transfer functions of a simplified spectromètre de mobilité electrique circulaire (SMEC) for nano particles. *Journal of Aerosol Science* 29(3):289-293.

12. Knutson, E. O. & Whitby, K. T. (1975) Aerosol classification by electric mobility: apparatus, theory, and applications. *Journal of Aerosol Science* 6(6):443-451.

13. Hurd, F. K. & Mullins, J. C. (1962) Aerosol size distribution from ion mobility. *Journal of Colloid Science* 17(2):91-100.

14. Qi, C., Chen, D.-R., & Greenberg, P. (2008) Performance study of a unipolar aerosol mini-charger for a personal nanoparticle sizer. *Journal of Aerosol Science* 39(5):450-459.

15. Hussin, A., Scheibel, H. G., Becker, K. H., & Porstendörfer, J. (1983) Bipolar diffusion charging of aerosol particles—I: experimental results within the diameter range 4–30 nm. *Journal of Aerosol Science* 14(5):671-677.

16. Chen, D.-R. & Pui, D. Y. H. (1999) A high efficiency, high throughput unipolar aerosol charger for nanoparticles. *Journal of Nanoparticle Research* 1(1):115-126.

17. Adachi, M., Romay, F. J., & Pui, D. Y. H. (1992) High-efficiency unipolar aerosol charger using a radioactive alpha source. *Journal of Aerosol Science* 23(2):123-137.

18. Abdel-Salam, M. (1992) Influence of humidity on charge density and electric field in electrostatic precipitators. *Journal of Physics D: Applied Physics* 25(9):1318.

19. Bruzewicz, D. A.*, et al.* (2011) Reversible uptake of water on NaCl nanoparticles at relative humidity below deliquescence point observed by noncontact environmental atomic force microscopy. *The Journal of Chemical Physics* 134(4):044702-044710.

20. User manual, TSI (2006) P-Trak Ultrafine Particle Counter Model 8525.

21. User manual, TSI (2006) Model 3010 Condensation Particle Counter.

Chapter 3 :Data inversion scheme and performance evaluation of the precipitator-type electrical ultrafine particle sizer

3.1. Introduction

The size distribution of ultrafine particles is a fundamental property of an ultrafine aerosol stream, and is one of the most essential parameter for personal ultrafine particle exposure assessment. To determine its particle size distribution, an aerosol stream needs to be passed through instruments called particle size spectrometers [1]. The spectrometers classify particles into different size bins based on their optical equivalent size, aerodynamic size, electrical mobility equivalent size, diffusion equivalent size, or other size equivalent parameters [2]. However, obtaining the particle size distribution from the raw instrument data is not straightforward, because there is not an ideal one to one correspondence between the measured bins and actual size classes [3]. In most cases, particles in a particular size bin are not entirely the particles in that certain size range, but might include particles from multiple neighboring bins. This non-ideal overlapping introduces a degree of indeterminacy into the size distribution retrieval process, and thus causes continuous controversy for determining a best "retrieved" solution.

The retrieval process is known as data inversion. Twomey described the inversion process thus: "the set of numbers which comprises the answer must be 'unraveled', as it were, from a tangled set of combinations of these numbers" [4]. Several mathematical techniques can be used for data inversion, briefly summarized as follows.

One of the simplest techniques for handling aerosol data is the histogram method. It displays a histogram distribution of the sampled aerosols. Typically, the bin size range of interest is first determined, and then measurements are made to determine the population in each bin. It is a straightforward approach for instruments with fairly sharp size cutoffs,

i.e., those with natural size bin boundaries. However, no instrument can achieve ideally sharp cutoff sizes for the discrete bins. Therefore, besides of the size cutoff sharpness requirement, the histogram method also loses detailed size resolution, as there is no size distribution information available inside each size bin to generate a spline line for the whole size range [5].

Linear inversion approaches can also be applied to the data inversion of aerosol size distributions, such as least-squares solution, regularization, and decomposition techniques using basis functions. The least-squares solution requires the number of measurements to be more than the number of unknowns. A parametric form also needs to be assumed for further successive iterations to converge to the unique solution, and this initial guess has a decisive effect on the final solution [6]. Regularized linear methods, such as the widely applied constrained least-squares method, was first developed by Philips in 1962, and later introduced into the aerosol measurement field by Twomey in 1965 [7]. Rizzi et al. reported that, to retrieve agreeable size distribution data, this constrained method had a maximum error tolerance of 5% in the measurements [8].

Nonlinear inversion was proposed for the aerosol measurement applications also by Twomey in 1975, as a substitute for linear inversion approaches. In his study, Twomey used a nonlinear iterative scheme for the data inversion of some typical atmospheric aerosol distributions, and got more reasonable results than the linear inversion solutions with the same input raw data [9]. Similar to the linear algorithm, constraints can also be applied to the nonlinear inversion method for optimized solutions, as proposed by Cooper and Spielman in 1976. The constraints applied to the inversion scheme, such as physical constraints, can help get a well-fit solution if the measured size distribution is very

similar to the initial guess. On the other hand, these physical constraints also lose detailed information by limiting the size distribution profile [10].

From all the above methods, to choose the most suitable algorithm for a size distribution measurement study, there is always a trade-off between algorithmic complexity, calculation speed, and the accuracy of reconstruction [11]. In the data inversion scheme, complexity of the algorithm does not always guarantee accuracy of solution [12]. Besides reproducible performance of the inversion scheme itself, for a miniaturized instrument, the computational effort to do the inversion also needs to be taken into consideration for determining the data inversion scheme [13].

To evaluate the size distribution reproducibility of the chosen data inversion scheme, and as well to demonstrate the sizing performance of the entire electrical ultrafine particle sizer (EUPS), evaluations of the EUPS size distribution measurements are also required. In this study, measurements were made of both laboratory generated polydisperse aerosols and real ambient aerosols.

3.2. Data inversion scheme

As in the precipitator-type electrical ultrafine particle sizer operation, a size spectrum of 12 evenly distributed size bins on a log scale were used to represent the size range from 20 to 500 nm, and there was no ideal one-to-one correspondence between the measured bins and the actual size classes. Thus a data inversion scheme representative of the components' performance was necessary to relate the P-Trak readings to the particle size distribution information of the measured aerosols.

3.2.1. Presumed log-normal scheme

The data inversion scheme was first developed by presuming a functional format for the particle size distribution. In this scheme, the particle number size distribution was presumed to be a log-normal distribution profile, and the relationship between the particle number size distribution and P-Trak® readings was then established by a prediction based on the average charges of particles exiting the mini-charger and particle penetrations through the precipitator. We assumed the particle number size distribution was a log-normal function:

$$f = \frac{1}{\sqrt{2\pi}\ln\sigma_g} exp\left[\frac{\ln d_p - \ln CMD}{2(\ln\sigma_g)^2}\right] \text{[14]}. \quad (3\text{-}1)$$

There are three variables, including the count median diameter (*CMD*) in nm, geometric standard deviation σ_g, and total number concentration N_t in #/cm^3. The following equation was then used to describe a unimodal size distribution based on particle number concentration:

$$N(d_p) = \frac{N_t}{d_p\sqrt{2\pi}\ln\sigma_g} exp\left(\frac{-(\ln d_p - \ln CMD)}{2(\ln\sigma_g)^2}\right) \text{[14]}. \quad (3\text{-}2)$$

The three variables were determined by successive approximations. For each data set, several possibilities for the three variables could fit the above equation. To pick out the most representative values, a criteria error function χ was defined to express the differences between the measured values and the values calculated by applying each possible set of the three variables:

$$\chi(CMD, \sigma_g, N_t) = \frac{\sum_{i=1}^{m}|P_i - M_i|}{m}, \quad (3\text{-}3)$$

in which, P_i is the calculated penetration when the precipitator is operated at voltage V_i, M_i is the measured penetration at precipitation voltage V_i, and m is the number of voltage steps applied to the mini-disk precipitator. By scanning through the entire preset value range for each variable, the set of variables producing the minimum criteria error function χ_{min} was identified as the final result.

For retrieving the more complicated bimodal log-normal particle size distributions, the problem was simplified and treated as a combination of two unimodal log-normal distributions. Thus there were in total six variables to be determined for a bimodal distribution, which required much more calculation by the working unit, and resulted in an undesirable increase in instrument response time.

3.2.2. Constrained least square scheme

As the electrical ultrafine particle sizer unit was primarily designed for personal use or spatial measurement in the field, the size distributions of the target aerosols would vary more dynamically than those of laboratory generated particles. This dynamic characteristic of the targeted aerosols requires a fast instrument response to get representative measurements of the particle size distributions. Therefore, to meet the requirements of quick measurements and flexible distribution profiles, a fast mode data inversion scheme was developed for the precipitator-type EUPS. This new scheme was established based on the constrained least-squares method, which is a linear inversion method introduced by Twomey [3]. For the EUPS size distribution measurements, the error E, i.e., the difference between the measured and calculated values, has its square E^2 defined as

$$E^2 = ([QA]_{M\times N} \cdot [C]_{N\times 1} - [R]_{M\times 1})^T ([QA]_{M\times N} \cdot [C]_{N\times 1} - [R]_{M\times 1}), \quad (3\text{-}4)$$

in which

$$[QA] = [A] + \lambda \cdot [H]. \quad (3\text{-}5)$$

In the above equations, N represents the number of size bins for the whole size distribution profile in the final output, M is the number of voltage steps applied on the mini-disk precipitator in each run, and λ is the smoothness conditioning parameter. $[H]$ is a nearly diagonal conditioning matrix determined by the chosen smoothing constraint, and $[A]$ is the calibrated penetration matrix for particles with sizes of the N size bins, classified through the mini-disk precipitator at M steps of voltage respectively. $[QA]$ is the conditioned penetration matrix, $[C]$ is the number concentration of each size bin, and $[R]$ is the Condensation Particle Counter (CPC) reading at each voltage step.

A lower square of the error indicates a more precise inversion. Then, to get the minimum square of the error, i.e., the minimum E^2, the calculations were performed as follows:

$$\frac{\partial(E^2)}{\partial C} = 0, \quad (3\text{-}6)$$

$$[QA]^T[QA][C] - [QA]^T[R] = 0, \quad (3\text{-}7)$$

$$[C] = ([QA]^T[QA])^{-1} \cdot [QA]^T[R], \text{ and} \quad (3\text{-}8)$$

$$[C] = [M] \cdot [R], [M] = ([QA]^T[QA])^{-1} \cdot [QA]^T. \quad (3\text{-}9)$$

As the matrix $[M]$ was accurately calculated from the calibration results in advance, and could later be directly preinstalled onboard the electrical ultrafine particle sizer unit, the matrix $[C]$ could then be quickly obtained by a simple matrix multiplication right after $[R]$ was read out. The multiplication product $[C]$ showed the particle number

concentrations of each corresponding size bin, and thus was output as the final result of particle size distribution based on number concentration.

This new data inversion scheme has several advantages over the previous presumed log-normal one. First, there is no presumption of the size distribution profile, and each size bin is monitored individually, so it more universally measures the size distributions, especially for irregularly distributed particles which could hardly fit in any log-normal distribution profile. Second, because it requires only the simple matrix calculus to get the final particle size distribution results, the time span of each size distribution measurement is much shorter, and thus the instrument responds much faster to variations in the size distribution of measured aerosols.

Moreover, the new data inversion scheme also enables a new feature of the instrument, described as *Identification of the Time-variation of Particle Size Distributions*. It is a dynamic monitoring function that zooms in on the specific size bin causing a dynamic change in the particle size distribution. This function is achieved by comparing and identifying the variation characteristics of P-Trak readings according to Table 3-1, when quickly switching the precipitator applied voltage between two selected values.

The matrix [*M*] in equation (3-9) was calculated from the component calibration results, and therefore was fixed for the system operated at the optimized settings. To simplify the table structure, every two neighboring size bins of the original 12 bins were regrouped into one size group, and there were finally six size groups for the identification table. For every voltage step, added up the elements in each size group, yielding a 6×12 matrix. By comparing the summed elements in each column, the two columns

representing voltages V_1 = 0 V and V_2 = 50 V were selected from the 12 voltage steps, choosing the most distinct different profile combinations among all six size groups. By normalizing the matrix elements with "+1" for element values > 0.2, "-1" for values < -0.2, and "0" for values between -0.2 and 0.2, a normalized identification table was obtained, as shown in Table 3-1.

Table 3-1. Identification table for V_1 = 0 V and V_2 = 50 V

Size Group Number	V_1	V_2
1	-1	+1
2	+1	+1
3	+1	-1
4	0	+1
5	0	-1
6	+1	0

To identify time variations, we compared the readings of the changing profiles with the identification table for each size group respectively, with "+1" for number concentration increases, "-1" for number concentration decreases, and "0" for imperceptible changes. Therefore, by quickly switching between the two selected voltages, 0 and 50 V, we could immediately identify the size group which has a concentration change. Take a concentration increase condition for example: if there was an increased V_1 reading and a decreased V_2 reading, i.e., a changing profile of "+1, -1", according to Table 3-1, it was then identified that intruding aerosols in size group 3 were causing the increase of the total particle number concentration. With this dynamic

identification feature, the size range of the aerosols causing the size distribution change can be easily nailed down, equipping the precipitator-type electrical ultrafine particle sizer with a new function as an emission source tracker, in addition to its capability as a particle size distribution monitor.

3.3. Laboratory evaluation of the p-type EUPS performance

With all the components calibrated, the data inversion scheme developed, and the sizer unit assembled, we next evaluated the precipitator-type electrical ultrafine particle sizer for its particle size distribution monitoring performance. Three parameters needed to be evaluated: the size distribution measurement reliability and flexibility, the fast-response capability, and the dynamic-identification functionality. Therefore, the performance evaluation included three experimental settings respectively: steady stream aerosol measurements with aerosols of unimodal and bimodal distributions, unsteady stream aerosol measurements, and dynamic identification of time variations in aerosol size distribution.

3.3.1. Steady stream aerosol measurements

In the steady stream aerosol measurements, two parameters were evaluated. One was the size distribution measurement reliability, which was represented as the comparability of particle size distribution results measured by the p-type EUPS and the reference distributions measured by the SMPS™ spectrometer (Model 3081, 3085, and 3025A, TSI Inc., Shoreview, MN) simultaneously. The other was the size distribution measurement flexibility benefitting from the updated data inversion scheme. Because no size distribution profile presumption was needed for the data inversion process, the p-type

EUPS should be able to measure particle size distributions in any profile with one single data inversion scheme. In this experiment, both unimodal and bimodal polydisperse aerosols were used to evaluate the p-type EUPS measurement flexibility.

One of the most widely used generators for obtaining a steady stream of laboratory-generated polydisperse aerosols is the Collison atomizer, which normally has a jar for spray solution, a spray nozzle, and a baffle for impacting the droplets [15]. By pumping a steady stream of compressed air through the spray nozzle, the spray solution is atomized to small droplets, and then partly dried to form a unimodal polydisperse aerosol stream [16]. To generate the bimodal polydisperse aerosols for testing size distribution measurement flexibility, two Collison atomizers with different spray solutions were used in the generation system for this evaluation, as shown in the experimental setup schematic in Figure 3-1. Two atomizers sprayed sodium chloride solutions of different volume concentrations, providing two streams of unimodal polydisperse sodium chloride aerosols with different geometrical median sizes. A ball valve added to one of the two generation lines was operated as a mixing valve, which allowed two choices of the aerosol size distribution profile downstream. When the mixing valve was open, the two streams of generated unimodal distributed sodium chloride aerosols were mixed and formed a stream of bimodally distributed aerosols after the mixing point. While if the mixing valve was closed, only aerosols generated by Atomizer 2 could pass through the mixing point, and thus the aerosols detected by instruments downstream had a unimodal size distribution profile.

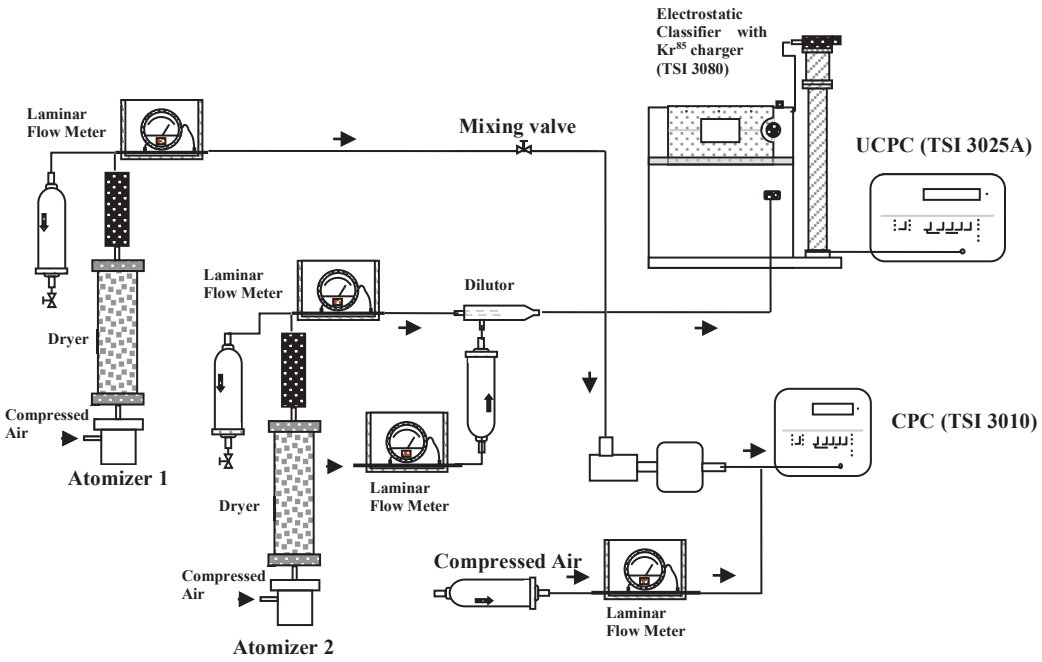

Figure 3-1. Experimental setup for lab evaluation of steady aerosol measurement

For the particle number concentration detector of the precipitator-type EUPS, the P-Trak was temporarily replaced with a CPC 3010 (TSI Inc., Shoreview, MN), which had the same operation principle as the P-Trak, but the CPC 3010 could be remotely controlled, and was more convenient to be started simultaneously with the referencing instrument SMPS™ spectrometer (TSI Inc., Shoreview, MN) for a better comparion. As the working flowrate of the CPC 3010 was 1.0 lpm, a 0.3 lpm make-up flow was added downstream to ensure a 0.7 lpm operation flowrate through the p-type EUPS classifier, to be consistent with the designed operation conditions.

The first part of the steady stream aerosol evaluation was the unimodal size distribution measurement. With the mixing valve closed, only Atomizer 2 was atomizing solution and generating unimodal sodium chloride aerosols, with a geometrical mean size around 100 nm. Downstream, the p-type EUPS and an SMPS™ spectrometer were

measuring the size distribution simultaneously. The SMPS™ measurement results were output with 8 channel (in a decade) resolution setting in the Aerosol Instrument Manager® (TSI Inc., Shoreview, MN).

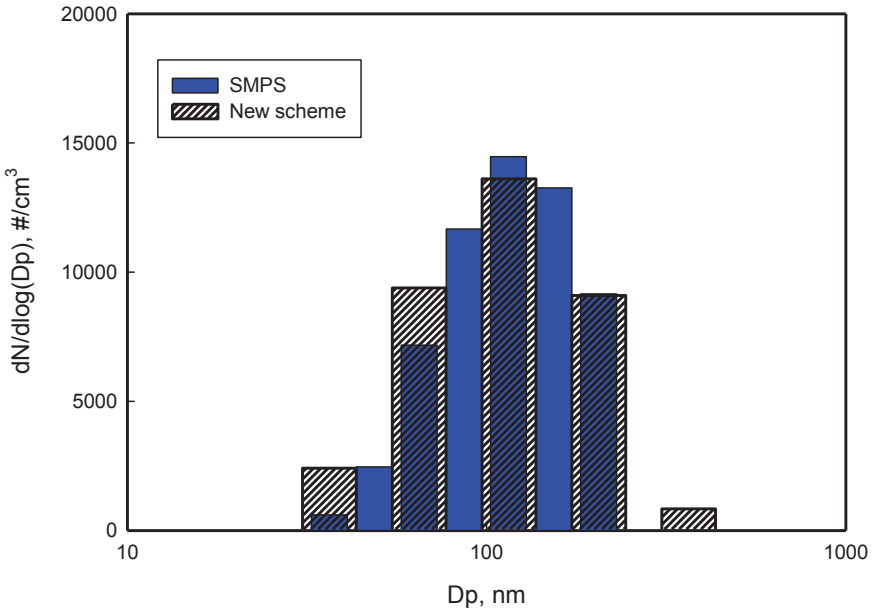

Figure 3-2. Comparison of unimodal size distribution measurements for steady stream aerosols

The comparative measurement results demonstrated an excellent agreement between the two sizing instruments, as shown in Figure 3-2. The agreement proved the p-type EUPS' sizing ability for measuring unimodal particle size distributions.

The second part of the steady stream aerosol measurement evaluated the p-type EUPS'ability to size a steady stream of aerosols with a bimodal size distribution. To obtain the bimodal distribution aerosols, the mixing valve was set at open, and the compressed air flows for both atomizers were turned on. For the (a) smaller particle sizes measurement, one atomizer atomized ultrapure water, and the other one atomized a 0.01% by volume potassium sulfate (K_2SO_4) solution. While for the (b) larger particle sizes

measurement, one atomizer atomized the 0.01% K_2SO_4 solution, and the other atomized a 10% by volume sodium chloride (NaCl) solution. The two solutions of different volume concentrations generated two streams of unimodal aerosols with different geometrical median sizes. By opening the mixing valve as shown in Figure 3-1, the two streams of unimodal aerosols were mixed and formed a stream of aerosols with bimodal size distribution. Downstream, the size distribution of this mixture of aerosols was simultaneously measured by both the p-type EUPS and an SMPS™ spectrometer. The size distributions for the p-type EUPS measurements were retrieved by using the new constrained least square data inversion scheme. Comparisons of measurement results are shown in Figure 3-3.

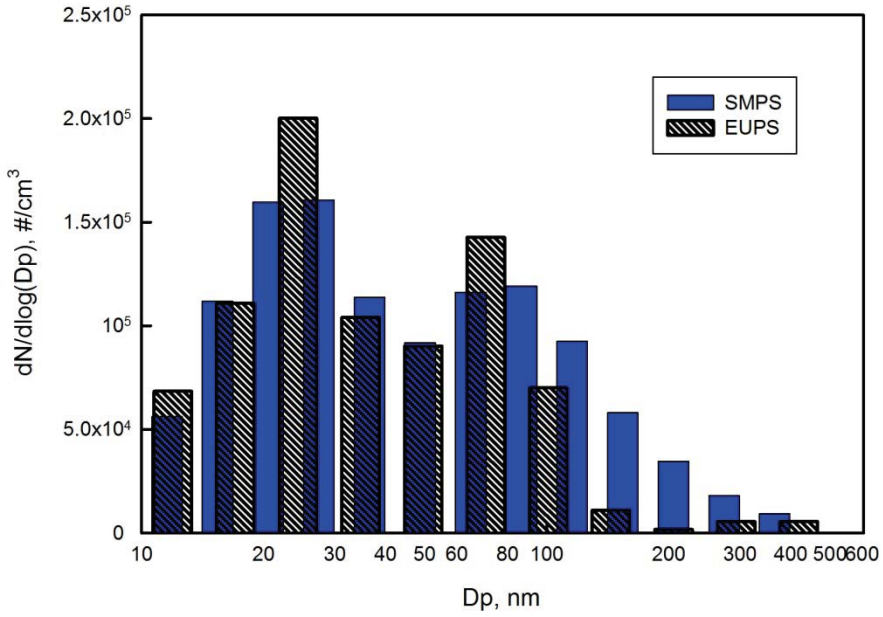

(a) Smaller particle sizes

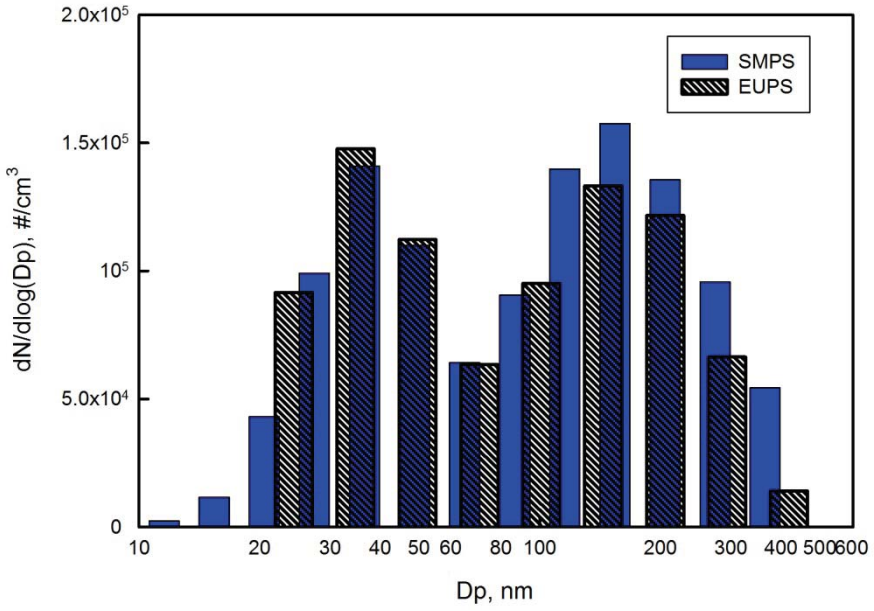

(b) Larger particle sizes

Figure 3-3. Comparison of bimodal size distribution measurements for steady stream aerosols

3.3.2. Unsteady stream aerosol measurements

To fully establish that the p-type EUPS is qualified for both personal exposure and spatial distribution measurements, it was also necessary to evaluate the measurement ability and reliability of the sizer unit responding to unsteady aerosols.

As shown in Figure 3-4, a dynamic aerosol dilutor was designed, constructed, and used along with a Collison atomizer for simulating a laboratory dynamic aerosol generator. By controlling the dilution air flowrate according to the programmed dilution profile shown in Figure 3-5, the steady stream of polydisperse aerosols from the atomizer was dynamically diluted. So, an unsteady stream of aerosols was generated for the evaluation of the EUPS' dynamic response to a changing aerosol source.

However, for this dynamic evaluation measurement, the SMPS™ spectrometer was not a suitable reference instrument, because it requires at least two minutes for each size distribution scan. To provide fast size distribution measurements, the Engine Exhaust Particle Sizer™ spectrometer (EEPS™, model 3090, TSI Inc., Shoreview, MN) was used instead, as the simultaneous reference instrument for this dynamic evaluation experiment. The EEPS™ spectrometer also measures particle size distributions based on electrical mobility classification and electrostatic precipitation, and the whole instrument weighs 32 kg. It has a detectable size range from 5.6 to 560 nm, with a sizing resolution of 16 channels per decade, and a total of 32 channels for the full size spectrum [17]. Particles are positively charged to a predictable level using a corona charger, and then charged particles are introduced into the measurement region near the center of a high-voltage electrode column, and transported down the column surrounded by HEPA-filtered sheath air. A positive high voltage applied to the electrode creates an electric field that repels the positively charged particles outward according to their electrical mobility. Charged particles strike the respective electrometers and transfer their charge. A particle with higher electrical mobility strikes an electrometer near the top; whereas, a particle with lower electrical mobility strikes an electrometer lower in the stack. This multiple-detector arrangement using highly sensitive electrometers allows for simultaneous concentration measurements of multiple particle sizes. The multi-electrometer detection enables the the EEPS™ spectrometer to measure particle emissions in real time, which meets the requirement of dynamic measurement in this experiment.

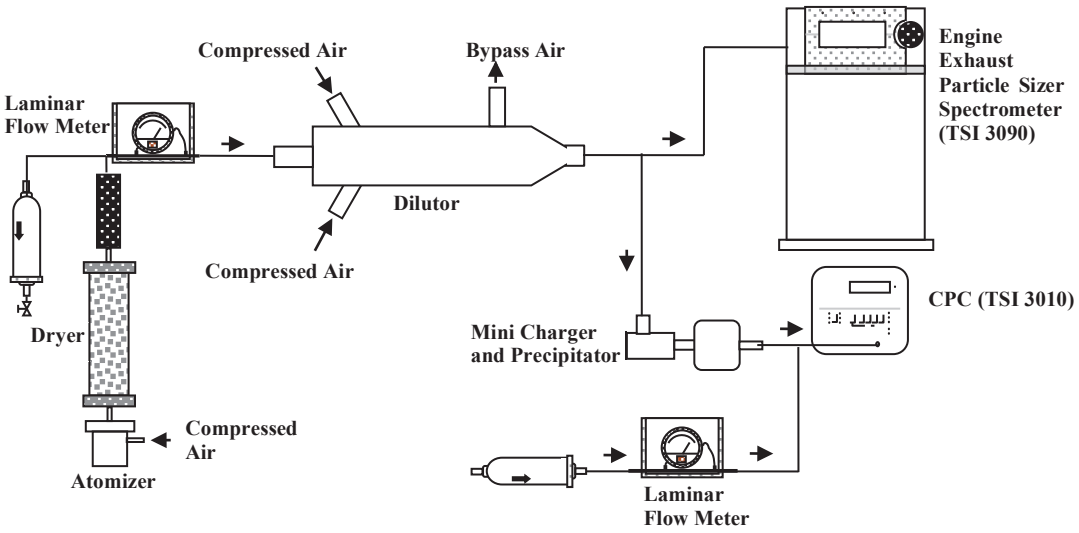

Figure 3-4. Experimental setup for evaluation of dynamic aerosol measurement

With the EEPS™ spectrometer providing the simultaneous reference measurement, the dynamically diluted aerosol stream was then measured by the EUPS system downstream, as shown in Figure 3-4.

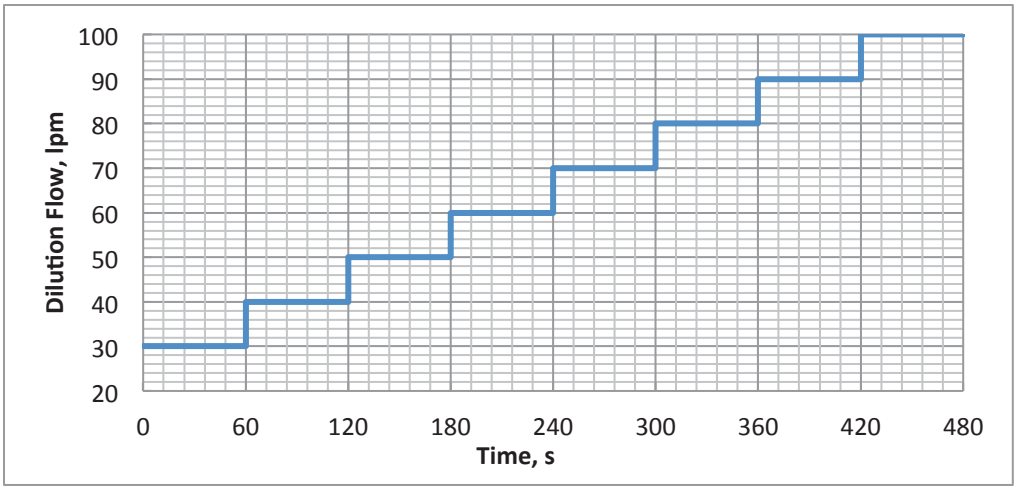

Figure 3-5. Dilution flow profile for the dynamic aerosol dilutor

As with the steady stream aerosol measurements, both size distribution measurement mode and time-variation identification mode were used for evaluating the unsteady aerosol size distribution measurement of the p-type EUPS.

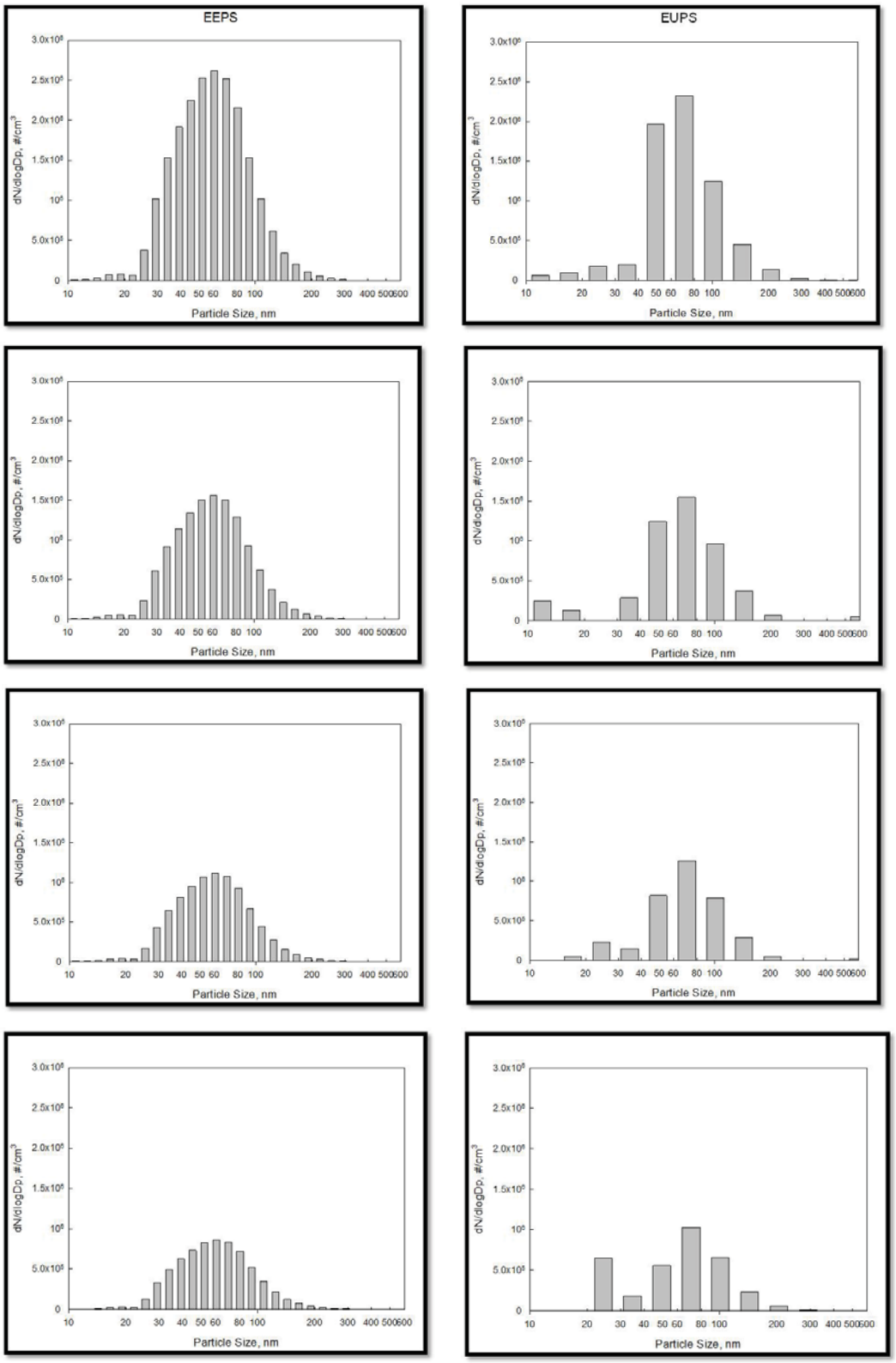

Figure 3-6. Comparison of dynamic aerosol measurements between EEPS (left) and EUPS

The size distribution measurement mode monitored the variation of the whole size distribution profile, with the EEPS™ as a reference. The comparative simultaneous size distribution measurement results are shown in Figure 3-6, in time increments of one minute.

The comparison clearly shows a simultaneous changing trend of the EUPS measurements with the referenced EEPS measurements. Meanwhile, very substantial agreements were also observed for the geometrical mean sizes, total number concentrations, and standard deviations in each paired set of size distribution profiles.

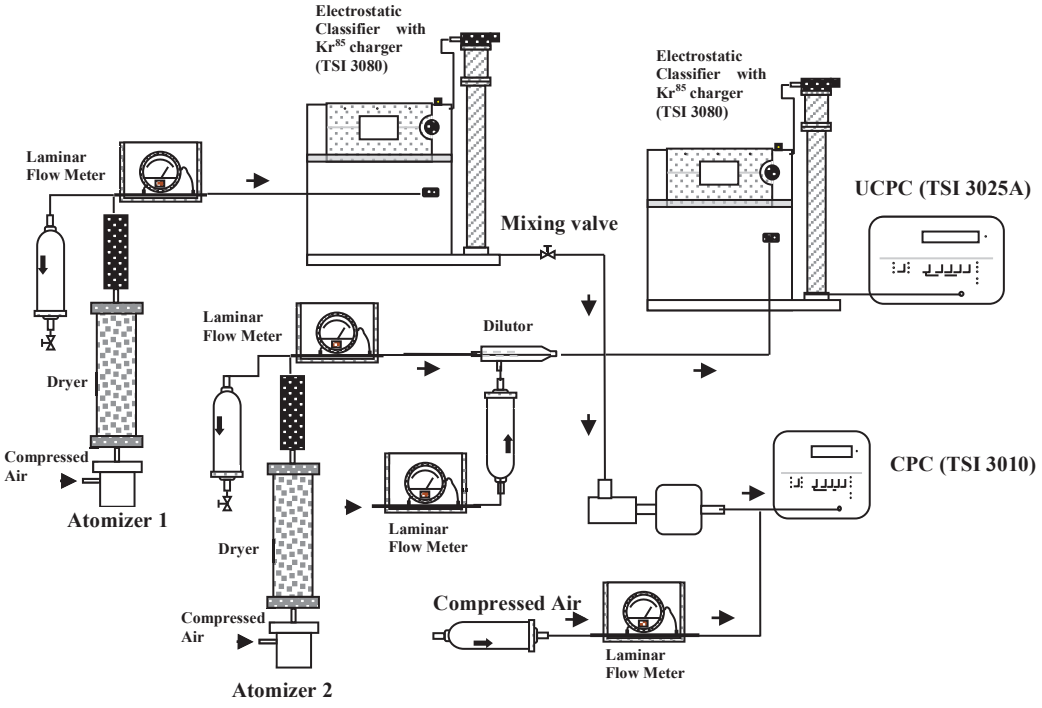

Figure 3-7. Experimental setup for verifying the dynamic identification mode

The other evaluation was of the dynamic identification feature realized by the least square data inversion scheme. Measurements were taken by simply switching the precipitator operation voltage between $V_1 = 0$ V and $V_2 = 50$ V. The experimental setup is shown in Figure 3-7. The time-variation for a specific size range was simulated by

introducing a stream of DMA classified aerosols into the original steady aerosol flow at a set time point. By comparing the variation profile of particle count readings at the two voltage steps with the identification Table 3-1, the size group of the intruding aerosols was then identified with a 3 s quick measurement. The results are shown in Figure 3-8. The p-type EUPS successfully identified the size group of the DMA classified aerosols introduced when opening the mixing valve.

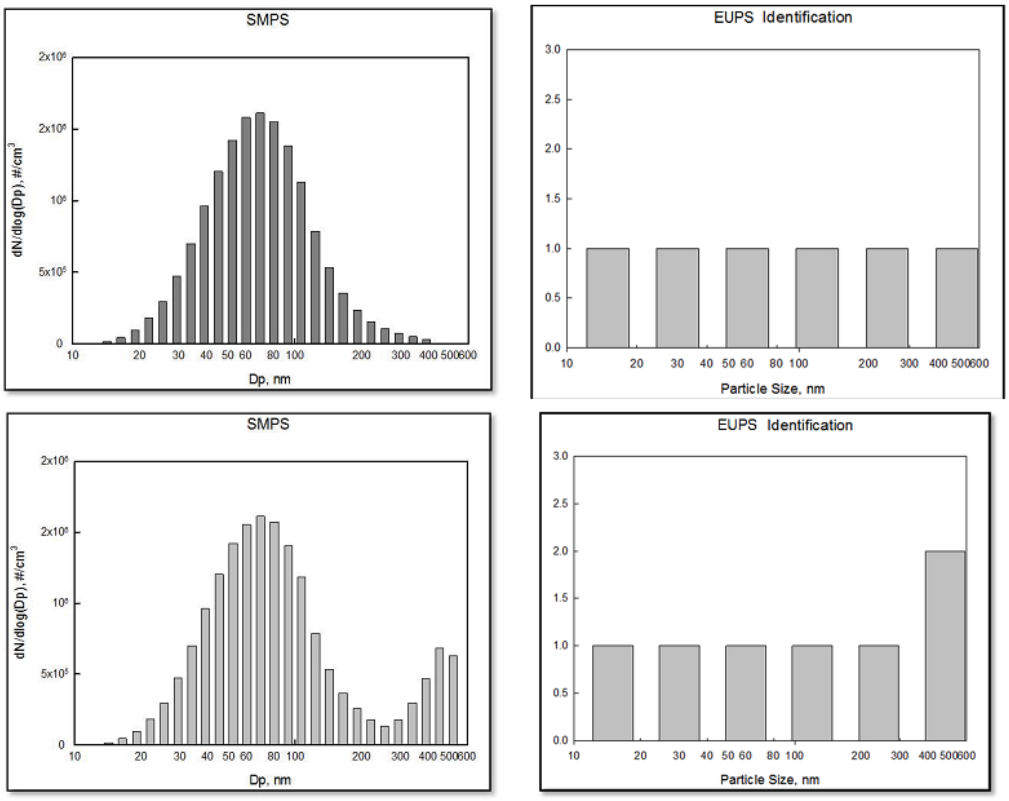

Figure 3-8. Evaluation of the dynamic identification mode measurement

The evaluation results of unsteady aerosol measurement demonstrated the dynamic measuring ability of the p-type EUPS for monitoring particle size distributions. The dynamic identification mode was also proved to be a fast and efficient way to identify the size range of an immediately intruding aerosol source into the working environment.

3.4. Field evaluation of the p-type EUPS performance

Beyond the laboratory evaluations, a field evaluation was also required to validate the measuring ability of the p-type EUPS, to comprehensively demonstrate its size distribution measuring reliability and flexibility, fast-response capability, and dynamic-identification functionality as a portable particle sizer. In the last part of the p-type EUPS evaluation, the system was taken out of the lab and set up to measure real outdoor aerosols. Both SMPS™ and EEPS™ measurements were taken simultaneously as references. The particle size distribution measurements were compared with the SMPS results to evaluate the measurement reliability and flexibility. The dynamic monitoring results were compared with the EEPS measurements to validate the fast-response capability and dynamic-identification functionality.

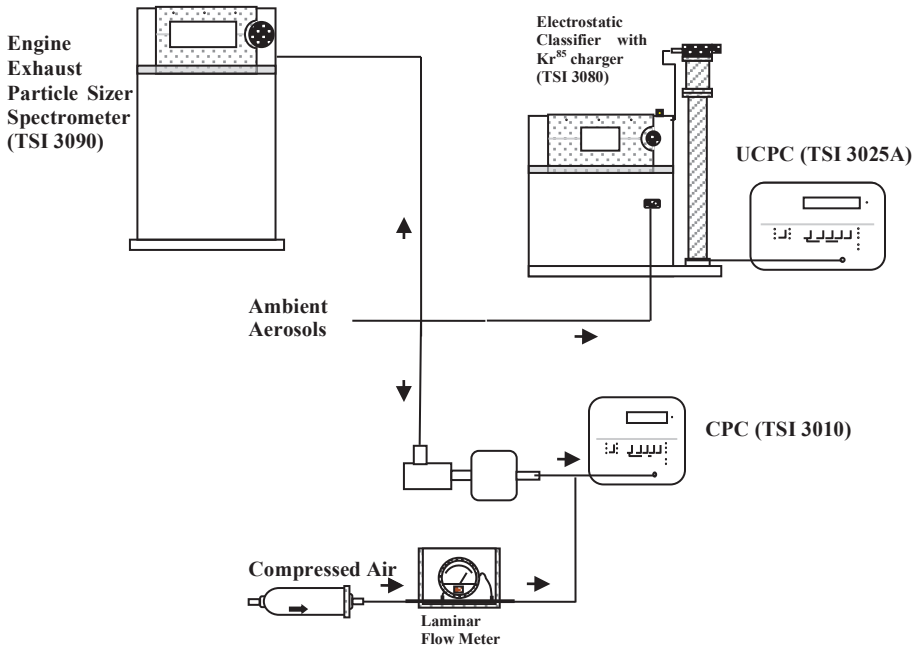

Figure 3-9. Experimental setup for field evaluation of ambient aerosol measurement

A simple field study was taken to measure the aerosol size distributions at the loading dock behind our department building, about 20 meters away from Forest Park Parkway, during moderate traffic at that time (10:00 am to 1:00 pm on a sunny August day). As references, both the SMPS™ and the EEPS™ were operated simultaneously with the p-type EUPS to measure the particle size distributions. The comparative size distribution measurement results are presented in Figure 3-10.

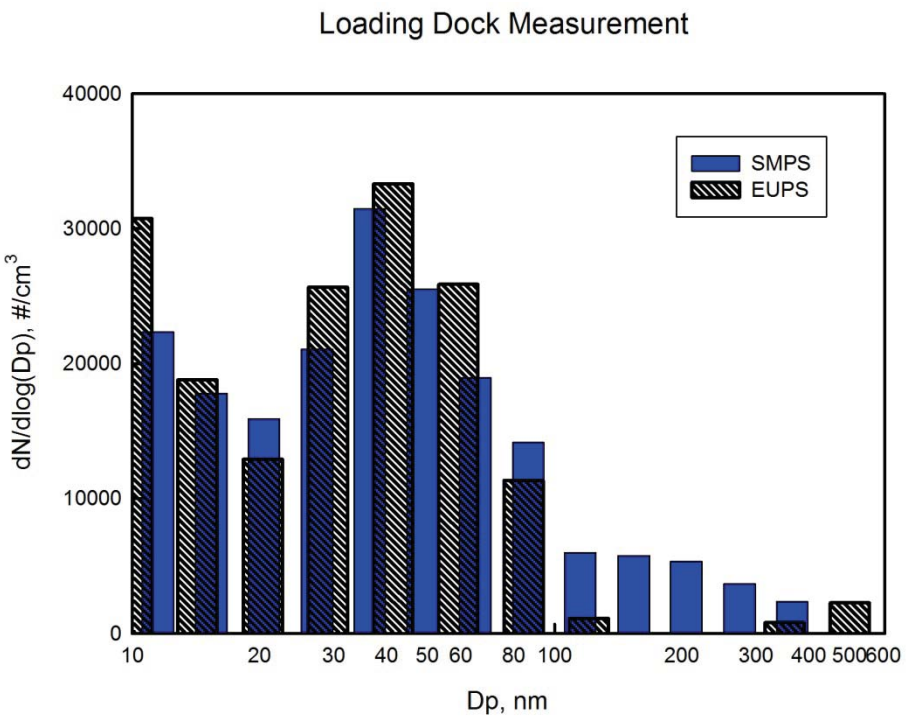

Figure 3-10. Comparative outdoor aerosol measurements

In addition to the particle size distribution measurement, the dynamic identification feature for time-varying aerosols was also verified by operating the voltage switching measurements during the unloading process of an Airgas® truck. Shown in Figure 3-11, the three sets of comparisons respectively represent three measuring conditions: (a) before the truck arrived, (b) when the truck arrived, and (c) after the truck shut down its engine. As demonstrated by the results, the handheld p-type EUPS well identified the

changes in particle size distribution caused by the unexpected foreign aerosols from the truck unloading process, and provided comparable time variation information to the measurement results from the 32 kg EEPS™ spectrometer.

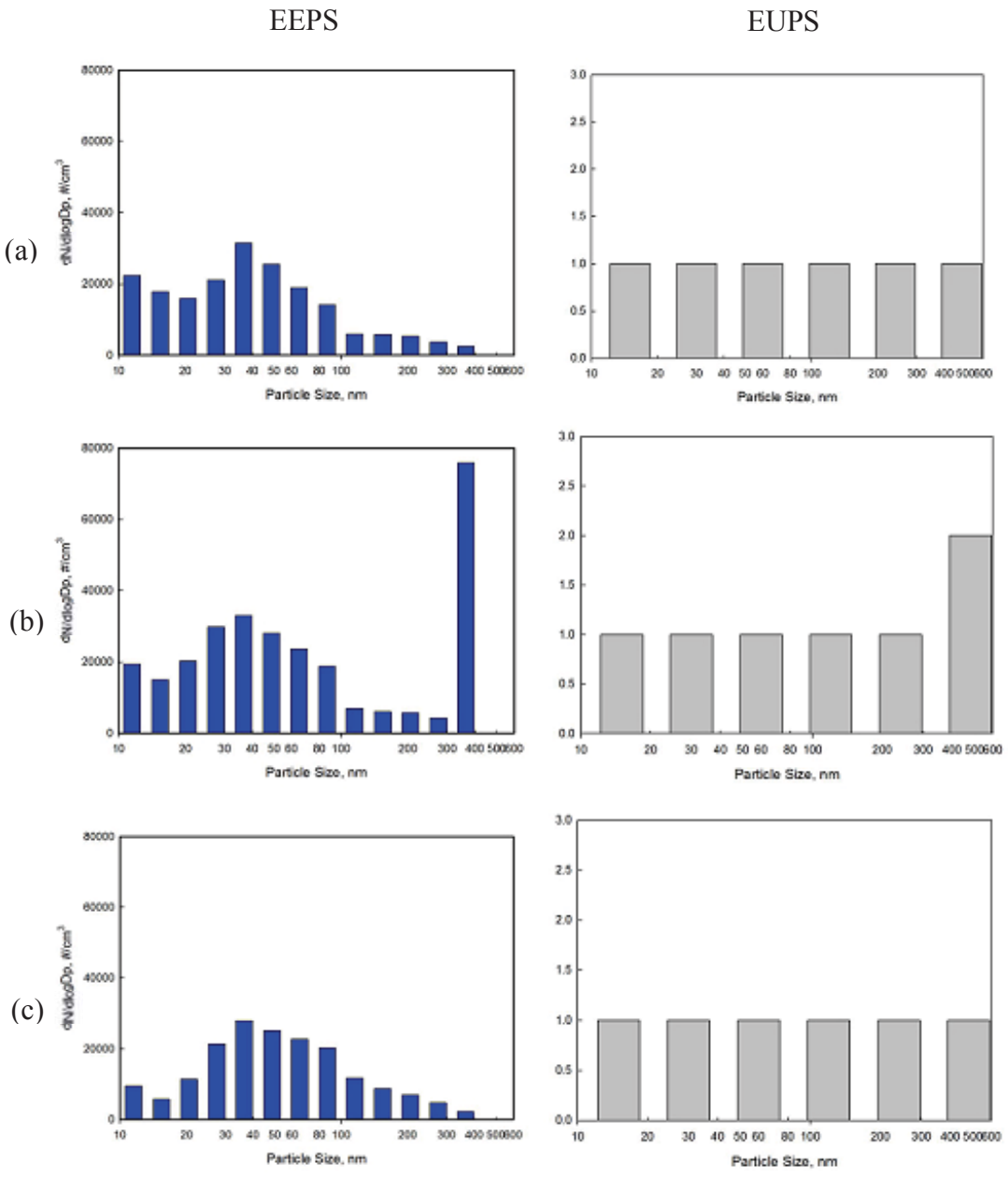

Figure 3-11. Field evaluation of dynamic identification mode

3.5. Conclusions

Based on the component calibration results reported in Chapter 2, a data inversion scheme was developed for deconvoluting particle size distribution from measured signals. To reduce the response time and calculation power, the scheme was established as a penetration matrix, which used the conditioned least square method instead of a presumed log-normal distribution method. As there was only one step of linear algebra calculation between getting the penetration data and outputting the size distribution profile, the inversion scheme enabled the fast-response measurement, taking 48 s for a whole size distribution. It also enabled a new function, as dynamic identification, which identified the time-variation of aerosol size distributions with a quick 3 s measurement.

For evaluating the measuring performance of the prototype unit, both laboratory and field tests were made. The promising results strongly verified the p-type EUPS measurement reliability and flexibility in size distribution measurements, fast response to size distribution changes, and the dynamic-identification functionality of the p-type EUPS.

3.6. References

1. Kousaka, Y., Okuyama, K., & Adachi, M. (1985) Determination of particle size distribution of ultra-fine aerosols using a differential mobility analyzer. *Aerosol Science and Technology* 4(2):209-225.

2. McMurry, P. H. (2000) A review of atmospheric aerosol measurements. *Atmospheric Environment* 34(12–14):1959-1999.

3. Kandlikar, M. & Ramachandran, G. (1999) Inverse methods for analysing aerosol spectrometer measurements: a critical review. *Journal of Aerosol Science* 30(4):413-437.

4. Twomey, S. (2002) *Introduction to the mathematics of inversion in remote sensing and indirect measurements* (Courier Dover Publications).

5. Crump, J. G. & Seinfeld, J. H. (1981) A new algorithm for inversion of aerosol size distribution data. *Aerosol Science and Technology* 1(1):15-34.

6. Gonda, I. (1984) Letter to the editor: on "inversion" of aerosol size distribution data. *Aerosol Science and Technology* 3(3):345-347.

7. Twomey, S. (1965) The application of numerical filtering to the solution of integral equations encountered in indirect sensing measurements. *Journal of the Franklin Institute* 279(2):95-109.

8. Rizzi, R., Guzzi, R., & Legnani, R. (1982) Aerosol size spectra from spectral extinction data: the use of a linear inversion method. *Applied Optics* 21(9):1578-1587.

9. Twomey, S. (1975) Comparison of constrained linear inversion and an iterative nonlinear algorithm applied to the indirect estimation of particle size distributions. *Journal of Computational Physics* 18(2):188-200.

10. Cooper, D. W. & Spielman, L. A. (1976) Data inversion using nonlinear programming with physical constraints: Aerosol size distribution measurement by impactors. *Atmospheric Environment (1967)* 10(9):723-729.

11. Voutilainen, A., Kolehmainen, V., & Kaipio, J. P. (2000) Statistical inversion of aerosol size distribution data. *Journal of Aerosol Science* 31, Supplement 1(0):767-768.

12. Ramachandran, G. & Kandlikar, M. (1996) Bayesian analysis for inversion of aerosol size distribution data. *Journal of Aerosol Science* 27(7):1099-1112.

13. Pandis, S. N., Baltensperger, U., Wolfenbarger, J. K., & Seinfeld, J. H. (1991) Inversion of aerosol data from the epiphaniometer. *Journal of Aerosol Science* 22(4):417-428.

14. Friedlander, S. K. (2000) *Smoke, dust, and haze* (Oxford University Press New York).

15. May, K. (1973) The Collison nebulizer: description, performance and application. *Journal of Aerosol Science* 4(3):235-243.

16. Liu, B. Y. & Lee, K. (1975) An aerosol generator of high stability. *The American Industrial Hygiene Association Journal* 36(12):861-865.

17. User manual: TSI (2010) Engine Exhaust Particle Sizer™ 3090.

Chapter 4 :A high efficiency, miniature unipolar charger for the electrical ultrafine particle sizer

4.1. Introduction

Aerosol chargers are important, because they are needed for particle collection by electrostatic precipitation, particle size characterization by electrical mobility classification, and many other applications in aerosol research [1]. The development of ultrafine aerosol chargers are greatly needed, by the increasing demand for aerosol chargers with high charging efficiency in ultrafine and submicron size range [2]. Recently, a variety of aerosol chargers have been developed and investigated as the essential component of an aerosol size distribution classifier. The most commonly used aerosol chargers are radioactive neutralizers, which utilize radioactive sources to ionize the gas molecules and then produce the particles charged in an equilibrium bipolar charge distribution within a sufficient residence time [3]. This bipolar charging technique has been shown to be effective in the measurement of submicron particles [4]. However, due to safety perceptions and other regulatory provisions, the radioactive material may not be suitable for personal monitoring or spatial distribution measurements [5]. Besides, it has also been reported that the bipolar chargers have poor effectiveness for nanometer aerosols [6]. For example, the Kr^{85} neutralizer implemented in the Scanning Mobility Particle Sizer (SMPS™) spectrometer (TSI Inc., Shoreview, MN) to charge particles for Differential Mobility Analyzer (DMA) classification, yields less than 1% particles charged for particle size at 3 nm [1, 7]. Therefore, the unipolar charging process, which can achieve higher charging efficiency without the recombination of ions with opposite polarity, is still the preferred choice for the design of the new miniaturized aerosol charger.

There are several approaches to conduct the unipolar charging process. The electrical separation of the bipolar ions, produced by radioactive material [1, 8], raises serious safety concerns. As alternatives, we can consider either the soft X-ray photo-ionization process, or choose corona discharge as used in the previous mini-charger design. Soft X-ray can also produce bipolar ions as radioactive materials [9], while avoiding the transportation regulations for radioactive materials. But the expense for soft X-ray sources makes them unsuitable for a low-cost personal instrument [10]. Besides the cost concerns, the material dependence of the photo-ionization charging performance [8] is also considered a drawback for ambient aerosol measurements. Therefore, the corona discharge process, which we have utilized for the first generation mini-charger, is still considered the most effective unipolar aerosol charging method for a personal charger.

For the design of a charger, where the particles get electrically charged, charging efficiency is the most critical priority. By evaluating the charging performance of the previous mini-charger, it was observed that we got only 80% as the highest extrinsic charging efficiency, reached by particles sized larger than 80 nm. In other words, only 80% of the particles entering the charger could ultimately be used for the following electrical mobility classification, and this ratio would be even less for particles smaller than 80 nm. Thus, improving the charging efficiency and reducing particle loss inside the charging chamber was the first objective for perfecting the charger design. Besides, during the experimental evaluation of the mini-charger, it was noticed that the corona tip could easily be contaminated by particles accidentally entering the corona tip chamber. It then required frequent tip cleaning to maintain stable charging performance. Therefore, to

make the new charger more reliable and longer-lasting, another objective was to solve the tip contamination problem in the new charger design.

4.2. Hardware design

Considering its applicability as a personal aerosol charging source, the corona-discharge unipolar charging mechanism was chosen again for designing a new miniature charger for the electrical ultrafine particle sizer (EUPS). To achieve a higher yield of charged particles, i.e., to charge the incoming particles at a higher charging efficiency, modifications and updates were made to both flow field and electric field configurations for designing the new unipolar charger. Although the flow field and electric field configurations vary greatly between different chargers, all the currently available unipolar charger designs can be classified into two groups according to the relative direction of the aerosol flow stream to the ion-driving electrical field [8]. The perpendicular configuration, the more common one, has the aerosol flow stream introduced into the charging zone perpendicularly to the electrical field, which was used in the first generation mini-charger design. The other type is categorized as the parallel configuration, this type of charger design has the aerosol flow direction parallel to the electric field, and was first developed by Adachi, Romay et al. [11]. The perpendicular flow chargers initially appeared to have a high intrinsic charging efficiency, which meant few neutral particles could exit from the charger. However, charged particles had difficulty exiting the charging zone too, and were mostly lost inside the charger, yielding a relatively low extrinsic charging efficiency for nanometer particles, and thus causing low efficiency and accuracy for the following electrical mobility classification process [12].

In the year of 1999, Chen and Pui presented a table to compare the construction characteristics and charging performance of different unipolar charger designs [8]. In this study, by adding the miniature corona-discharged unipolar charger designed for the first generation of EUPS, the comparison table was re-summarized and updated as Table 4-1.

Table 4-1. Comparison of different unipolar chargers

Investigators	Ion source	Sheath air	Aerosol/ion direction	Extrinsic charging efficiency
Liu and Pui, 1997 [13] Pui et al., 1988 [14]	Corona	YES	Perpendicular	1.3% at 6 nm (+)
Adachi et al., 1985 [1]	Am^{241}	YES	Perpendicular	58% at 15 nm (+)
Wiedensohler et al., 1994 [15]	Cm^{244}	YES	Perpendicular	7.5% at 7 nm (190 V)
Büscher and Schmidt-Ott, 1992 [16]	Corona	YES	Perpendicular	4% at 5 nm
Qi et al., 2008b [5]	Corona	NO	Perpendicular	35% at 20 nm (40 V)
Chen and Pui, 1998 [6]	Po^{210}	YES	Parallel	43% at 4 nm (+)
Adachi and Masuda, 1990 [17]	Po^{210}	NO	Parallel	51% at 10 nm (3kV)
Romay et al., 1991 [18]	Po^{210}	NO	Parallel	--

It can be noticed from the table that the parallel direction configuration has higher extrinsic charging efficiency than the perpendicular direction design. Thus, higher charging efficiency could be achieved for the new charger by designing it as a corona-discharge based parallel flow unipolar charger. In addition to the parallel flow configuration for the new charger design, the length of the aerosol flow pathway was shortened to decrease the residence time to minimize particle loss inside the charger. And

a subtle sheath flow was also introduced into the corona chamber to protect the corona tip from contamination by sampled particles.

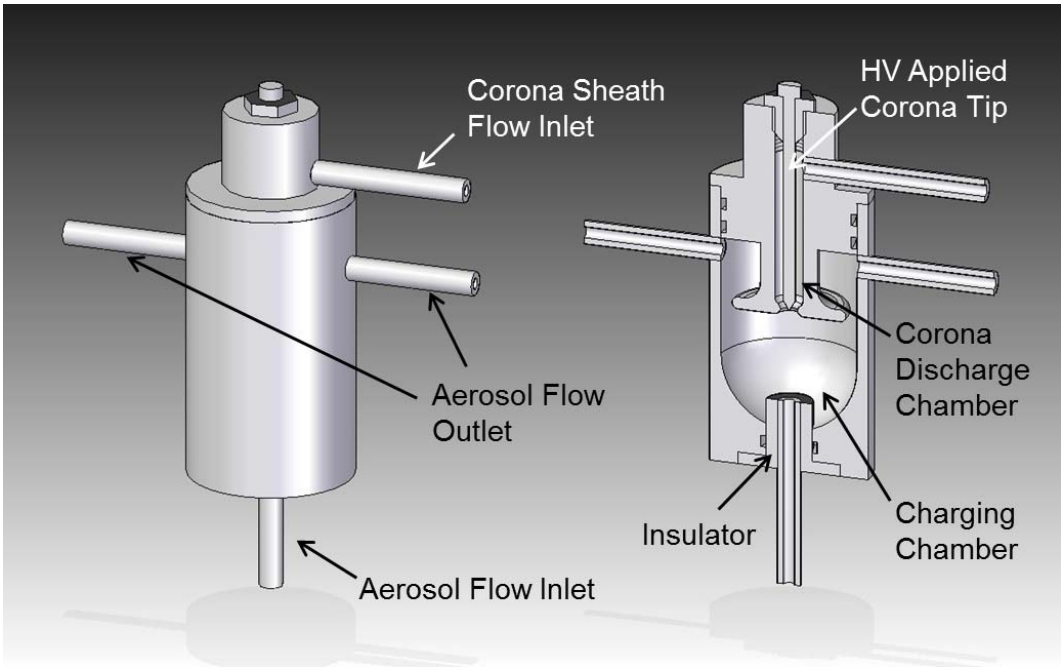

Figure 4-1. Schematic of the new miniaturized charger design

The prototype charger was constructed with a tubular brass case as the charging chamber, with a corona discharge chamber hermetically inserted within it. High voltage was applied on the tungsten tip to initiate the corona discharge process for generating high concentration of unipolar ions. A low ion-driving voltage was applied on the entire tubular brass case. A subtle air flow was introduced into the corona discharge chamber through the sheath flow inlet. The ions exiting from the corona discharge chamber then got mixed with the incoming sampled particles, which were introduced into the charging chamber through the aerosol flow inlet at the bottom, and in a parallel direction to the electrical field. The aerosol flow inlet was grounded and electrically insulated from the tubular case by a tubular delrin sleeve. The inner surface of the tubular case, or the

charging chamber, was filleted to reduce the inner volume, the particle residence time, and thus the particle loss inside the charger. This filleted structure also helped the charged particles quickly exit from the charging zone once they got electrically charged by the diffusing ions, and the charged particles then exited from the charger through the two aerosol flow outlets. The schematic of the new charger design is shown in Figure 4-1.

4.3. Numerical modeling of the charger performance

4.3.1. Flow and electrical field modeling

To verify the minimum particle loss effect of parallel flow design before the manufacture, a better understanding of both flow field and electrical field inside the miniature unipolar charger was required. Therefore, a numerical model was developed to investigate the flow field and electrical field inside the charger under different design geometries. The calculated flow field and electrical field characteristics were then used for predicting the particle moving trajectories in, and the particle penetrations through the charging chamber. By comparing the modeling results for different geometrical parameters, the miniature unipolar charger design was optimized and finalized for hardware construction.

To conduct the numerical modeling, a finite element algorithm of COMSOL Multiphisics® was utilized, which is a commercial software available for solving numerical models coupled by multiple physical phenomena. The model consisted of two parts, modeling both the flow field and electrical field.

The flow field was governed by the incompressible Navier-Stokes equation, along with the continuity equation as

$$\rho_f \left(\frac{\partial \overrightarrow{u_f}}{\partial t} + \overrightarrow{u_f} \cdot \nabla \overrightarrow{u_f}\right) = -\nabla p_f + \mu_f \nabla^2 \overrightarrow{u_f} + \overrightarrow{F_f}, \quad (4\text{-}1)$$

and

$$\frac{\partial \overrightarrow{u_f}}{\partial x} + \frac{\partial \overrightarrow{u_f}}{\partial y} = 0\ . \quad (4\text{-}2)$$

In the above two equations, ρ_f is the fluid density, $\overrightarrow{u_f}$ is the fluid velocity vector, p_f is the local pressure, μ_f is the fluid viscosity, and $\overrightarrow{F_f}$ is the body force per unit of volume. Three assumptions were made for using these governing equations: (1) the flow is axial-symmetric, incompressible, and in steady-state, (2) the fluid is isotropic and homogeneous, and (3) there is a uniform velocity profile by area at the flow inlet.

For the inlet boundary conditions, both the aerosol flow and sheath flow inlets were set with uniform velocity profiles. While at the outlet boundary, which was chosen as the pressure reference in the flow field modeling, the absolute pressure of one point on the boundary was set to zero. Non-slip wall boundary conditions were imposed on all other outside boundaries of the computational domain. The shape functions of the elements for this finite element computation were of the second order in velocity $\overrightarrow{u_f}$ and the first order in pressure p_f.

For the electrical field inside the miniature unipolar charger, Gauss' law for the electrical field was applied for governing the electrical flux,

$$\nabla \cdot \overrightarrow{D_e} = \rho_e, \quad (4\text{-}3)$$

where ρ_e is the free electrical charge density, and $\overrightarrow{D_e}$ is the electrical displacement field. In the condition of homogeneous, isotropic, non-dispersive, and linear materials, the electrical displacement field $\overrightarrow{D_e}$ was related to the electrical field $\overrightarrow{E_e}$ by:

$$\overrightarrow{D_e} = \varepsilon \overrightarrow{E_e}, \tag{4-4}$$

where ε is the electrical permittivity of the material.

Corresponding electrical potentials (ground or a certain electrical potential, depending on the applied voltage) were imposed on all solid walls, while for the flow inlets and outlets, boundary conditions were set to a zero free electrical density. In this part, the third order shape functions were used to describe the electrical displacement field.

As the whole charging chamber was axial-symmetric, a calculation in a two-dimensional half cutoff plane was enough for representing the whole three-dimensional cylindrical charging zone. Therefore, the calculation of electrical field distribution in the charging zone was taken in a half cutoff plane. The entire brass tubular case was set at a positive ion-driving voltage of 20 V, the corona chamber was electrically connected to the outer case, and the aerosol flow inlet was electrically grounded. With above electrical potential settings, the electrical field distribution result is shown in Figure 4-2. The electrical potential gradient was toward the aerosol flow inlet, which would help drive ions generated from the corona-discharge process toward that direction for a more efficient mixing of the ions with the incoming particles. Besides, the electrical potential gradient was also focused around a small region, which also avoided interfering with particle motions of the charged particles, and thus increased the particle penetration from the miniature unipolar charger.

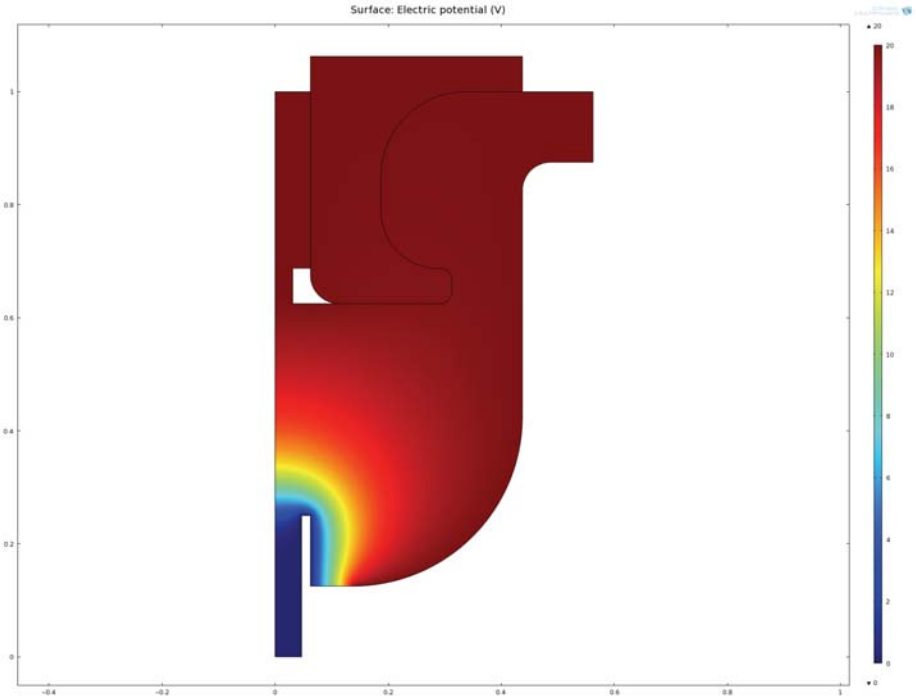

Figure 4-2. Electrical field in the charger, tubular case at 20 V, and aerosol flow inlet grounded.

The flow field was also modeled for the miniature unipolar charger in the same computational domain as the electrical field modeling. The inlet aerosol flowrate was set at 1.5 lpm, and a 0.3 lpm air flow was introduced into the corona chamber as the sheath flow. The calculation result is shown in Figure 4-3, 0.3 lpm sheath flow was high enough to prevent sampled particles entering the corona chamber and contaminating the corona tip. Meanwhile, the 0.3 lpm sheath flow was not overly strong to push back the incoming particles away from the ions emitted from the corona-discharge process of the tungsten tip. After the mixing of the aerosol stream and ion stream, most of the mixed flow exited through the aerosol flow outlet on the right side, while a small fraction of the flow was trapped in the chamber by flow recirculation.

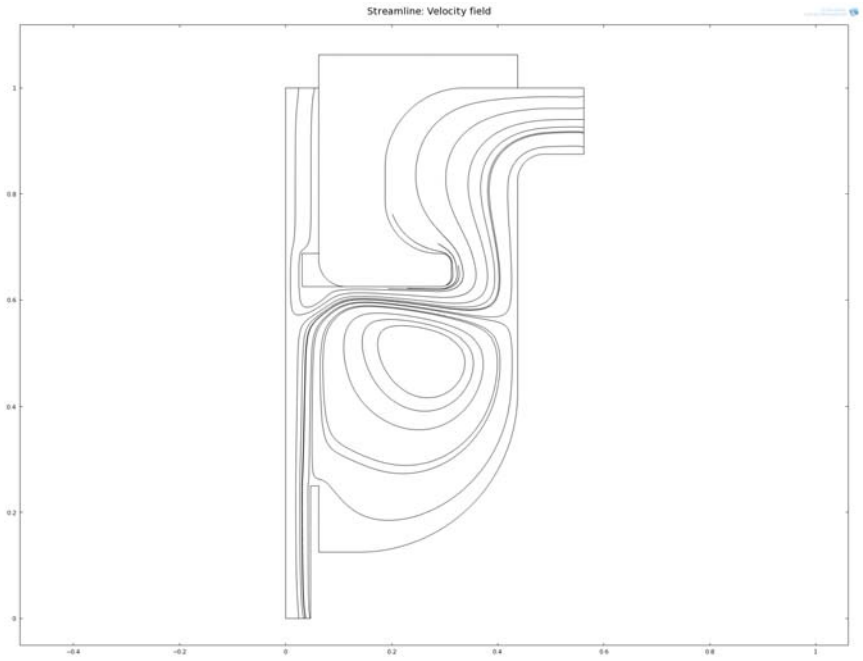

Figure 4-3. Flow field in the charger, aerosol flow at 1.5 lpm, corona sheath flow at 0.3 lpm

4.3.2. Modeling of particle penetration through the charger

It was important to investigate how much the recirculation would affect charged particle penetration through the charger. Therefore, in addition to the previous two calculations of the flow field and electrical field modeling, particle deposition inside and particle penetration through the miniature unipolar charger were also modeled. For this particle motion modeling, computation results of the flow field and electrical field were required. With the flow and electrical field modeling results imported into the Matlab software via a compatible syntax, particle motions were then computed and modeled by solving the Langevin equation of particle translation:

$$m_p \frac{\partial \vec{u}_p}{\partial t} = \vec{F} = \vec{F}_d + \vec{F}_e + \vec{F}_b, \tag{4-5}$$

where m_p and $\vec{u}_p$ are the particle mass and translation velocity vector. $\vec{F}_d$, $\vec{F}_e$, and $\vec{F}_b$ are drag force, electrical force, and Brownian force, respectively. Gravity, shear-induced lifting force, and other forces were negligible in this modeling.

According to Friedlander, the drag force acting on a spherical particle can be expressed as

$$F_d = \frac{C_D \frac{\pi}{8} \rho_g {d_p}^2 U^2}{C_C} \text{ , [19]} \tag{4-6}$$

in which ρ_g is the density of the fluid, d_p is the particle size, U is the relative velocity between fluid and particle, and C_D is the drag coefficient, which can be expressed as

$$C_D = \frac{24}{Re}(1 + 0.15Re^{0.687}) \text{ , [19]} \tag{4-7}$$

with Re known as the particle Reynolds number. C_C is the Cunningham correction factor [20] and can be estimated as

$$C_c = 1 + \frac{\lambda}{d}\left[2.34 + 1.05 \exp\left(-0.39\frac{d}{\lambda}\right)\right], \tag{4-8}$$

where λ is the mean free path of the air at room temperature and ambient pressure.

The electrical force acting on the particles is

$$\overrightarrow{F_e} = ne\overrightarrow{E_e}, \tag{4-9}$$

where $\overrightarrow{E_e}$ is the electrical field obtained from COMSOL Multiphysics® calculation, e is the elementary charge, and n is the number of elementary charges on a charged particle.

The Brownian force, which indicates the particle diffusion effect, was ignored for simplification in this numerical modeling.

Four particle sizes were used for the particle trajectory modeling, including 10, 50, 100, and 200 nm. All particles were singly positively charged, and released near the inner wall of the aerosol flow inlet as the worst scenario for charged particle deposition in the charger chamber.

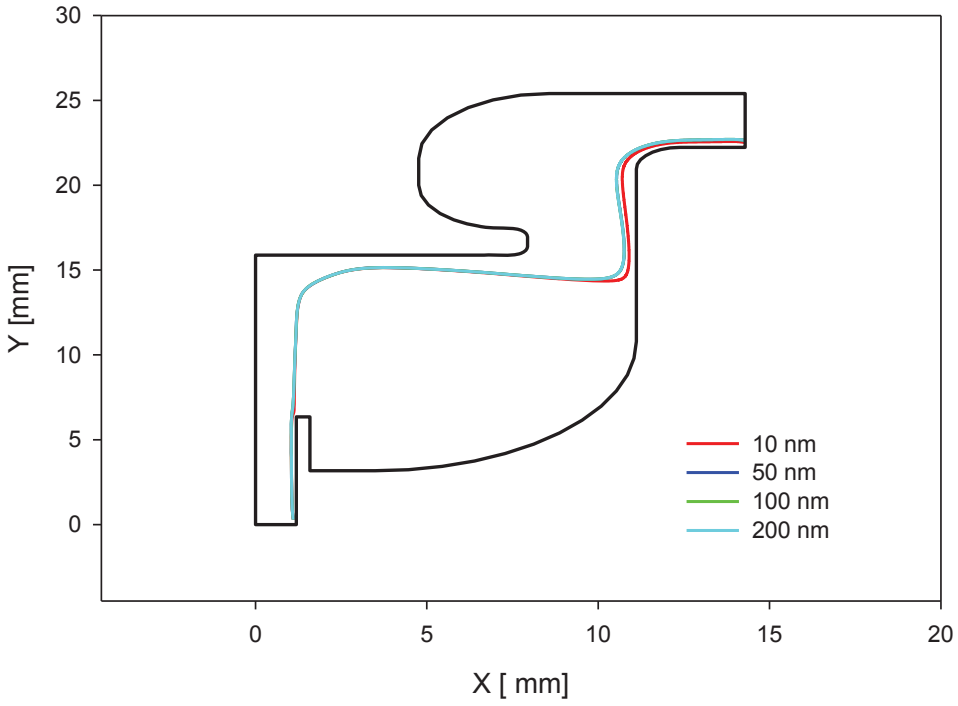

Figure 4-4. Particle trajectory modeling results for the miniature unipolar charger

Particle trajectory modeling results were plotted with the aerosol flow domain as reference, as shown in Figure 4-4. Origin of the plane-coordinate system was set at the center of the bottom plane of the aerosol flow inlet (particle releasing plane), X and Y were the coordinates of computational node in x and y axis respectively. The results indicated that there was no particle deposition loss inside the charging chamber for particles at the four modeled sizes, all particles safely penetrated through the charging zone and exited the charger, for following electrical mobility classification.

4.4. Experimental evaluation of the unipolar charger

Similar to the previous mini-charger evaluations, three charging performance parameters were evaluated for the new miniature unipolar charger, including two charging efficiencies, as extrinsic charging efficiency and intrinsic charging efficiency, and the average number of elementary charges on charged particles.

The extrinsic charging efficiency η_{ex} represents the charged particle fraction in the total particle stream exited from the unipolar charger. Similar to the one previously mentioned in Chapter 2, η_{ex} was defined as

$$\eta_{ex} = \frac{(N_3 - N_1)\cdot Q_t}{N_4 \cdot Q_{in}}, \tag{4-10}$$

where N_1 is the number concentration of neutral particles measured downstream of the working charger. N_3 is the number concentration of all particles exiting the charger, N_4 is the total number concentration of particles entering the charger, Q_t is the total flowrate exiting from the charger, and Q_{in} is the aerosol flowrate entering the charging chamber.

The neutral particle number concentration N_1 was measured by filtering all charged particles using an electrostatic particle precipitator (charged particle remover). Because neutral particles might also deposit inside the precipitator, N_1 was calculated as

$$N_1 = \frac{N_1'}{P_{cpr}}, \tag{4-11}$$

in which N_1' is the number concentration measured after the charged particle remover, P_{cpr} is the penetration of neutral particles through the charged particle remover as a function of particle size, and was evaluated separately for the charged particle remover before the charger's performance evaluation.

While the measurement of extrinsic charging efficiency counted only the charged fraction of particles exiting the charger (i.e., charged particles did not penetrate the charger chamber were not counted into the charging efficiency), intrinsic charging efficiency had a totally different treatment of the charged particle loss during charging and transportation processes. It measured only the neutral particles exiting the charged particle remover downstream of the charger, thus all the particles lost before the exit were counted into the charging efficiency. The charged fraction, i.e., the intrinsic charging efficiency η_{in} was obtained by subtracting the neutral fraction of particles exiting the second particle remover, as defined by Adachi, Romay et al. [11]:

$$\eta_{in} = 1 - \frac{N_1}{N_2}. \tag{4-12}$$

In the equation, N_1 is the number concentration of neutral particles, same as those that appeared in the extrinsic charging efficiency measurement. N_2 is neutral particle penetration through the charger-remover system, which was measured similarly to N_1, but with the voltages for the corona discharge module and the second charged particle remover turned off.

Besides the number concentration measurement route, there was a second flow route with a Faraday cage and an electrometer installed, for measuring the current carried by the charged particles. The measured current could then be used along with the particle number concentration of the aerosol flow for calculating the average number of elementary charges on the charged particles, using the equation

$$n = \frac{I}{V_a \cdot C \cdot e}. \tag{4-13}$$

Here n is the average number of charges, I is the current captured by the Faraday cage and measured by the electrometer, V_a is the total volume of air passing through the Faraday cage during the current sampling time, C is the concentration measured by Ultrafine Condensation Particle Counter (UCPC, model 3025A, TSI Inc., Shoreview, MN), and e is the elementary charge as 1.6×10^{-19} C.

For all the experimental evaluations of the miniature unipolar charger, the aerosol flowrate going into the charger was kept exactly at 1.5 lpm, the sheath flowrate through the corona chamber was 0.3 lpm, and therefore the flowrate at the aerosol flow outlet was 1.8 lpm.

4.4.1. Experimental Setup for miniature unipolar charger evaluation

With high voltage applied, the miniature unipolar charger was maintained at a stable working current of 2.0 μA. With the grounding voltage applied to the outer case, we calibrated the charger's performance as a function of the charged particle size. The test aerosols were monodisperse NaCl particles selected by a Differential Mobility Analyzer (DMA, Model 3081 and 3085, TSI Inc., Shoreview, MN) with sizes ranging from 20 nm to 500 nm (the lower size limit of 20 nm was determined by the detection limit of the P-Trak particle counter). Figure 4-5 is a schematic diagram of the experimental setup used for monodisperse particle generation.

Similar to the generation system introduced in Chapter 2, two different systems were used for generating polydisperse sodium chloride particles for the miniature unipolar charger evaluation. For particles with mean diameters smaller than 50 nm, a furnace was used for generating particles via the evaporation-condensation process described by

Hussin [21]. A combustion boat loaded with test particle material, sodium chloride powder for our experiment, was placed in a ceramic tube passing through a tube furnace. When the furnace was heated to the required high temperature, the sodium chloride powder evaporated to form a rich vapor in the ceramic tube. A stream of inert gas passed through the furnace tube, carrying the vapor-rich stream to the dilutor, where the hot vapor-rich stream was quenched by another stream of particle-free inert gas at room temperature. Polydisperse nanoparticles were then formed during this quenching process, and sent to the Nano-Differential Mobility Analyzer (Nano-DMA, model 3085, TSI Inc., Shoreview, MN) system downstream, where they were classified and the monodisperse nanoparticles needed for the following evaluation experiment were obtained.

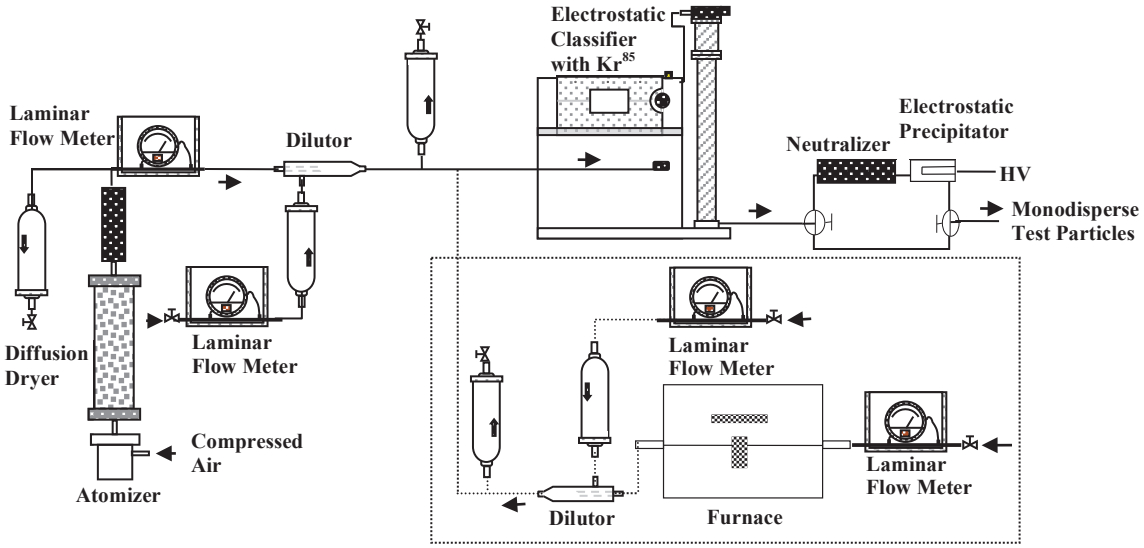

Figure 4-5. Experimental setup for the particle generation and particle size characterization

For larger polydisperse particles, with mean diameters ranging from 50 to 500 nm, the generator system was a homemade Collison mechanical atomizer, which is a widely used generator for obtaining a steady stream of laboratory-generated polydisperse

aerosols. The Collison atomizer normally consists of a jar for the spray solution, a spray nozzle, and a baffle for impacting the droplets [22]. By pumping a steady stream of compressed air through the spray nozzle, the spray solution is atomized to small droplets, and then partly dried to form a unimodal polydisperse aerosol stream [23]. The droplets were then thoroughly dried by the two diffusion dryers filled with silicon desiccant and connected in series. The final yield was dry polydisperse sodium chloride particles at the outlet of the second diffusion dryer. Downstream, a standard DMA (model 3081, TSI Inc., Shoreview, MN) classified the monodisperse particles with diameters larger than 50 nm. Since DMA classification is based on particle electrical mobility, all the classified monodisperse particles exiting from the DMA systems were electrically charged. To get the monodisperse neutral particles needed for the charger evaluation experiment, both a Po^{210} neutralizer and a high voltage applied charged particle remover were used downstream of the DMAs. To get monodisperse singly charged particles for the penetration measurement, there was also an optional bypass flow route parallel to the charge-removing route.

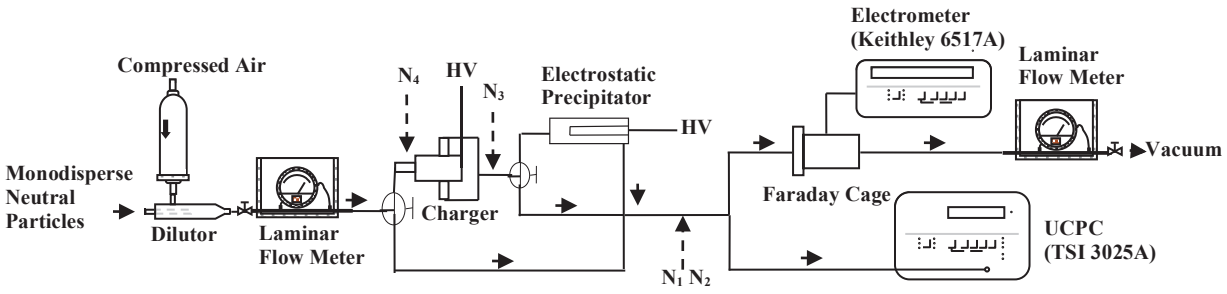

Figure 4-6. Experimental setup for the miniature unipolar charger calibration

Using monodisperse neutral test particles, we calibrated the mini-charger for extrinsic charging efficiency, intrinsic charging efficiency, and average charge of the

charged particles, using the experimental setup shown in Figure 4-6. To conduct the charging efficiency measurement, another electrostatic precipitator was added downstream of the mini-charger, removing the charged fraction of particles from the passing aerosol flow, with only neutral particles surviving. As before, the second charged particle remover could also be bypassed to get the number concentration of all the particles, charged and neutral, exiting from the mini-charger. The UCPC (model 3025A, TSI Inc., Shoreview, MN) was then used to measure all the particle number concentrations needed to investigate the neutral or charged fractions in the aerosol flow passing through the mini-charger.

4.4.2. Calibration results of the miniature unipolar charger

With monodisperse test particles from 10 to 500 nm, the charger was calibrated under the optimized operation settings for intrinsic charging efficiency, extrinsic charging efficiency, and average number of elementary charges per charged particles. All the three calibration results were shown in comparison of the previous mini-charger calibration.

For both charging efficiency evaluations, the results were similar to the previous mini-charger evaluations, an "exponential growth to a maximum" trend with particle size was observed in both intrinsic and extrinsic charging efficiencies respectively, as shown in Figure 4-8 and Figure 4-8. The intrinsic charging efficiency started from 75% for particle size of 10 nm, 91% at 20 nm, and increased to 100% for particle sizes larger than 40 nm. As compared to the previous mini-charger, which had the intrinsic charging efficiency of 82% at 20 nm and reached the 100% intrinsic charging efficiency for particle sizes larger than 60 nm, the new miniature unipolar charger made obvious improvement. This improvement in intrinsic charging efficiency indicated that, with the

aerosol flow introduced in the counter direction of the ion flow in the new charger design, both the mixing efficiency and ion attachment effectiveness were increased as compared to the previous perpendicular mixing profile. With the higher ion-particle collision efficiency, more particles were charged in the charging chamber, thus fewer neutral particles were detected downstream of the charger.

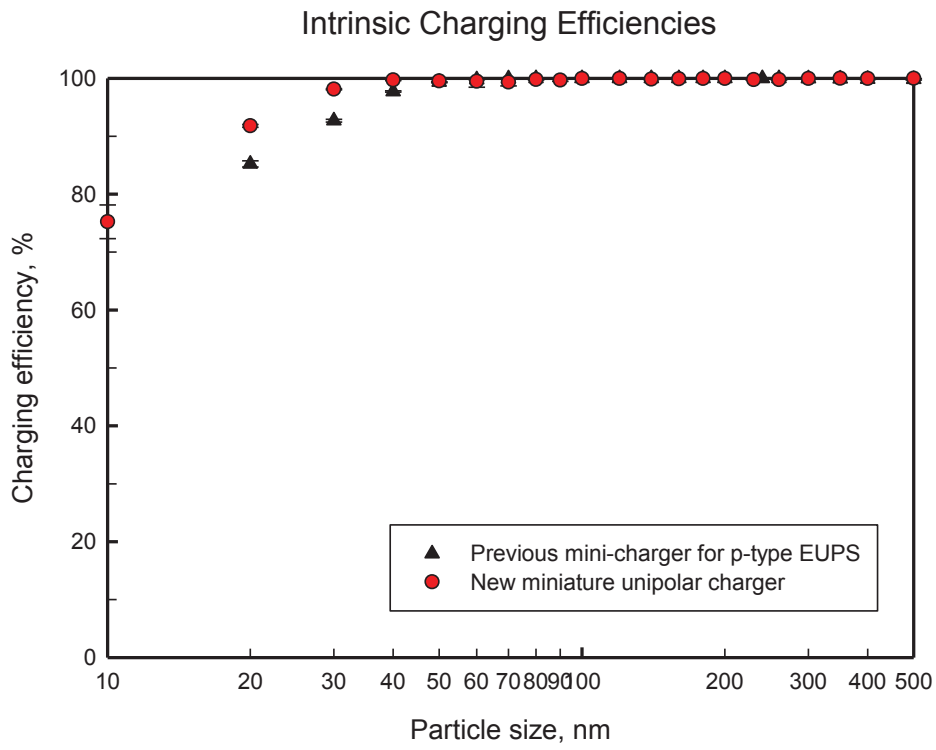

Figure 4-7. Intrinsic charging efficiency of the new miniature unipolar charger, compared with the previous mini-charger

Another obvious increase was also observed in the extrinsic charging efficiency results. Starting from the efficiency of 22% at particle size of 10 nm, the extrinsic charging efficiency later approached 100% when particle sizes exceeded 100 nm. As compared to the 43% extrinsic charging efficiency at 20 nm of the previous mini-charger for the p-type EUPS, the new miniature unipolar charger had an efficiency of 55% for the same particle size, as shown in Figure 4-8. The significant improvement in extrinsic

charging efficiency indicated that not only the charging efficiency was improved by the parallel flow direction, but the particle loss inside the charging chamber was also effectively reduced due to the flow field design. The filleted curvature decreased the residence time of charged particles in the charging zone, and the narrow opening (the circular slit) between the charging zone and the aerosol flow outlet also helped charged particles quickly leave the charging zone and then exit through the outlet.

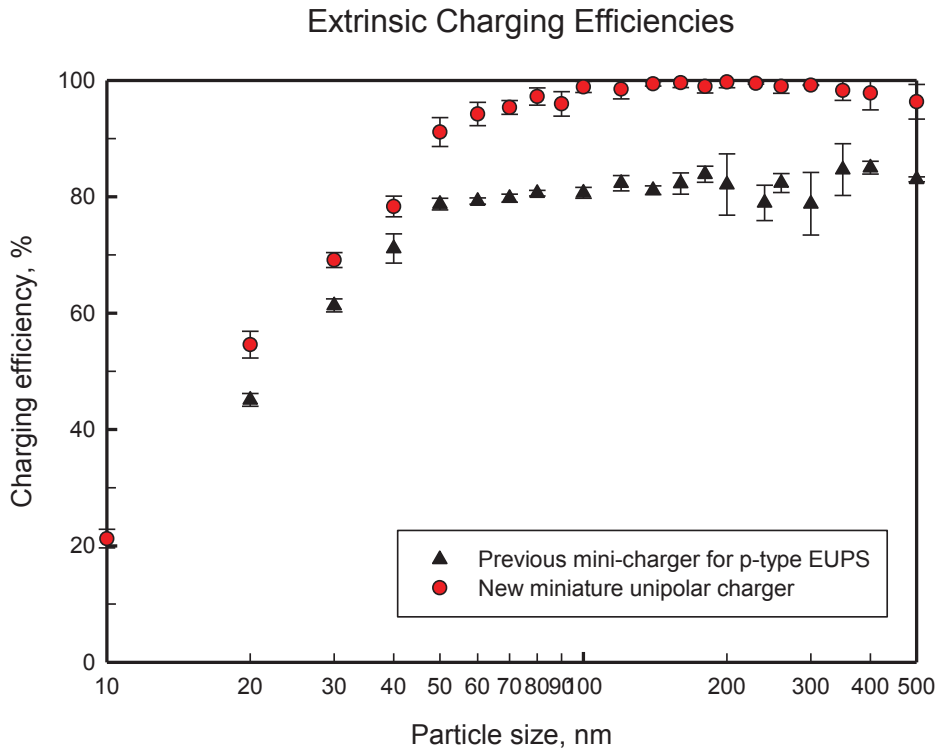

Figure 4-8. Extrinsic charging efficiency of the new miniature unipolar charger, compared with the previous mini-charger

Because of the significant increase in ion-particle mixing and collision efficiency, the average number of elementary charges per charged particle was also increased, which was no surprise. Similar to the average charge results of the previous mini-charger, the average number of elementary charges per charged particle also had an approximately linear relationship with particle size in the new miniature unipolar charger evaluation, as

shown in Figure 4-9. The minimum value was one elementary charge per particle, because the averaging was applied for charged particles only, and the elementary charge is undividable. With particle size increasing, the average number of charges increased and reached 65 as the highest value in the evaluated size range, for 500 nm particles. Although the new miniature unipolar charger charged particles with higher average charges, it had a more stable charging performance as compared to the previous mini-charger, especially for the larger particle sizes.

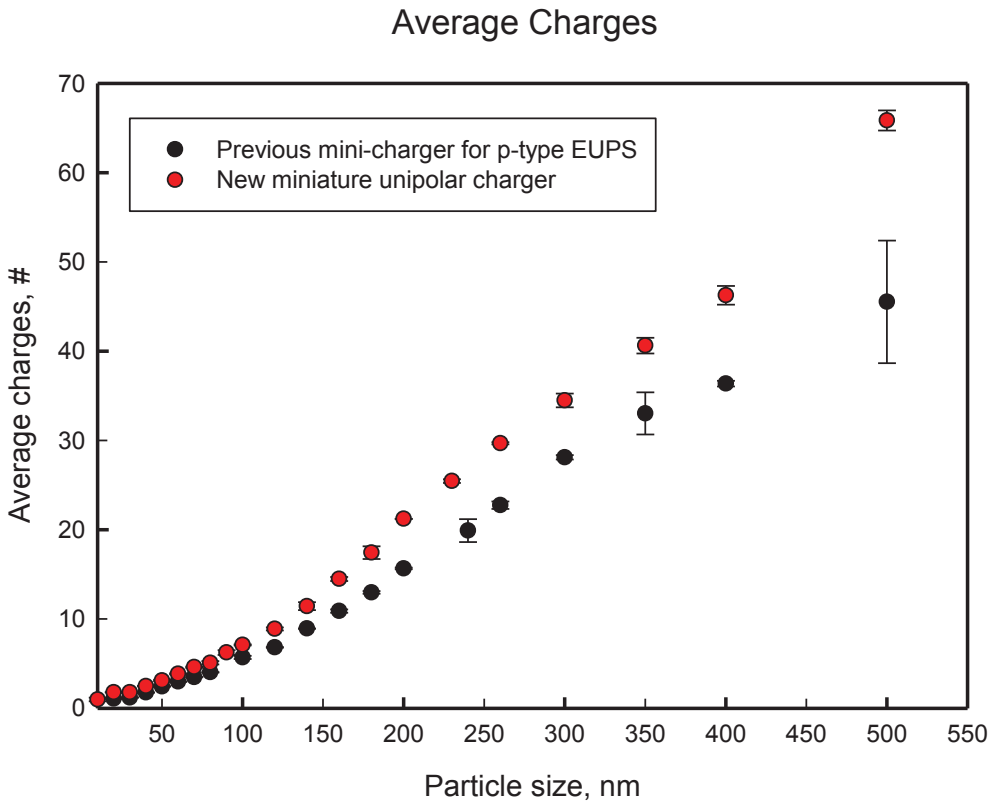

Figure 4-9. Average number of elementary charges per charged particle for the new miniature unipolar charger, compared with the previous mini-charger

4.5. Conclusions

In this study, a corona-discharge based, miniature unipolar aerosol charger was developed and evaluated. The prototype miniature unipolar charger was a parallel ion-aerosol flow design, with 50 mm in length and 22 mm in diameter, and the construction of the prototype consisted of two major components. The bigger part, as the charging chamber, was a brass tubular case with one axial tube as the aerosol flow inlet at the bottom, and two radial tubes as aerosol flow outlets at its shoulder. The smaller part, with a cylindrical corona discharge chamber in the center, was inserted into the charging chamber to seal the charging zone, and it also included a radial tube as the inlet for a corona tip sheath flow.

For operating the miniature unipolar charger, a pointed tungsten needle electrode was inserted into the corona-discharge chamber and was electrically insulated from the brass case, and a 0.3 lpm sheath flow was introduced into the corona discharge chamber via the sheath flow inlet tube. With high voltage supplied and the outer case grounded, corona discharge was initiated, and the incoming aerosols toward the ion outlet were electrically charged.

Calibrations based on three parameters were performed to evaluate the charging performance of the prototype miniature unipolar charger. The three parameters included extrinsic charging efficiency, intrinsic charging efficiency, and average number of elementary charges per charged particle. As shown in the results, significant improvements were observed in both intrinsic and extrinsic charging efficiencies, resulting from the higher ion attachment efficiency and lower particle loss inside the

charger. As for 20 nm particles, an 8% increase in intrinsic charging efficiency and an 11% increase in extrinsic charging efficiency were both achieved with the new miniature unipolar charger design. As for average charge measurement, more charges were obtained by each charged particle according to the results, but more stable charging performance was observed for the new design, especially for larger particle sizes. This stable and repeatable performance promises to be an indispensable basis, for ensuring the reproducibility of the data inversion scheme in the following electrical mobility classification procedure.

The compact size and largely improved charging performance made the prototype miniature unipolar charger an ideal substitute for the previous mini-charger in the p-type EUPS design, and a good candidate for the future EUPS development. In addition to being an improved charger design for the EUPS development, for its low particle loss characteristic, the flow pattern and hardware configuration of this prototype miniature unipolar charger also offer many other potential applications.

4.6. References

1. Adachi, M., Kousaka, Y., & Okuyama, K. (1985) Unipolar and bipolar diffusion charging of ultrafine aerosol particles. *Journal of Aerosol Science* 16(2):109-123.

2. Alguacil, F. J. & Alonso, M. (2006) Multiple charging of ultrafine particles in a corona charger. *Journal of Aerosol Science* 37(7):875-884.

3. Fuchs, N. A. (1963) On the stationary charge distribution on aerosol particles in a bipolar ionic atmosphere. *Pure and Applied Geophysics* 56(1):185-193.

4. Wang, S. C. & Flagan, R. C. (1990) Scanning electrical mobility spectrometer. *Aerosol Science and Technology* 13(2):230-240.

5. Qi, C., Chen, D.-R., & Greenberg, P. (2008) Performance study of a unipolar aerosol mini-charger for a personal nanoparticle sizer. *Journal of Aerosol Science* 39(5):450-459.

6. Chen, D.-R. & Pui, D. Y. H. (1998) A novel charger for nanometer aerosols. *Journal of Aerosol Science* 29, Supplement 2(0):S1023-S1024.

7. Reischl, G. P., Mäkelä, J. M., Karch, R., & Necid, J. (1996) Bipolar charging of ultrafine particles in the size range below 10 nm. *Journal of Aerosol Science* 27(6):931-949.

8. Chen, D.-R. & Pui, D. Y. H. (1999) A high efficiency, high throughput unipolar aerosol charger for nanoparticles. *Journal of Nanoparticle Research* 1(1):115-126.

9. Han, B., Shimada, M., Choi, M., & Okuyama, K. (2003) Unipolar charging of nanosized aerosol particles using soft X-ray photoionization. *Aerosol Science and Technology* 37(4):330-341.

10. Li, L. & Chen, D.-R. (2011) Performance study of a DC-corona-based particle charger for charge conditioning. *Journal of Aerosol Science* 42(2):87-99.

11. Adachi, M., Romay, F. J., & Pui, D. Y. H. (1992) High-efficiency unipolar aerosol charger using a radioactive alpha source. *Journal of Aerosol Science* 23(2):123-137.

12. Büscher, P. & Schmidt-Ott, A. (1990) A new concept for a unipolar diffusion charger. *Journal of Aerosol Science* 21, Supplement 1(0):S567-S570.

13. Liu, B. Y. H. & Pui, D. Y. H. (1977) Unipolar diffusion charging of aerosols in the continuum regime. *Journal Name: J. Colloid Interface Sci.; (United States); Journal Volume: 58:1*:Medium: X; Size: Pages: 142-149.

14. Pui, D. Y. H., Fruin, S., & McMurry, P. H. (1988) Unipolar diffusion charging of ultrafine Aerosols. *Aerosol Science and Technology* 8(2):173-187.

15. Wiedensohler, A.*, et al.* (1994) A novel unipolar charger for ultrafine aerosol particles with minimal particle losses. *Journal of Aerosol Science* 25(4):639-649.

16. Büscher, P. & Schmidt-Ott, A. (1992) A new compact aerosol charger for unipolar field-diffusion charging. *Journal of Aerosol Science* 23, Supplement 1(0):385-388.

17. Adachi, M. & Masuda, S. (1990) *Aerosols: Science, Industry, Health and Environment* p 439.

18. Romay, F. J., Pui, D. Y. H., & Adachi, M. (1991) Unipolar diffusion charging of aerosol particles at low pressure. *Aerosol Science and Technology* 15(1):60-68.

19. Friedlander, S. K. (2000) *Smoke, dust, and haze* (Oxford University Press New York).

20. Hinds, W. C. (1999) *Aerosol technology: properties, behavior, and measurment of airborne paticles* (Wiley) 2nd edition Ed.

21. Hussin, A., Scheibel, H. G., Becker, K. H., & Porstendörfer, J. (1983) Bipolar diffusion charging of aerosol particles—I: experimental results within the diameter range 4–30 nm. *Journal of Aerosol Science* 14(5):671-677.

22. May, K. (1973) The Collison nebulizer: description, performance and application. *Journal of Aerosol Science* 4(3):235-243.

23. Liu, B. Y. & Lee, K. (1975) An aerosol generator of high stability. *The American Industrial Hygiene Association Journal* 36(12):861-865.

Chapter 5 :A miniature dumbbell electrostatic aerosol classifier (Dumbbell EAC) for the electrical ultrafine particle sizer

5.1. Introduction

Nanoparticles, or ultrafine particles, are ubiquitous in ambient environment [1], and they hold potential risks for human health [2, 3]. The adverse health effects caused by ultrafine particles have been proven to be size-related [4, 5]. As concerns mount over this size-related health effect caused by personal ultrafine particle exposure, it is important to develop ultrafine particle sizers which are capable of measuring personal exposure and spatial distribution of ultrafine particles [6]. Among all the sizing techniques, an electrical mobility classification based particle sizing technique easily beat others, such as optical detection, inertial separation, and deposited sampling techniques, to be the principle technique for sizing submicron and ultrafine particles. The superiority results from its low sensitivity to particle material, high resolution for sizing submicron and ultrafine particles, and real time online measurement ability [7]. Some low-cost, electrical mobility classification based ultrafine particle sizers, such as the precipitator-type electrical ultrafine particle sizer (p-type EUPS), were thus developed to achieve the requirement for personal monitoring and spatial measurement task [8, 9]. However, as the p-type EUPS used a mini-disk precipitator as the electrical mobility classifier, the sizing resolution of the instrument was poor. To improve the sizing resolution, while still covering the particle size range from 10 to 500 nm, a new miniature electrical mobility classifier needs to be developed as an improvement and replacement for the mini-disk precipitator in the next generation of a low cost electrical ultrafine particle sizer design.

There are three types of electrical mobility classifiers, based on the classification mechanisms in three orders respectively, as shown in Figure 5-1. The zero-th order classification is electrostatic precipitation, which uses precipitator as the classifier. In the

electrostatic precipitation, no sheath flow is used, so polydisperse particles can enter the classification region anywhere in the inlet plane, i.e. in different distances from the central electrode. Therefore, particles of any electrical mobility can penetrate the classifier, and then be collected at the outlet [10]. In the first order classification, a sheath flow is introduced into the classification region, which limits and unifies the entering position of all particles, and this type of classifier is named as Electrical Aerosol Classifier (EAC). In the operation of EAC, all particles then have the same migration distance, and only particles with electrical mobility lower than a critical mobility can exit the classifier [11]. The second order classifier is the most widely used type of electrical mobility classifier, known as the Differential Mobility Analyzer (DMA). In the DMA operation, not only the particle entering position is limited by the sheath flow, the particle outlet is also limited to a narrow slit, i.e., only particles with one specific electrical mobility value can exit through the particle outlet [12]. The electrical mobility classifying resolution successively increases with the classification order. For the p-type e-UPS, a mini-disk precipitator, a zero-th order classifier, was used for the electrical mobility classification. Although the mini-disk precipitator performed well in altering the size distribution of downstream sampled particles by changing its precipitation voltage, it could not separate charged particles via a preselected electrical mobility due to its zero-th order resolution. Therefore, to more finely classify the electrical mobility of the charged sample particles, a higher order classifier, such as the Electrostatic Aerosol Classifier (EAC, as the first order), or the Differential Mobility Analyzer (DMA, as the second order), should be utilized in the design of a new EUPS classifier. By introducing sheath

air for the classification process, more precise particle size distribution information can be retrieved from the penetration measurements [7].

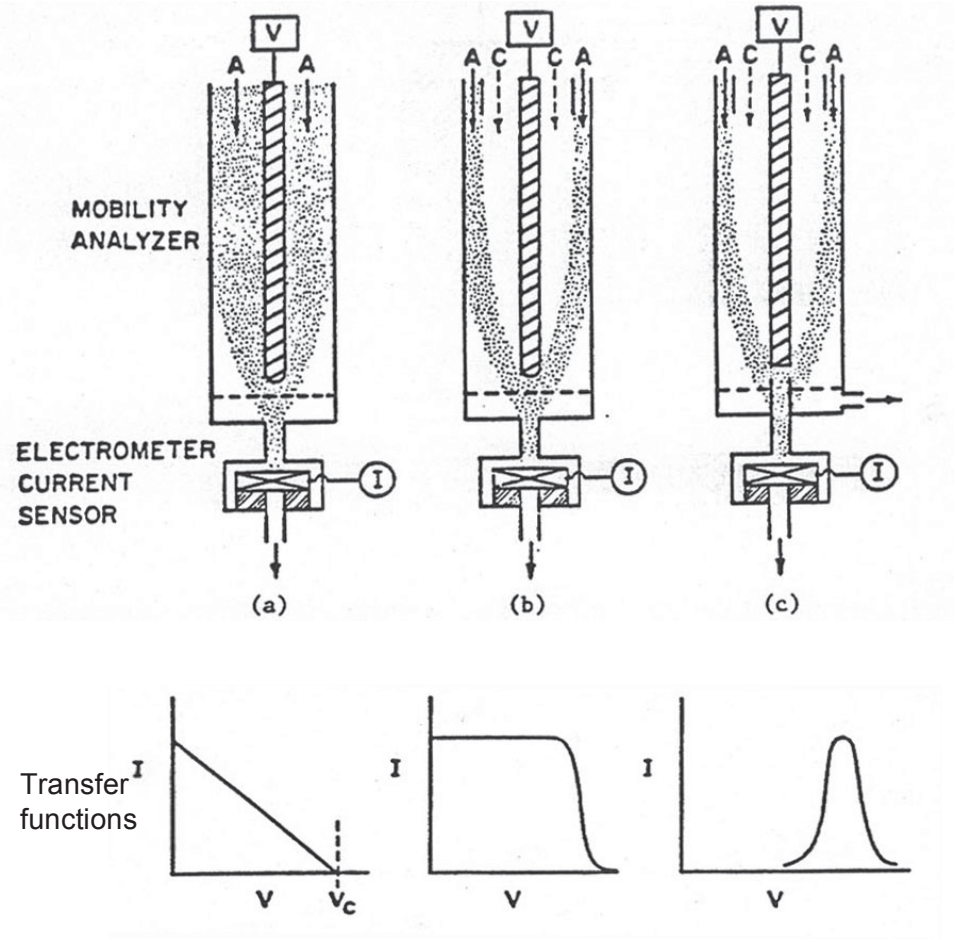

Figure 5-1. Schematics and transfer functions of the three generations of electrical mobility classifiers: (a) precipitator, (b) electrical aerosol analyzer, and (c) differential mobility analyzer [11]

The most commonly employed electrical mobility classifier is the cylinder type DMA developed by Knutson and Whitby [13], which is used as a part of the scanning mobility particle sizer (SMPS) for precisely measuring distributions in the submicron and nanometer range [14]. However, the cylinder type DMA, which measures about 45 cm in length, is too large for personal use. Also, the characteristic length is one of the most critical components for DMA performance, and cannot be simply shortened for

miniaturization. There is another, more compact type of DMA, known as the radial type DMA, with several designs available, including the Spectrometre de Mobilite Electrique Circulaire (SMEC) [15] and the Radial Differential Mobility Analyzer (RDMA) [16]. The radial type DMA has a classification zone formed by a parallel arrangement of two circular electrodes. During the classification process, both the polydisperse aerosol flow and the sheath flow entering from the edge of the flow chamber are merged in the classification zone and classified there by the applied voltage. After that, the excess airflow exits through the outlet at the center of the same disk that the polydisperse aerosol flow enters, while the classified monodisperse particles are extracted from a port in the circular electrode that is opposite to the aerosol inlet [17]. However, the construction of this radial type DMA is expensive for a low cost EUPS, and the operation is still too complicated for personal use, although it can be manufactured to a much more compact size than the cylinder DMA. Thus, an EAC type electrical mobility classifier is a better choice for designing the new classifier.

In 2009, Li, Chen et al. developed a low cost, miniaturized disk electrostatic aerosol classifier (mini-disk EAC), and it was reported to be more suitable than the previous mini-disk precipitator for use in a miniaturized electrical ultrafine particle sizer. Figure 5-2 shows a design schematic of the mini-disk EAC, which measures 44.45 mm in diameter and 46.23 mm in height. The performance of the mini-disk EAC was also characterized under different operating flowrates by Li, during which the penetration efficiency was measured as a function of applied voltage at each aerosol flowrate. The results show that the mini-disk EAC has a highest total operational flowrate of 1.5 lpm (0.5 lpm aerosol flowrate and 1.0 lpm sheath flowrate), and an upper limit of 120 nm for

the detectable size range. The short characteristic length and the confined classification region of the mini-disk EAC caused this limitation. According to Li's design schematic, the mini-disk EAC has a characteristic length of only 19 mm in length.

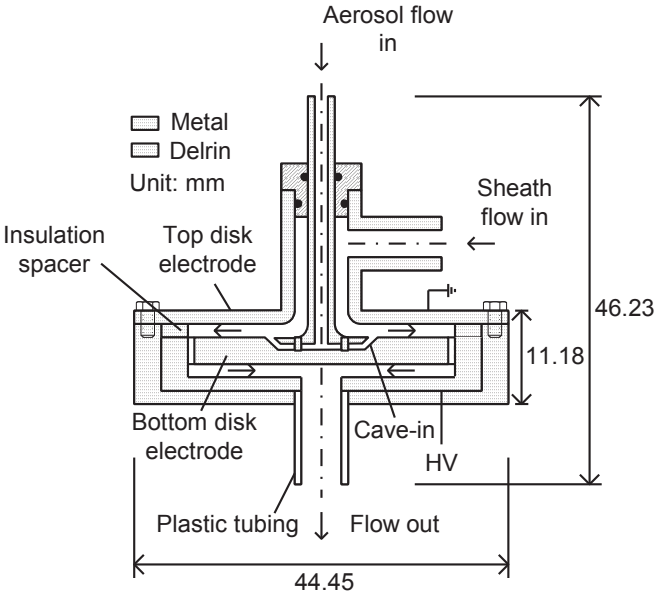

Figure 5-2. Schematic diagram of the mini-disk EAC (units in mm) [17]

Therefore, to be applied as the electrical mobility classifier in the electrical ultrafine particle sizer (EUPS), a new EAC design must be made, with an extended detectable size range for a better application in ambient aerosol measurements.

5.2. Hardware design

5.2.1. Why Dumbbell EAC?

To extend the size detection limit of the EAC type classifier means to extend the particle residence time, or to extend the particle classification length, i.e., the characteristic length of the classification channel, within an operational range of sampling flowrates. However, the new design of EAC was also expected to be as compact as the

mini-disk EAC, or even more compact in overall size, if possible. Under the prerequisite to keep a compact overall size, the design concept of the new EAC was to maximize the characteristic classification length by applying an axial-symmetric curved flow channel as the particle classification zone, as shown in the cutoff view in Figure 5-3. As the shape of the axial-symmetric curved classification channel was like a dumbbell, the new miniature EAC was named Dumbbell EAC accordingly. As for a complete design of the Dumbbell EAC, there was an aerosol flow at the top, which was followed by a disk shape chamber to buffer and evenly distribute the aerosol flow. The curved classification channel was connected to the distribution chamber with an angled slit. The angled channel was used for guiding the aerosol flow to enter the classification region tangentially, and also for reducing the occurrence of any possible flow turbulence. For the sheath flow, a ring-shaped distribution chamber was designed for the sheath flow inlet, and there was also an angled circular oblique incision to restrict the sheath flow to be evenly distributed, and to smoothly enter the classification channel in a laminar condition. At the classified aerosol outlet, a perforated plate was used to restrict the flow out and thus keep a stable laminar flow pattern in the classification region.

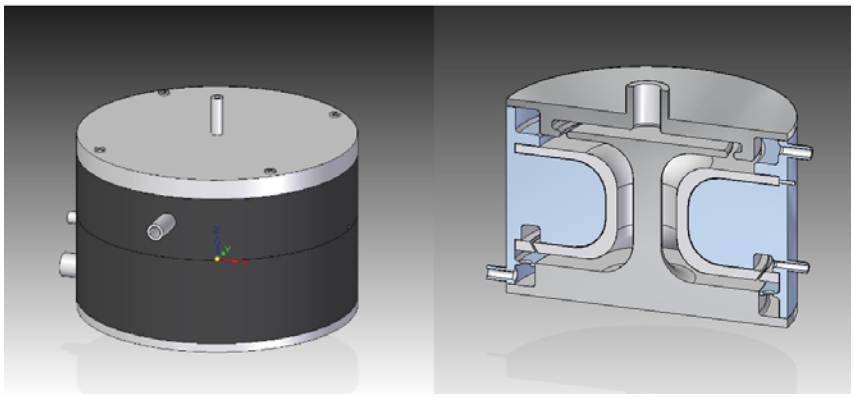

Figure 5-3. Overall and cutoff view of the Dumbbell EAC design

5.2.2. Optimization of design parameters

While the curved flow channel significantly increased the characteristic length within a miniaturized package, its bending sections also brought potential risks to the EAC classification, which requires laminar flow throughout the process [18]. To investigate how curvature and spacing of the characterization channel would affect the flow laminarity in the classification region, a numerical modeling of the flow field was executed by COMSOL Multiphysics® for the Dumbbell EAC with different structure parameters.

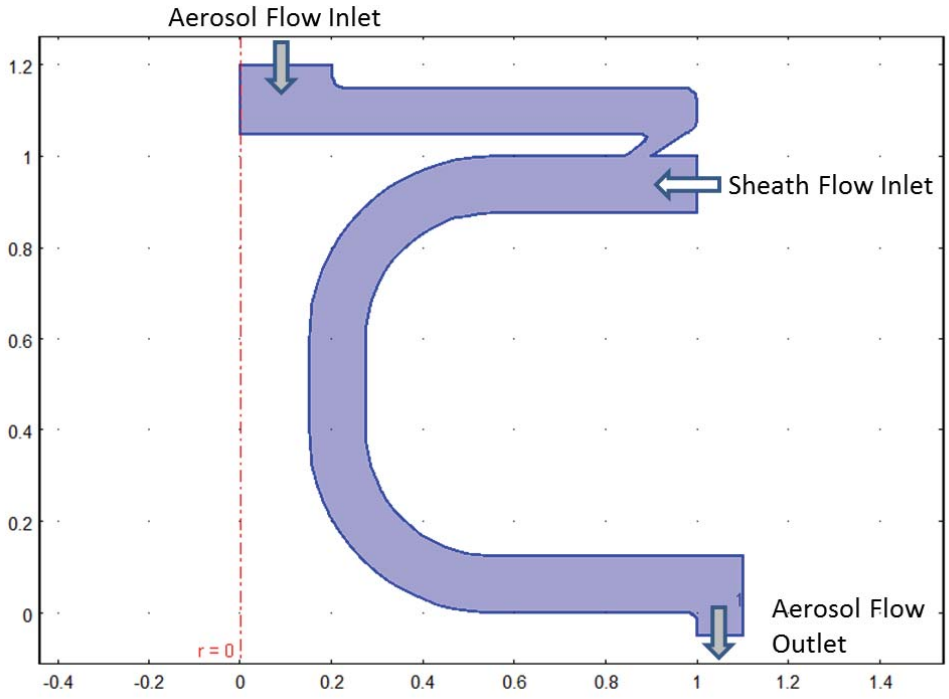

Figure 5-4. Computational domain for Dumbbell EAC flow field modeling

Similar to the flow field modeling for the miniature unipolar charger, a half cutoff plane of the flow channel was chosen as the computational domain for this axial-symmetric modeling, as shown in Figure 5-4. Aerosol flow was introduced into the classification region through the aerosol inlet from the top, sheath flow was introduced

through the sheath flow inlet from the side, and classified aerosol flow exited from the Dumbbell EAC through the aerosol flow outlet at the bottom.

For flow field modeling, the incompressible Navier-Stokes equation

$$\rho_f \left(\frac{\partial \overrightarrow{u_f}}{\partial t} + \overrightarrow{u_f} \cdot \nabla \overrightarrow{u_f}\right) = -\nabla p_f + \mu_f \nabla^2 \overrightarrow{u_f} + \overrightarrow{F_f}\,, \tag{5-1}$$

was used as the governing equation, along with the continuity equation as

$$\frac{\partial \overrightarrow{u_f}}{\partial x} + \frac{\partial \overrightarrow{u_f}}{\partial y} = 0\,. \tag{5-2}$$

In the above two equations, ρ_f is the fluid density, $\overrightarrow{u_f}$ is the fluid velocity vector, p_f is the local pressure, μ_f is the fluid viscosity, and $\overrightarrow{F_f}$ is the body force per unit of volume. To apply the two governing equations the flow field modeling of the Dumbbell EAC, three assumptions were made: (1) the fluid is isotropic and homogeneous, (2) the flow is axial-symmetric, incompressible, and in steady-state throughout the whole computational domain, and (3) the flow velocity profile is uniform by area at each flow inlet.

Therefore, boundary conditions were set according to the three assumptions for solving the two equations in EAC's computational domain. At the flow inlets, both aerosol flow and sheath flow were introduced into the classification region with uniform velocity profiles. For the boundary at the classified aerosol outlet, one point on the boundary had the absolute pressure set as zero, and this point was used as the pressure reference in this flow field modeling. Non-slip wall boundary conditions were imposed on all other boundaries of the computational domain. The shape functions of the elements in this finite element computation were of the second order in velocity $\overrightarrow{u_f}$ and the first order in pressure p_f.

Three parameters were investigated in this field modeling and design parameter iteration, including angle α of the circular oblique incision to the horizontal reference, aerosol flowrate Q_a and sheath flowrate Q_s, and spacing of the classification channel d. The modeling results were represented as streamlines in the flow field.

In the modeling of the circular oblique incision angle, the other two parameters, as the flowrates and the spacing of the classification channel, were both set constant, with Q_a = 0.5 lpm, Q_s = 3 lpm, and d = 3.175 mm. Results of the aerosol slit channel angle modeling are shown in Figure 5-5.

(a)

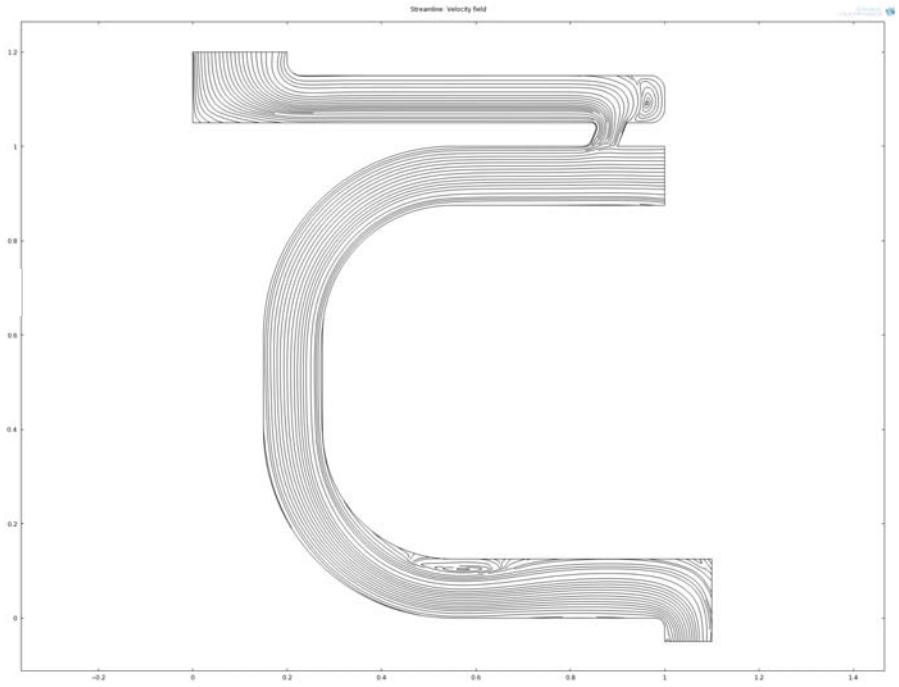

(b)

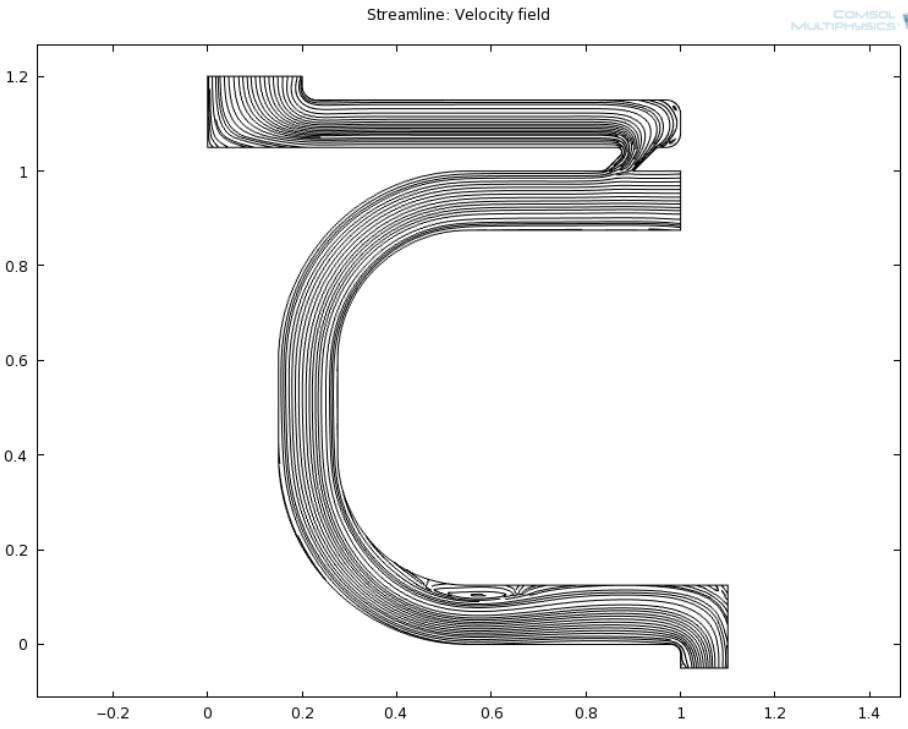

(c)

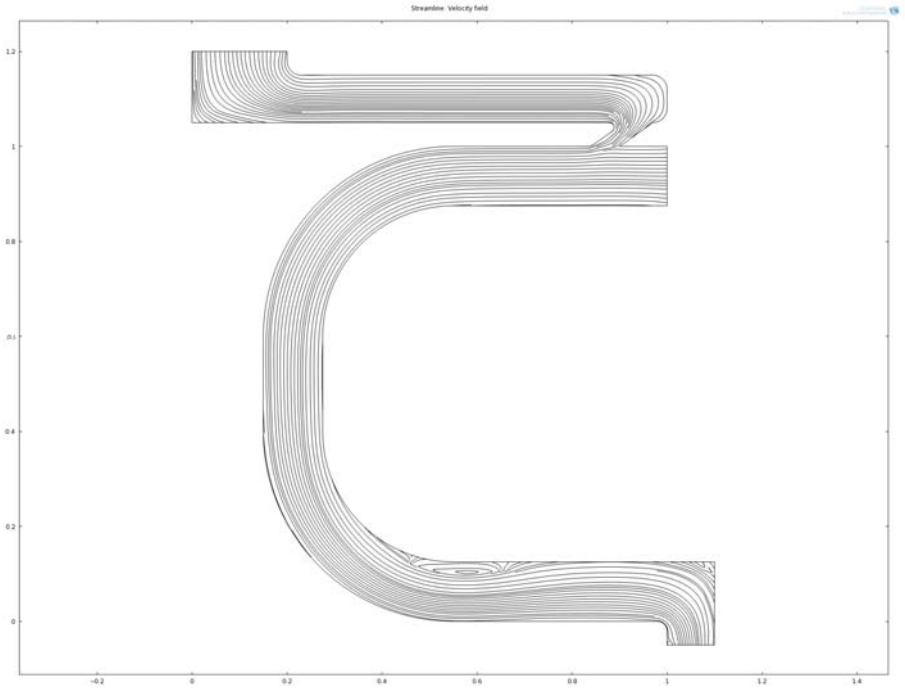

Figure 5-5. Modeling of the aerosol slit channel angle: (a) $\alpha = 60°$, (b) $\alpha = 45°$, and (c) $\alpha = 30°$.

Three different angles were used for the modeling, as 60°, 45°, and 30°. As the angle decreased, less turbulence or recirculation was observed in the flow pattern near the slit channel. For a smooth introduction of aerosol flow into the classification channel, small angles were preferred for the aerosol slit channel design.

Similar to the circular oblique incision angle modeling, for flowrate modeling, all the other parameters were set as constant, with the circular oblique incision angle $\alpha = 30°$, and classification channel spacing $d = 3.175$ mm. Results of the flowrate modeling were also represented in streamlines, and five flowrate settings are shown here in Figure 5-6.

(a)

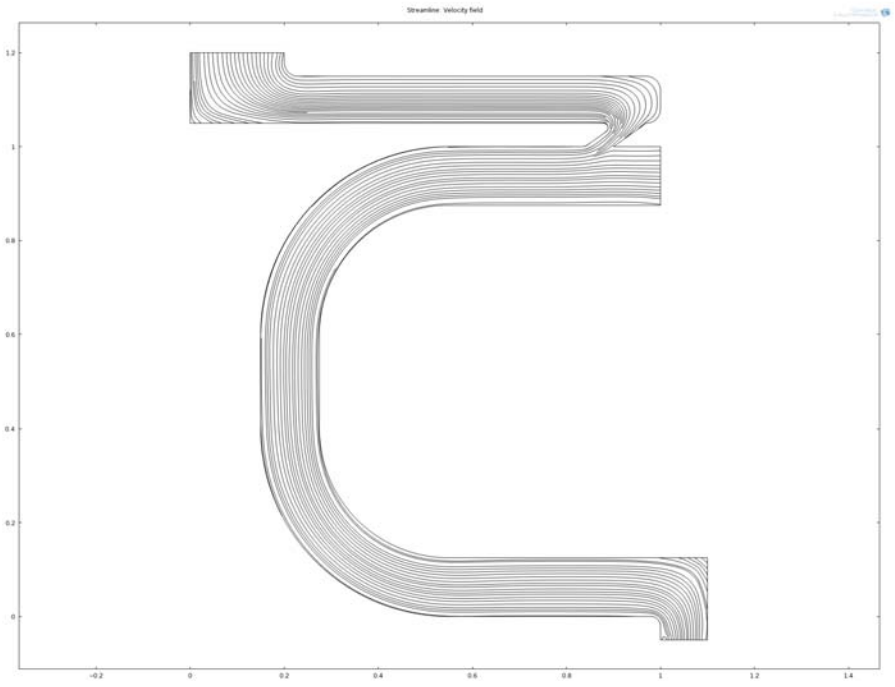

(b)

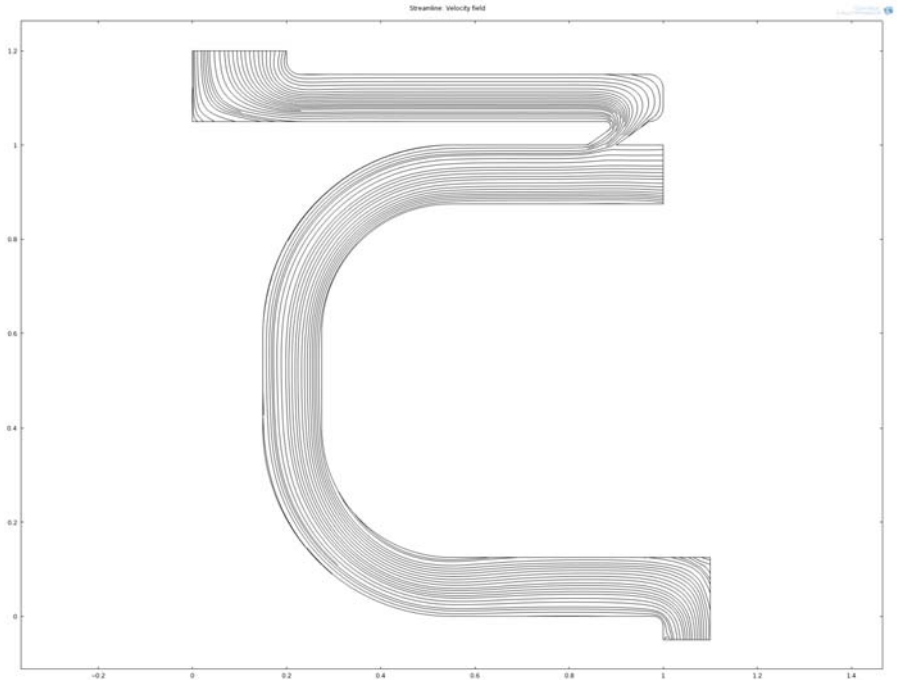

(c)

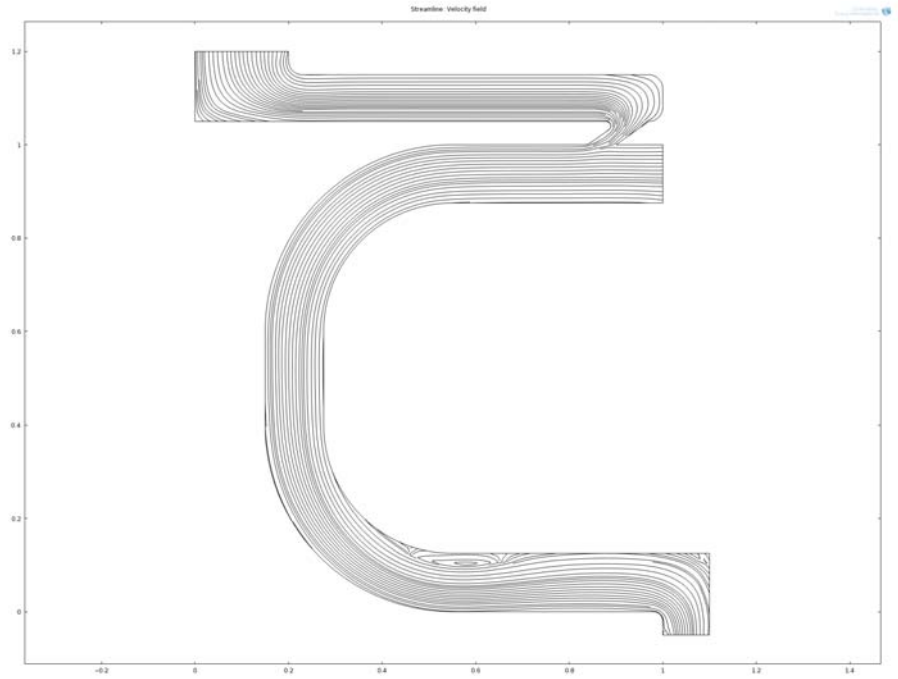

(d)

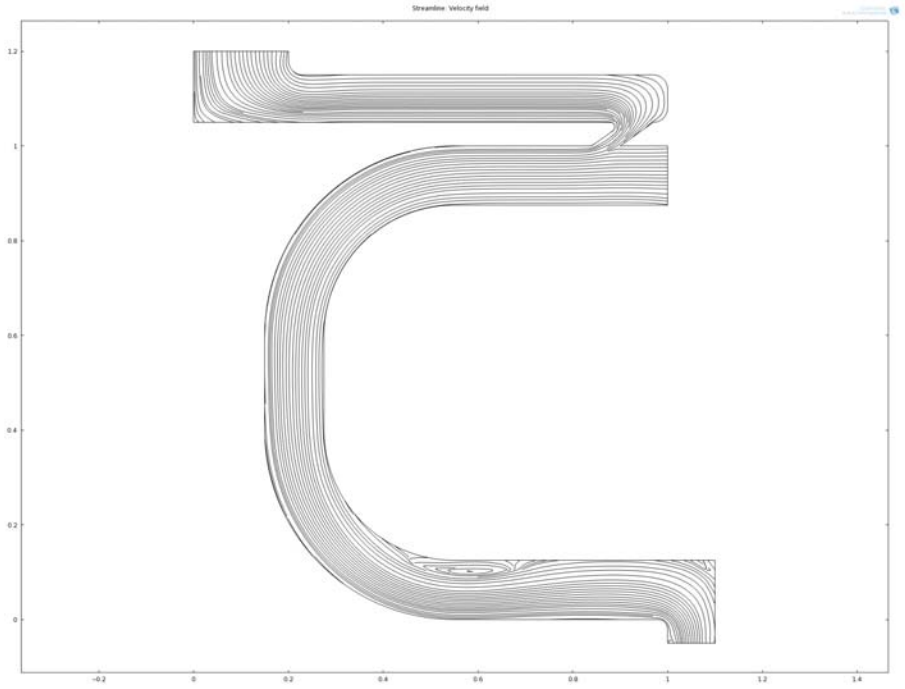

(e)

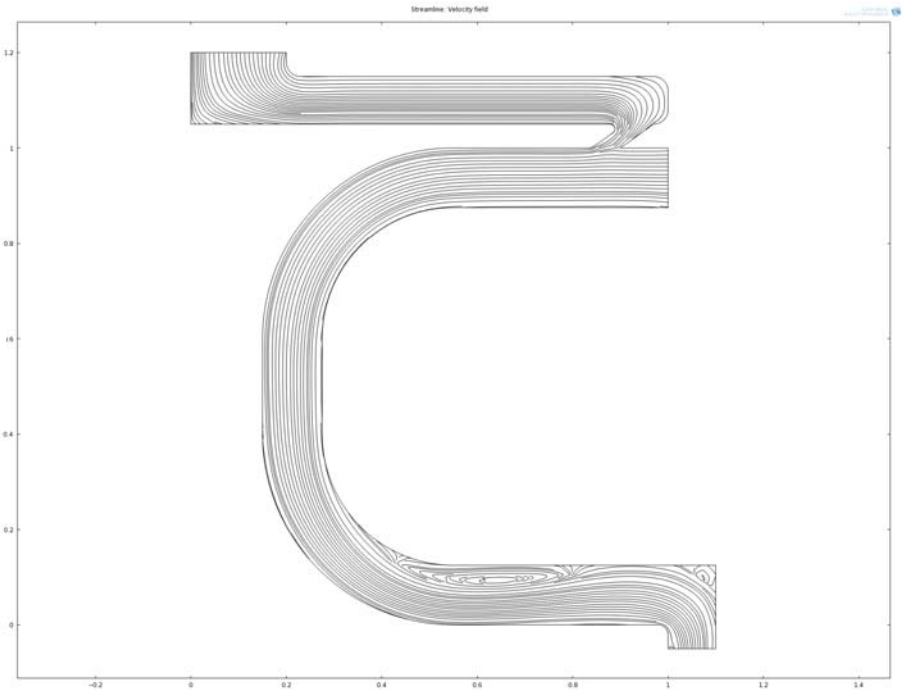

Figure 5-6. Modeling of the aerosol and sheath flowrats: (a) Q_a = 0.5 lpm, Q_s = 1 lpm, (b) Q_a = 0.5 lpm, Q_s = 2 lpm, (c) Q_a = 0.5 lpm, Q_s = 3 lpm, (d) Q_a = 1 lpm, Q_s = 3 lpm, and (e) Q_a = 0.5 lpm, Q_s = 4 lpm

Dividing the entire classification channel into three sections (as horizontal inlet section, vertical section, and horizontal outlet section), when the total flowrate exceeded 2.5 lpm, a secondary flow was developed in the horizontal outlet section, as the recirculation observed in the modeling results.

To eliminate the recirculation that occurred near the horizontal outlet section, and to improve the EAC design to achieve a higher operational flowrate limit, the effect of classification channel spacing on flow field was thus investigated.

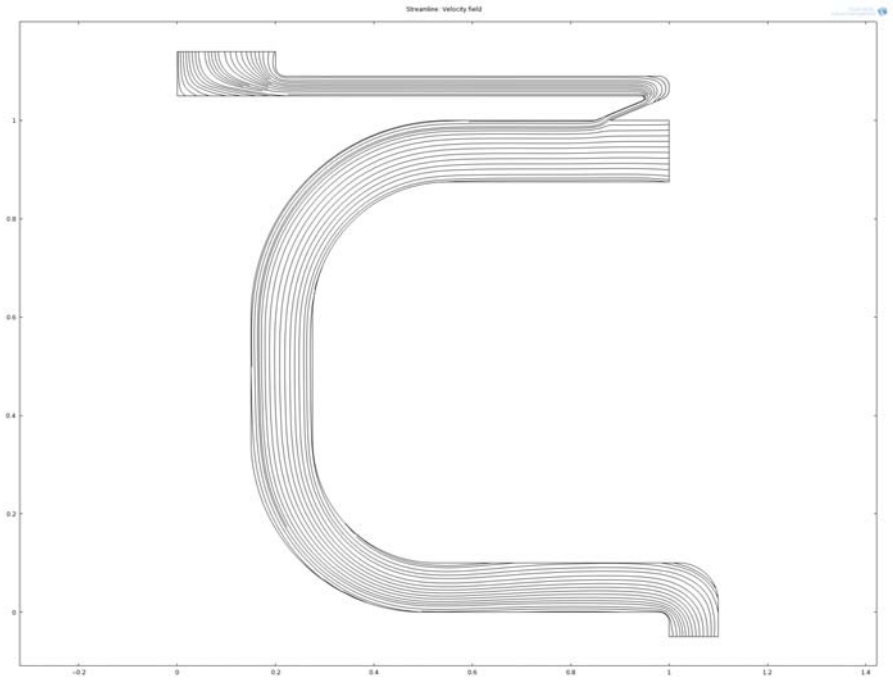

Figure 5-7. Modeling of the classification channel spacing

As lower Reynolds number (Re) indicates a lower possibility of secondary flow development in a flow channel, the channel spacing of the horizontal outlet section was narrowed down to d = 2.381 mm (3/32 inch) for this part of modeling. In addition, spacing of the aerosol flow distribution chamber was also narrowed down to 1 mm, to decrease aerosol residence time, and as a result decrease particle diffusional loss inside

the chamber for a higher sizing resolution of the Dumbbell EAC. The circular oblique incision angle and flowrate parameters were set as α = 30°, Q_a = 0.5 lpm, and Q_s = 4 lpm. The streamline result shown in Figure 5-7 clearly demonstrates the recirculation problem was solved by the new channel geometry settings, and the flow pattern throughout the whole Dumbbell EAC classification region was kept at the laminar flow state.

5.2.3. Design of the Dumbbell EAC

According to numerical modeling results, the design of the Dumbbell EAA was optimized and finalized, as the circular oblique incision was cut in an angle of 30° to the horizontal reference; the first two sections of the classification channel were spaced at 3.175 mm (1/8 inch); and the last section, as the horizontal outlet section had a spacing of 2.381 mm (3/32 inch). The cutoff section of the final Dumbbell EAA design is shown in Figure 5-8, with dimensions given in mm.

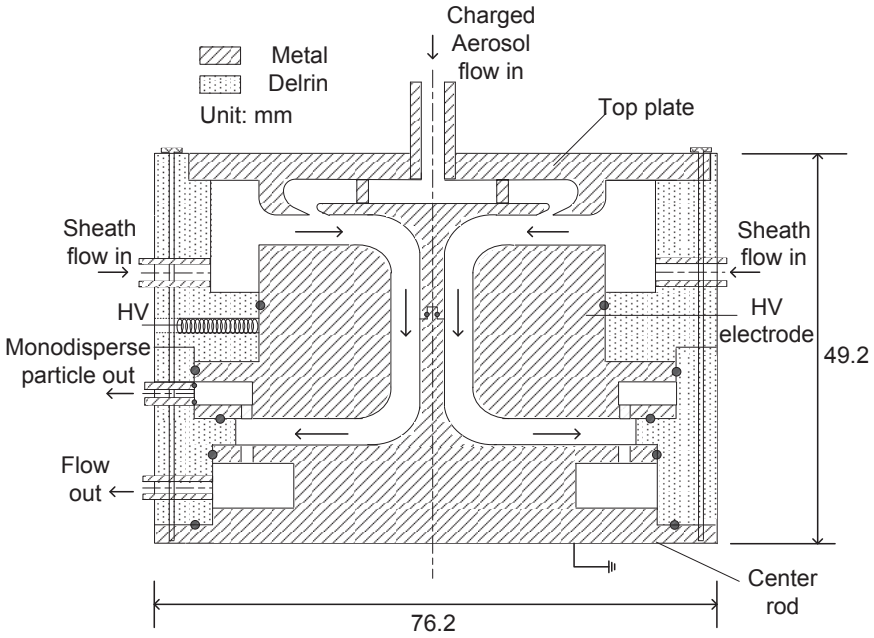

Figure 5-8. Schematic diagram of the Dumbbell EAC

The top plate and center rod were electrically connected and grounded. The HV electrode, as shown in the schematic, was applied with high voltage via a high voltage cable connected. To establish a stable electrical field, the HV electrode was electrically separated from the grounded parts by Delrin® insulators. A curved electrical field was then established in the curved classification region.

For the Dumbbell EAC flow operation, an electrically charged aerosol stream was introduced into the EAC chamber through a central tube connected to the top plate. After quickly passing through the cramped distribution chamber, the aerosol stream tangentially slid into the classification channel via a circular oblique incision, moved inwards radially, and then flew downstream. The sheath flow was introduced into the sheath flow chamber through two 180° symmetrical tubes connected to the side. With a narrow opening between the sheath flow chamber and the classification channel, the sheath flow was laminarized before meeting the sliding out aerosol flow from the oblique incision. The exit for the classified aerosol flow was at the downstream of the entire classification zone, to the side and near the bottom of the center rod. There was also another aerosol outlet near the HV electrode on the side, which was designed as a monodisperse particle outlet for an optional DMA function of this classifier.

During the EAC size classifying operation, an electrical field was established in the classification region with a high voltage applied to the HV electrode, and trajectories of the charged particles were then deflected according to a different electrical mobility. All particles with sufficiently high electrical mobility were deposited on the inner surface of the HV electrode, while those with sufficiently low electrical mobility could fully escape and exit the device through the classified flow exit. Particles with median mobility were

partially deposited on the HV electrode, and the electrical mobility with 50% penetration was defined as the cutoff mobility under that specific operation condition. By using the cutoff electrical mobility and particle number concentration at the classified flow outlet, particle size distribution information could then be retrieved. To integrate the Dumbbell EAC into an electrical ultrafine particle sizer (EUPS) unit, a sensitive aerosol electrometer could be used downstream of the EAC to measure the number concentration of escaped charged particles. However, in the following component evaluation of the Dumbbell EAC, the focus was on the device's performance as an electrostatic aerosol classifier, so an Ultrafine Condensation Particle Counter (UCPC, model 3025A, TSI Inc., Shoreview, MN) was used to measure particle number concentration in the experiment.

5.3. Numerical modeling of the Dumbbell EAC performance

In addition to the flow field modeling for optimizing and finalizing the Dumbbell EAC hardware design, electrical mobility classification ability of the curved channel was also verified before the manufacture. The verification procedure included mainly two steps. First, a numerical model was used to investigate the flow field and electrical field inside the Dumbbell EAC under different design geometries. And then, particle movement trajectories were modeled by applying the calculated flow field and electrical field characteristics. By summarizing the particle trajectory results, particle penetrations through the Dumbbell EAC were calculated for different particles electrical mobility values, and then the transfer function of the EAC sizing function was obtained. With the calculated transfer function, electrical mobility classification ability of the Dumbbell EAC was verified and also numerically evaluated.

5.3.1. Flow and electrical field modeling

Flow field modeling was done using the same equations and procedure as described in the previous design optimization part. The electrical field modeling used Gauss' law for the electrical field,

$$\nabla \cdot \overrightarrow{D_e} = \rho_e, \tag{5-3}$$

for governing the electrical flux inside the Dumbbell EAC classification channel. In the equation, ρ_e is the free electrical charge density, and $\overrightarrow{D_e}$ is the electrical displacement field. Under the assumptions of homogeneous, isotropic, non-dispersive, and linear materials of the medium, the electrical displacement field $\overrightarrow{D_e}$ was related to the electrical field $\overrightarrow{E_e}$ by:

$$\overrightarrow{D_e} = \varepsilon \overrightarrow{E_e}, \tag{5-4}$$

where ε is the electrical permittivity of the medium material.

Depending on the grounding condition and the high voltage applied to the HV electrode, corresponding electrical potentials were imposed on all solid walls, as the boundary condition settings. For the non-solid wall boundaries, such as all the flow inlets and outlets, boundary conditions were set as zero free electrical density. The third order shape functions were used to describe the electrical displacement field in this part of the modeling.

The computational domain for the electrical field modeling matched the two-dimensional half cutoff plane as used for flow field modeling. In the electrical operation of the Dumbbell EAC, the top and bottom metal plates, as well as the center rod connected to both plates, were all electrically grounded, while the HV electrode was

connected to a high voltage power supply. Thus, as reflecting to the electrical potential settings in the computational domain, the left boundary line was electrically grounded, and the right boundary had high voltage applied. Figure 5-9 shows an example of the electrical field distribution in the computational domain, with both electrical potential and field streamline presented.

(a)

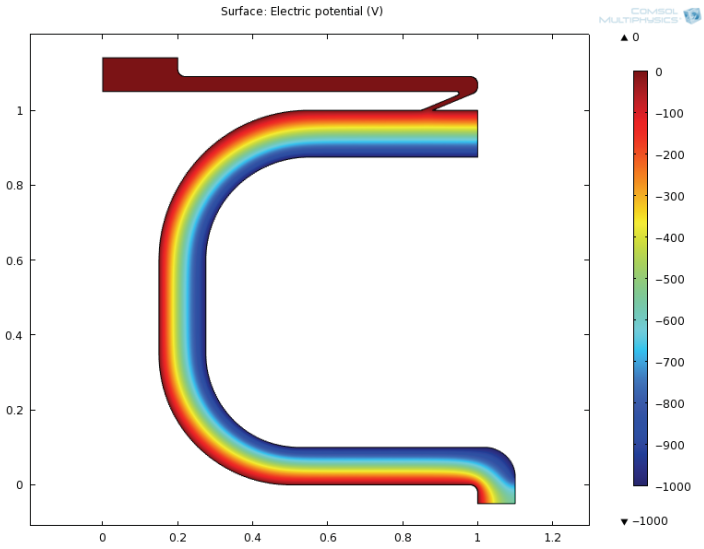

(b)

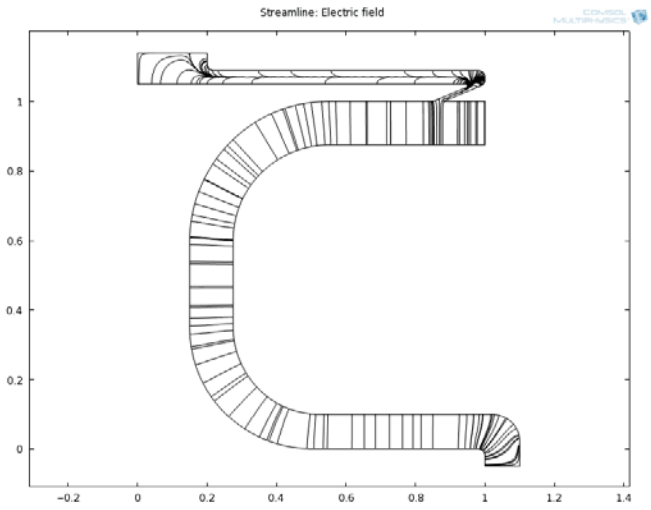

Figure 5-9. Electrical field modeling of the Dumbbell EAC: (a) electrical potential (V), and (b) streamline of the electric field

The modeling result was obtained by applying a negative high voltage of -1000 V to the HV electrode. It showed a uniform distribution of the electrical field throughout the classification region, which was promising for a stable classification performance of the Dumbbell EAC.

5.3.2. Particle Trajectory Modeling

Although the flow and electrical field modeling showed barely an adverse effect on flow laminarity and electrical field uniformity by the curved channel design, it remained unknown how much the bending sections would affect charged particle motion through the Dumbbell EAC classification region. Therefore, in addition to the flow field and electrical field modeling, particle electrical mobility classification ability of the Dumbbell EAC was also investigated, with the same procedure as used for the miniature unipolar charger.

To model charged particle motion through the classification channel, computation results from the flow field and electrical field modeling were utilized. With the flow and electrical field modeling results imported, the charged particle motions were then computed and modeled by solving the Langevin equation of particle translation:

$$m_p \frac{\partial \vec{u}_p}{\partial t} = \vec{F} = \vec{F}_d + \vec{F}_e + \vec{F}_b, \tag{5-5}$$

where m_p and $\vec{u}_p$ are the particle mass and translation velocity vector. $\vec{F}_d$, $\vec{F}_e$, and $\vec{F}_b$ are drag force, electrical force, and Brownian force, respectively. Other forces, as gravity, shear-induced lifting force, and rotational motion, were negligible and were not considered in this modeling.

Once the quantities in the particle translation equation were properly expressed, the equation was solved numerically using a fourth order Runge-Kutta integration technique with adaptive step size control. Thus, by tracking a group of particles randomly released into the classification region through the aerosol flow inlet, it was possible to obtain the deposition location of each single particle, as well as the overall deposition profile of the whole aerosol stream.

For evaluating the electrical mobility classification ability, six different negative operational voltages, ranging from 0.5 to 10 kV, were used in the modeling. Particles were assumed positively singly charged, and were uniformly released through the aerosol flow inlet all at once. Seven different particle sizes were tested, including 50, 60, 80, 100, 150, 200, and 300 nm, and were represented by different colors. Five particles were used for each particle size. After entering the classification channel, the particle would either deposit on the HV electrode surface, or exit the EAC via the classified aerosol outlet at the bottom. By tracking the particle movement trajectory, the deposition position of each single particle was recorded by x and y coordinates in the same coordinate system of the computational domain. To represent the deposition results, the HV electrode surface, as a particle collection surface, was used as a reference, as shown in Figure 5-10. The results clearly demonstrated a size classification ability of the Dumbbell EAC, as 50 nm particles, with the highest electrical mobility among all particle sizes, needed the least time to penetrate the sheath layer and to deposit on the collection surface. For the modeling case with operational voltage at 0.5 kV, only 50 nm particles were partially trapped in the EAC, all other particle sizes exited. When operational voltage increased, more particle sizes were trapped inside. For the highest voltage at 10 kV, only 300 nm particles could

exit.

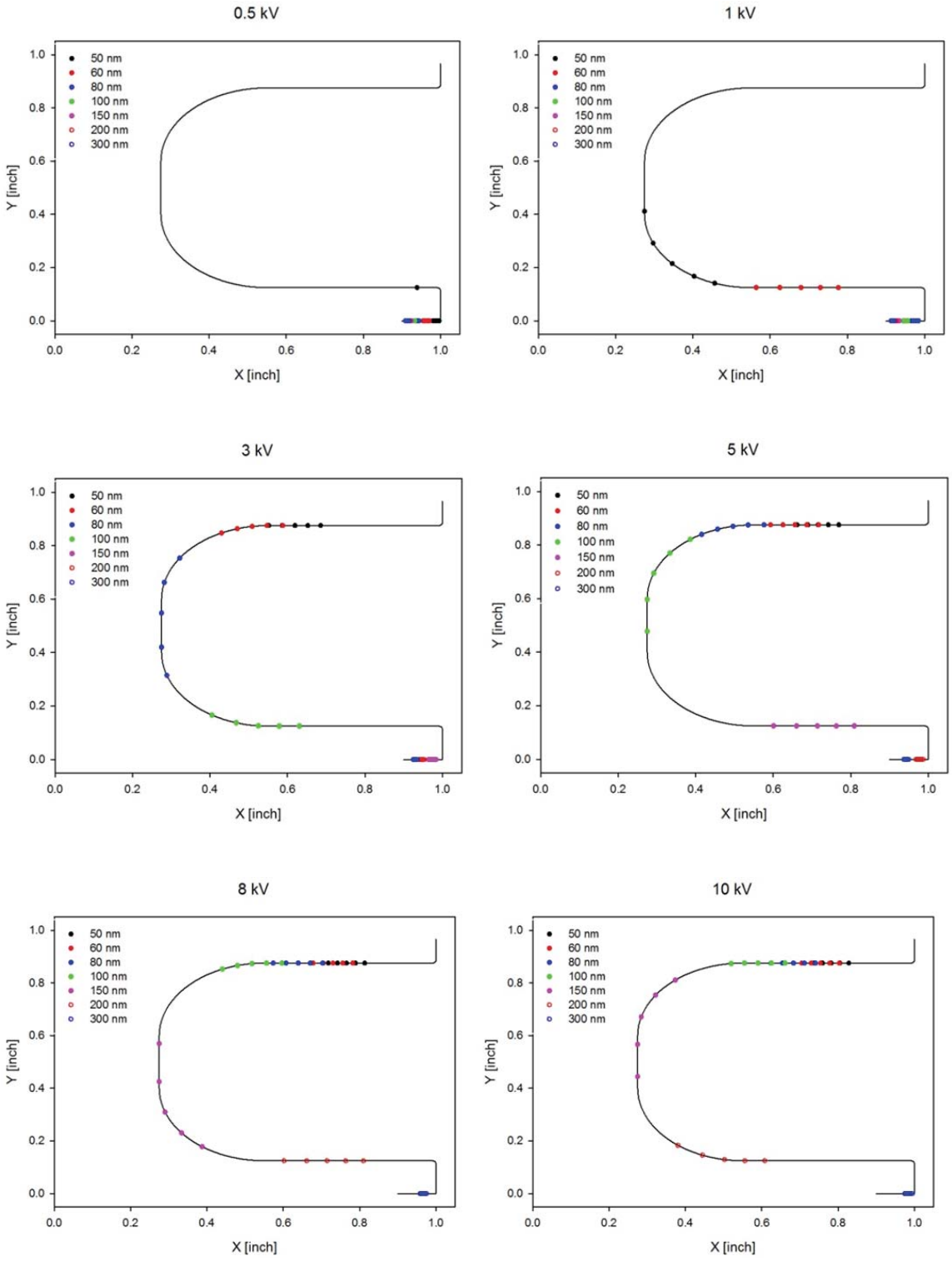

Figure 5-10. Particle trajectory modeling results for six different operational voltages

5.4. Experimental evaluation of the Dumbbell EAC

In addition of the numerical evaluation, the Dumbbell EAC classification performance was also experimentally evaluated after the construction of first prototype. Two parameters were used in the evaluation, including particle transmission efficiency through the nonworking EAC unit, and classified particle penetration through the classification region.

5.4.1. Experimental setup for the Dumbbell EAC evaluation

The Dumbbell EAA prototype was tested with DMA classified monodisperse particles, generated by a laboratory aerosol generation system as shown in Figure 5-11.

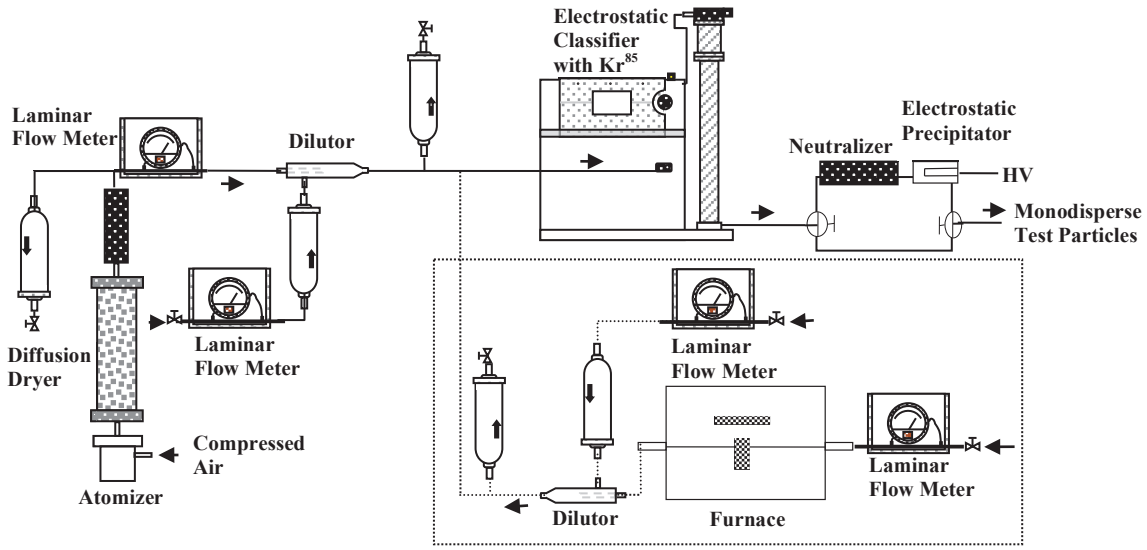

Figure 5-11. Experimental setup for particle generation and particle size characterization

Same as the generation system introduced in Chapter 2, two different systems were used for generating polydisperse sodium chloride particles for the Dumbbell EAC evaluation. For particles with mean diameters smaller than 50 nm, a furnace was used for generating particles via the evaporation-condensation process described by Hussin [19]. A

combustion boat loaded with test particle material, sodium chloride powder for our experiment, was placed in a ceramic tube passing through a tube furnace. When the furnace was heated to the required high temperature, the sodium chloride powder evaporated to form a rich vapor in the ceramic tube. A stream of inert gas passed through the furnace tube, carrying the vapor-rich stream to the dilutor, where the hot vapor-rich stream was quenched by another stream of particle-free inert gas at room temperature. Polydisperse nanoparticles were then formed during this quenching process, and sent to the Nano-Differential Mobility Analyzer (Nano-DMA, model 3085, TSI Inc., Shoreview, MN) system downstream, where they were classified, and the monodisperse nanoparticles needed for the following evaluation experiment were obtained.

For larger polydisperse particles, with mean diameters ranging from 50 to 500 nm, the generator system was a homemade Collison mechanical atomizer, which is a widely used generator for obtaining a steady stream of laboratory-generated polydisperse aerosols. The Collison atomizer normally consists of a jar for spray solution, a spray nozzle, and a baffle for impacting the droplets [20]. By pumping a steady stream of compressed air through the spray nozzle, the spray solution is atomized to small droplets, and then partly dried to form a unimodal polydisperse aerosol stream [21]. The droplets were then thoroughly dried by the two diffusion dryers filled with silicon desiccant and connected in series. The final yield was dry polydisperse sodium chloride particles at the outlet of the second diffusion dryer. Downstream, a standard DMA (model 3081, TSI Inc., Shoreview, MN) classified the monodisperse particles with diameters larger than 50 nm. Since DMA classification is based on particle electrical mobility, all the classified monodisperse particles exiting from the DMA systems were electrically charged. To get

the monodisperse neutral particles needed for the charger evaluation experiment, both a Po^{210} neutralizer and a high voltage applied charged particle remover were used downstream of the DMAs. There was also an optional bypass flow route parallel to the charge-removing route to get singly charged monodisperse particles for the Dumbbell EAC penetration measurement.

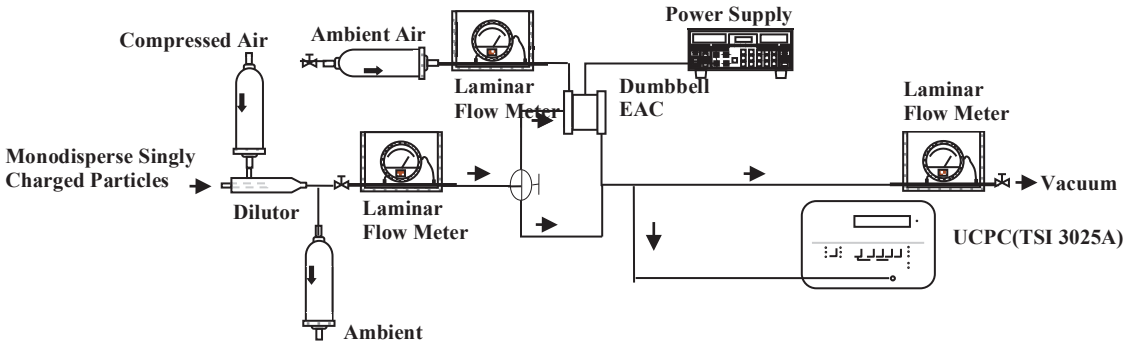

Figure 5-12. Experimental setup for Dumbbell EAC performance evaluation

Singly charged particles were used as the test particles and were directly fed into the Dumbbell EAC. Sheath flow was introduced into the EAC by a vacuum suction downstream, both aerosol flowrate and sheath flowrate were controlled by two Swagelok® needle valves, and monitored by two laminar flow meters respectively. The first evaluation parameter: particle transmission efficiency was then obtained as

$$Transmission = \frac{N_{dn}(0)}{N_{up}}. \qquad (5\text{-}6)$$

In the equation, $N_{dn}(0)$ is the singly charged particle number concentration measured downstream of the Dumbbell EAA with no voltage applied, and N_{up} is the concentration measured upstream. Particles with DMA classified sizes from 10 to 600 nm were tested.

All the number concentrations were measured by an ultrafine condensation particle counter (UCPC, model 3025A, TSI Inc., Shoreview, MN).

The second evaluation parameter: classified particle penetration through the classification region was measured for obtaining cutoff curves for Dumbbell EAC classification. In this part of evaluation, singly charged particles with different electrical mobility, i.e., with different particle sizes were tested, and the Dumbbell EAC was operated with a sequence of applied voltages successively. Downstream particle number concentrations N_{dn} were measured by the UCPC (model 3025A, TSI Inc., Shoreview, MN) correspondingly. Different from the precipitator operation, for EAC classification, charged particles began to be precipitated in the classifier only when the applied voltage reached certain critical values. However, one thing was similar to the precipitator that, a complete precipitation could also be experienced when sufficiently high voltage was applied. For a given $(Z_p \cdot V)$ value, the particle penetration is defined as

$$P = \frac{N_{dn}(Z_p \cdot V)}{N_{dn}(0)}. \tag{5-7}$$

In the equation, $N_{dn}(Z_p \cdot V)$ is the particle number concentration measured downstream when the operational voltage is on, while $N_{dn}(0)$ is the downstream number concentration when the voltage is off. To present the measurement results of the charged particle penetration through the classifier, all $(Z_p \cdot V)$ products were also normalized by the $(Z_p \cdot V)_{50}$ at 50% penetration, as

$$Nor(Z_p.V) = \frac{(Z_p \cdot V)}{(Z_p \cdot V)_{50}}. \tag{5-8}$$

By plotting the penetration as a function of the normalized $(Z_p \cdot V)$value, cutoff curves were obtained under different flow operations, which could then be used for retrieving the transfer function of the Dumbbell EAC as to represent its classification performance [22, 23].

5.4.2. Results of the Dumbbell EAC performance evaluation

Figure 5-13 shows evaluation results of particle transmission efficiency through the Dumbbell EAC. Monodisperse particles with a size range from 10 to 600 nm were used, and the evaluation included two flowrate settings, one had a total flowrate of 3.5 lpm, with aerosol flowrate Q_a = 0.5 lpm, sheath flowrate Q_s = 3.0 lpm; and the other had a total flowrate of 1 lpm, with Q_a = 0.5 lpm, Q_s = 0.5 lpm accordingly.

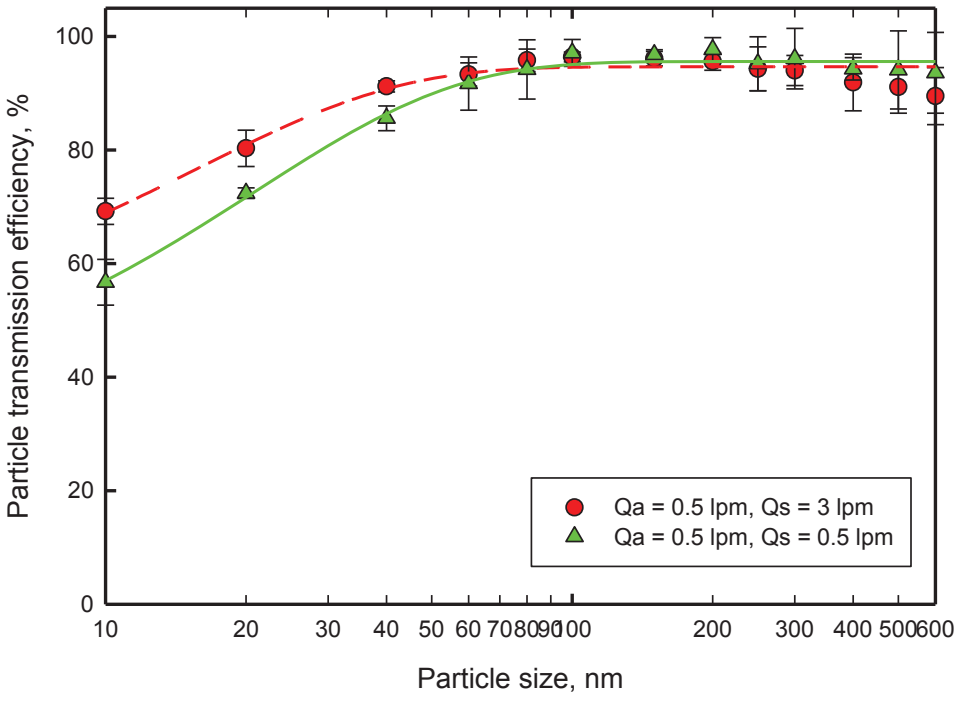

Figure 5-13. Particle transmission efficiency through the Dumbbell EAC

Both transmission efficiencies showed an exponential growth profile according to particle size increase. As compared with each other, a higher total flowrate had lower particle loss for particles sized between 10 and 60 nm, because of less diffusional loss within the shorter residence time. But the higher total flowrate had a higher loss of large particles, which was resulted from the impaction effect at the aerosol flow inlet. In contrast, a lower total flowrate had much less impaction effect at the aerosol inlet, and large particles could penetrate the device more safely, which helped Dumbbell EAC maintain a lower particle loss for 300 to 600 nm particles. However, when lowering the total operational flowrate, particle residence time inside the classification region was significantly increased, and longer residence time thus increased the probability of diffusional loss for small particles [24].

Charged particle penetration was plotted as a function of the normalized ($Z_p \cdot V$) to get the Dumbbell EAC cutoff curves for each operational flowrate setting respectively, as shown in Figure 5-14.

As the slope of an EAC cutoff curve (of the inclination part) is determined by an aerosol to sheath flowrate ratio of Q_a / Q_s , five different flowrate ratio settings were used for the evaluation. For aerosol to sheath flowrate ratios of Q_a : Q_s = 1:1, 1:2, and 1:3, the total flowrate (Q_a + Q_s) used was 3 lpm, while for the lower aerosol to sheath flowrate ratios of Q_a : Q_s = 1:4.5 and 1:5, a lower total flowrate of 1.5 lpm was used to avoid turbulent mixing in the classification channel. As expected, the evaluation showed that the transfer functions for lower Q_a : Q_s ratios were steeper than those for higher Q_a : Q_s ratios, i.e., an EAC-type classification performance, as higher classification resolution for

larger operational sheath to aerosol flowrate ratios, was experimentally proved for the Dumbbell EAC.

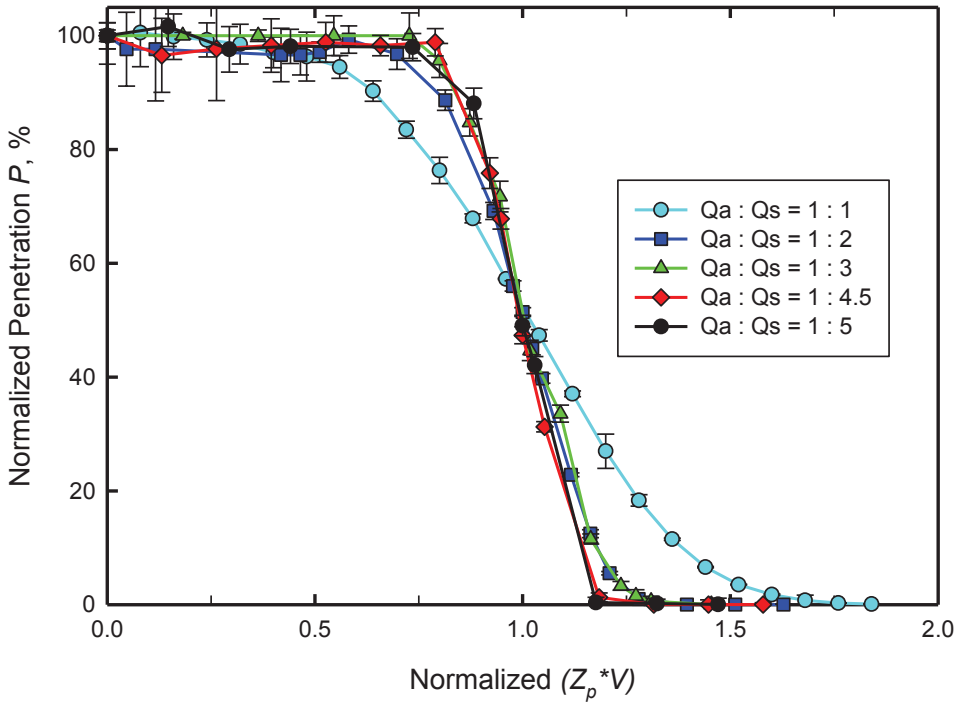

Figure 5-14. Cutoff curves of the Dumbbell EAC

The total flowrate effect on the Dumbbell EAC transfer function was also investigated, by operating the Dumbbell EAC at different total flowrate (Q_a + Q_s) settings, while keeping the same aerosol to sheath flowrate ratio as 1:1. Four total flowrate settings were tested, including $Q_a = Q_s$ = 0.25 lpm, $Q_a = Q_s$ = 0.40 lpm, $Q_a = Q_s$ = 1.00 lpm, and $Q_a = Q_s$ = 1.50 lpm. Correspondingly, four cutoff curves were obtained as the evaluation results plotted in Figure 5-15, which clearly showed all four cutoff curves had the same cutoff slope, overlapping with each other. This repeatability demonstrated that, within the total operational flowrate upper limit, as of 4 lpm from the previous evaluation, the

Dumbbell EAC classification performance had a low sensitivity to the total operational flowrate.

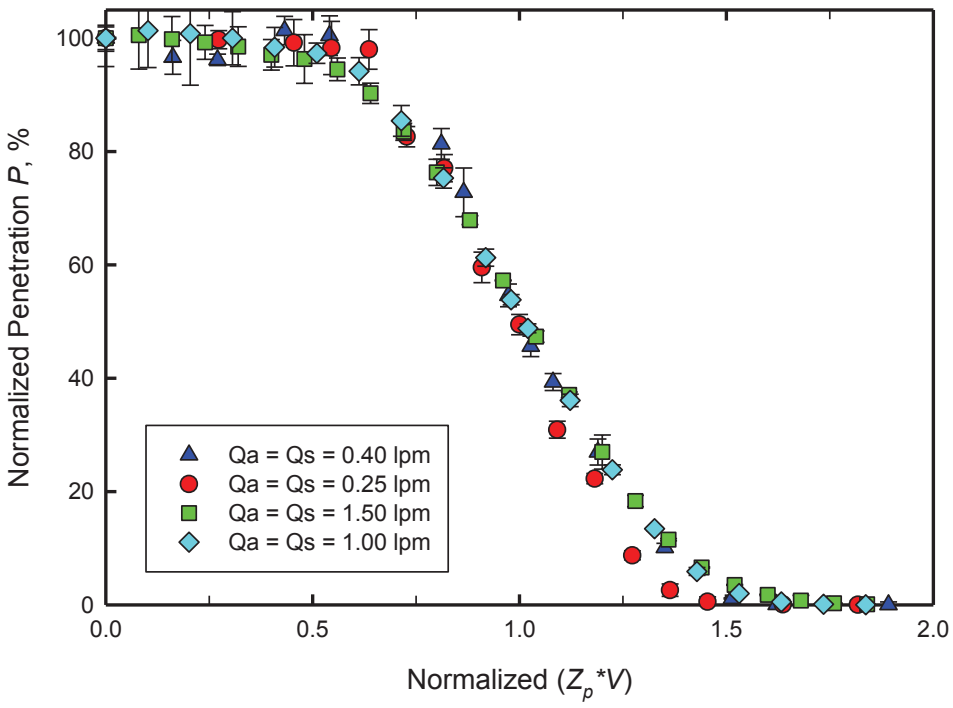

Figure 5-15. Same aerosol to sheath flowrate ratio cutoff curves for the Dumbbell EAC

Besides, the upper limit of the detectable size range was also investigated incidentally by the low flowrate evaluations. With an operational voltage of 2000 V was applied to the Dumbbell EAC, the upper size limit for the $Q_a = Q_s = 0.40$ lpm operation was 700 nm; while for the $Q_a = Q_s = 0.25$ lpm operation, it was 850 nm.

In order to predict the Dumbbell EAC classification performance when the operational condition is varied, the numerical model previously introduced was also used for getting cutoff curves. Modeling results were presented in comparison with the experimental results of cutoff curves, and Figure 5-16 showed an example case, with an aerosol flowrate $Q_a = 1$ lpm, and a sheath flowrate $Q_s = 2$ lpm.

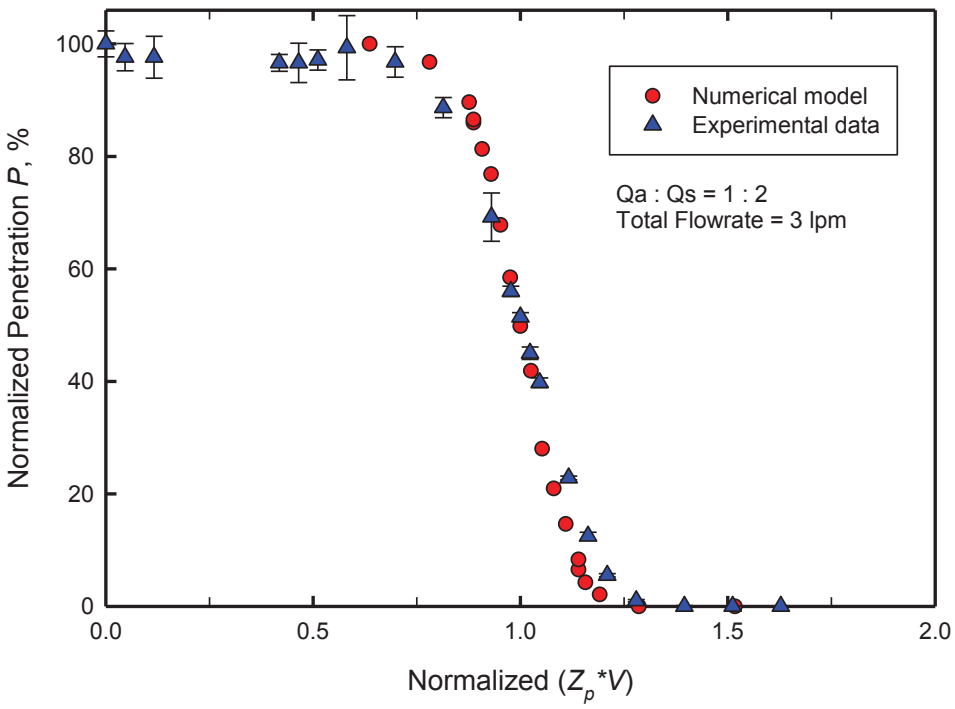

Figure 5-16. Comparison of modeled and experimental cutoff curves

The slope of the numerically modeled cutoff curve was slightly steeper than that of the experimental data, but the modeled cutoff size, as the singly charged particle size with 50% penetration, agreed quite well with the experimental data, which was 79.4 nm by numerical model, and 80 nm by experimental evaluation for the operational conditions shown in Figure 5-16.

5.5. Conclusions

In this study, a miniature electrostatic aerosol classifier (EAC) prototype was designed as a key component for an electrical ultrafine particle sizer. The hardware development and performance evaluation were done and reported. Distinct from conventional cylindrical or disk-type EAC designs, this new miniature prototype had a novel configuration as an axial-symmetric dumbbell-shaped curved classification channel,

and was named the Dumbbell EAC accordingly. With an extended classification length by the curved channel design, the Dumbbell EAC was able to achieve a wide detectable size range of 10 to 850 nm, while maintaining a compact overall device package. Particle transmission efficiency of the prototype was experimentally characterized in the laboratory using DMA classified monodisperse particles. Despite its compact size and curved classification channel, the Dumbbell EAC prototype had satisfactory transmission efficiency for singly charged particles, which was close to 100% for particles with sizes larger than 60 nm. In addition, the electrical mobility classification performance of the prototype was experimentally evaluated, represented by particle cutoff curves, i.e., normalized penetrations plotted as a function of normalized $(Z_p \cdot V)$values. Cutoff curves obtained under different operational flowrate settings proved a reliable classification performance with several optional resolutions for the Dumbbell EAC. The EAC performance was also numerically evaluated with a particle trajectory model with the same operational settings, and the numerical modeled results agreed well with the experimental data. With its palm-sized package size, high sizing resolution up to 1:5, and extended detectable size range, the Dumbbell EAC thus provided an improved solution for miniature electrical ultrafine particle sizers, which are now greatly needed in spatially distributed particle size distribution measurements or personal ultrafine particle exposure assessments.

5.6. References

1. Biswas, P. & Wu, C.-Y. (2005) Nanoparticles and the environment. *Journal of the Air & Waste Management Association* 55(6):708-746.

2. Hoet, P., Bruske-Hohlfeld, I., & Salata, O. (2004) Nanoparticles - known and unknown health risks. *Journal of Nanobiotechnology* 2(1):12.

3. Holl, M. M. B. (2009) Nanotoxicology: a personal perspective. *Wiley Interdisciplinary Reviews: Nanomedicine and Nanobiotechnology* 1(4):353-359.

4. Oberdörster, G. (2000) Pulmonary effects of inhaled ultrafine particles. *International Archives of Occupational and Environmental Health* 74(1):1-8.

5. Warheit, D. B. (2004) Nanoparticles: health impacts? *Materials today* 7(2):32-35.

6. Koch, W., Dunkhorst, W., & Lodding, H. (1999) Design and performance of a new personal aerosol monitor. *Aerosol Science and Technology* 31(2-3):231-246.

7. Flagan, R. C. (2011) Electrical mobility methods for submicrometer particle characterization. *Aerosol Measurement*, (John Wiley & Sons, Inc.): 339-364.

8. Torsten, T.*, et al.* (2013) NanoScan SMPS – A novel, portable nanoparticle sizing and counting instrument. *Journal of Physics: Conference Series* 429(1):012061.

9. Qi, C., Chen, D.-R., & Greenberg, P. (2008) Fundamental study of a miniaturized disk-type electrostatic aerosol precipitator for a personal nanoparticle sizer. *Aerosol Science and Technology* 42(7):505 - 512.

10. Hinds, W. C. (1999) *Aerosol technology: properties, behavior, and measurment of airborne paticles* (Wiley) 2nd edition Ed.

11. Liu, B. Y. H., Pui, D. Y. H., & Kapadia, A. (1976) *Electrical aerosol analyzer: history, principle, and data reduction* p Medium: ED; Size: Pages: 64.

12. Whitby, K. T. & Clark, W. E. (1966) Electric aerosol particle counting and size distribution measuring system for the 0.015 to 1 μ size range1. *Tellus* 18(2-3):573-586.

13. Knutson, E. O. & Whitby, K. T. (1975) Aerosol classification by electric mobility: apparatus, theory, and applications. *Journal of Aerosol Science* 6(6):443-451.

14. Wang, S. C. & Flagan, R. C. (1990) Scanning electrical mobility spectrometer. *Aerosol Science and Technology* 13(2):230-240.

15. Fissan, H.*, et al.* (1996) Experimental comparison of four differential mobility analyzers for nanometer aerosol measurements. *Aerosol Science and Technology* 24(1):1-13.

16. Zhang, S.-H., Akutsu, Y., Russell, L. M., Flagan, R. C., & Seinfeld, J. H. (1995) Radial differential mobility analyzer. *Aerosol Science and Technology* 23(3):357-372.

17. Li, L., Chen, D.-R., Qi, C., & Kulkarni, P. S. (2009) A miniature disk electrostatic aerosol classifier (mini-disk EAC) for personal nanoparticle sizers. *Journal of Aerosol Science* 40(11):982-992.

18. Brunelli, N. A., Flagan, R. C., & Giapis, K. P. (2009) Radial differential mobility analyzer for one nanometer particle classification. *Aerosol Science and Technology* 43(1):53-59.

19. Hussin, A., Scheibel, H. G., Becker, K. H., & Porstendörfer, J. (1983) Bipolar diffusion charging of aerosol particles—I: experimental results within the diameter range 4–30 nm. *Journal of Aerosol Science* 14(5):671-677.

20. May, K. (1973) The Collison nebulizer: description, performance and application. *Journal of Aerosol Science* 4(3):235-243.

21. Liu, B. Y. & Lee, K. (1975) An aerosol generator of high stability. *The American Industrial Hygiene Association Journal* 36(12):861-865.

22. Stratmann, F., Kauffeldt, T., Hummes, D., & Fissan, H. (1997) Differential electrical mobility analysis: a theoretical study. *Aerosol Science and Technology* 26(4):368-383.

23. Jiang, J.*, et al.* (2011) Transfer functions and penetrations of five differential mobility analyzers for sub-2 nm particle classification. *Aerosol Science and Technology* 45(4):480-492.

24. Winklmayr, W., Ramamurthi, M., Strydom, R., & Hopke, P. K. (1990) Size distribution measurements of ultrafine aerosols, dp > 1.8 nm, formed by radiolysis in a diameter measurement analyzer aerosol charger. *Aerosol Science and Technology* 13(3):394-398.

Chapter 6 :Dissertation Accomplishments and Recommendations for Future Work

6.1. Summary of accomplishments

Aimed at delivering low cost and portable solutions for size distribution measurements of ultrafine and submicron particles, this dissertation studied the development and miniaturization of electrical ultrafine particle sizers (EUPS), to meet the increasing demand for personal exposure monitoring and spatially distributed measurements. There are three essential components for developing a EUPS unit, including a charger to electrically charge the sample particles, an electrical mobility classifier to classify the charged particles, and a downstream particle count detector to measure the number concentrations. All three components were designed to be: low-cost, miniaturized, with minimal particle loss and high detection efficiency. Two generations of EUPS were developed within this dissertation, with detailed accomplishments summarized as follows.

6.1.1. The precipitator-type electrical ultrafine particle sizer

A precipitator-type electrical ultrafine particle sizer was assembled, with the three components developed and calibrated, including a miniature corona-discharge unipolar charger, a miniature disk-type precipitator, and a portable condensation particle counter.

The miniature charger was calibrated at a constant corona-discharge current of 2 μA, and an aerosol flowrate of 0.7 lpm. Three parameters were investigated for the miniature charger calibration: intrinsic charging efficiency, extrinsic charging efficiency, and average number of charges on charged particles. Differential mobility Analyzer (DMA, model 3081 and 3085, TSI Inc., Shoreview, MN) classified monodisperse particles with sizes from 20 to 500 nm were used as the test particles. The calibration results showed

"exponential growth to a maximum" trend for both charging efficiencies. The intrinsic charging efficiency increased from 80% at 20 nm to 100% for sizes larger than 60 nm, and the extrinsic charging efficiency increased from 37% at 20 nm to 80% for particle sizes larger than 80 nm. The humidity effect on charging performance was also evaluated for the miniature charger, by using both potassium sulfate (K_2SO_4) particles (hydrophobic) and sodium chloride (NaCl) particles (hydrophilic). The results showed the miniature charger was not sensitively affected by relative humidity conditions. However, some charging performance difference was observed in the NaCl measurement, which was caused by a deliquescence effect induced particle size increase of NaCl particles.

The calibration curve for the mini-disk precipitator was demonstrated as a function of the square root of penetration $P^{1/2}$ and the product of particle electrical mobility and operation voltage ($Z_p \cdot V$), and it showed an explicit linear relationship between the two parameters. The experimental evaluation results of the mini-disk precipitator well aligned with the semi-empirical model for its dual chamber precipitation. This consistency proved a predictable and stable performance of the modified mini-disk precipitator, for being used as an electrical mobility classifier in the EUPS assembly.

The counting efficiency of the particle number concentration detector was also calibrated in this study. DMA classified monodisperse particles with sizes from 20 to 500 nm were used as test particles, and an ultrafine condensation particle counter (UCPC, model 3025A, TSI Inc., Shoreview, MN) was used as the number concentration reference. The evaluation results showed an increasing counting efficiency as particle size increases.

Through the component calibration, operation conditions were optimized and performance was calibrated for all three components. Based on the component calibration results, a data inversion scheme was developed for deconvoluting particle size distribution from measured signals, based on the constrained least-squares method. With only one step of linear algebra calculation between getting the penetration data and outputting the size distribution profile, the inversion scheme effectively reduced both response time and calculation effort. In addition, it also revealed a new function as the dynamic identification of time-variation in aerosol size distributions. Thus, fast-response measurements were enabled for the precipitator-type EUPS, as 48 s for a whole size distribution, or a quick 3 s dynamic identification measurement.

After the construction of both component hardware and data inversion software, size distribution measurement performance of the p-type EUPS prototype was evaluated, with both laboratory generated aerosols and field ambient aerosols. A Scanning Mobility Particle Sizer (SMPS™, model 3080, 3081 and 3025A, TSI Inc., Shoreview, MN) and an Engine Exhaust Particle Sizer (EEPS™, model 3090, TSI Inc., Shoreview, MN) were used as the size distribution measurement reference. Evaluation results solidly verified the size distribution measurement reliability and flexibility of the p-type EUPS.

6.1.2. Component development and evaluation for the next generation electrical ultrafine particle sizer

According to the evaluation results for all three key components (the charger, the classifier and the particle detector) and the whole precipitator-type EUPS unit, several possible improvements were implied for a more precise EUPS size distribution

measurement. These improvements were realized in the second part of this dissertation, as the component development and evaluation for a second generation EUPS.

First, for the charger, a new corona-discharge based, miniature unipolar aerosol charger was developed and evaluated. The prototype was constructed with a brass tubular case as the charging chamber and a corona discharge chamber, and it maintained a miniaturized size with 50 mm in length and 22 mm in diameter. However, it had a totally different design in flow configuration, as the aerosol flow was introduced into the charging chamber in parallel to the ion flow, and a gentle sheath flow was used in the corona discharge chamber. Calibrations were also performed according to the three parameters as extrinsic charging efficiency, intrinsic charging efficiency, and average number of elementary charges per charged particle. The results showed significant improvements in both intrinsic and extrinsic charging efficiencies as compared to the previous mini-charger. As for 20 nm particles, an 8% increase in intrinsic charging efficiency and an 11% increase in extrinsic charging efficiency were both achieved with the new miniature unipolar charger design. The increases in charging efficiencies resulted from the higher ion attachment efficiency and lower particle loss inside the charger. For the average charge measurement, more charges were obtained by each charged particle without a doubt, because of the high ion attachment efficiency, but more stable charging performance was observed for the new design, especially for larger particle sizes, which can ensure good reproducibility in the following electrical mobility classification procedure. In addition to being an improved charger design for the EUPS development, for its low particle loss characteristic, the flow pattern and hardware configuration of this prototype miniature unipolar charger could also be applied in many other applications.

Second, a miniature electrostatic aerosol classifier (EAC) prototype was designed as an improved replacement of the mini-disk precipitator for the next generation miniature electrical mobility classifier. It was named as the Dumbbell EAC because it had an axial-symmetric dumbbell-shaped curved classification channel design. The curved channel design helped the Dumbbell EAC achieve an extended classification length within a compact overall device size, and thus endowed the Dumbbell EAC a wide detectable size range of 10 to 850 nm. The EAC prototype was determined to have satisfactory transmission efficiency for singly charged particles, which was close to 100% for particles with sizes larger than 60 nm. In addition, the electrical mobility classification performance of the prototype was experimentally evaluated, with cutoff curves obtained under different operational flowrate settings. A particle trajectory model was also used to numerically evaluate the Dumbell EAC classification performance. Based on the agreement between experimental and numerical results, a reliable classification performance with several optional classifying resolutions was proved for the Dumbbell EAC. This palm size device, with its high sizing resolution up to 1:5, and extended detectable size range from 10 to 850 nm, provided an improved solution for a next generation miniature electrical mobility classifiers, and would further be utilized to improve the EUPS design for more precise portable size distribution measurements.

6.2. Recommendations for Future Work

The increasing demand of size distribution measurement for personal ultrafine particle exposure assessment and spatially distributed monitoring has drawn more and more attention into the development of miniature ultrafine particle sizers. While significant progress was made in this dissertation, more investigations and research

efforts are still necessary to fully meet the market requirements for miniature particle sizers. The following recommendations are made for future researches related to the instrumentation of miniature electrical ultrafine particle sizers, inspired by the studies done within this dissertation.

Field study with the p-type EUPS for measuring real ambient aerosols: In this dissertation, the precipitator-type EUPS was mainly evaluated with laboratory generated aerosols and under laboratory conditions. Only one simple field evaluation was done with the p-type EUPS for measuring real ambient aerosols at the loading dock of our department building (Brauer Hall, Department of Energy, Environmental and Chemical Engineering, Washington University in St. Louis, MO). To better investigate the size distribution measurement performance of the p-type EUPS, more comprehensive field evaluations should be executed for the prototype. With multiple prototype units provided by TSI Inc. (three units were delivered, and the other three are pending), spatial distributed measurements can be made to demonstrate the particle size evolution according to the distance from an emission source. Personal exposure to ultrafine particles can also be monitored using the p-type EUPS prototype, as part of an epidemiology study. Besides the measurement applications, it will also be interesting to investigate the possibility of using the p-type EUPS as a smoke detector, which can more precisely identify combustion aerosols by their special size distribution characteristics than current detection mechanism of particle concentration monitoring. If possible, this feature can be a milestone improvement for smoke detection technology.

Use a Faraday cage and a sensitive electrometer as the EUPS particle counter: the particle count detectors used for current EUPS prototypes are P-Trak® condensation

particle counters (model 8525, TSI Inc., Shoreview, MN). In spite of its portability, the CPC type P-Trak® has several drawbacks as the EUPS particle counter. Primarily, as a condensation particle counter, it needs a supply of working fluid: 99.9% purified isopropanol alcohol (IPA) is recommended in the manual. This requirement is inconvenient for field study or remote monitoring. Besides, the P-Trak® requires frequent maintenance to clean the particle contamination from the optical detector, and the working fluid cartridge must be recharged every 8 hours for stable counting efficiency. Both requirements make the P-Trak® not suitable for long-term monitoring measurement. Besides contamination and working fluid problems, this optical detection based device also has a limited efficiency for counting particles smaller than 80 nm. To solve these problems of the CPC-type detector, an electrical detection technique can be investigated as a substitute for the particle count measurements, which measures particle charges by utilizing an aerosol Faraday cage along with a sensitive electrometer. The total charges carried by a stream of sampled particles, which will be an electrical current signal measured by the electrometer, can then be used to get the total number concentration of that sampled particle stream.

Multiple-charge problem by using unipolar aerosol charger: If using a Faraday cage as the particle count detector in EUPS design, the multiple charge problem of unipolar aerosol charger will be the very first challenge to be solved. Multiple charges on a single particle, especially for large particle sizes, is always an issue for using a corona-discharge aerosol charger as the ion source. Two possible approaches can be investigated for solving the multi-charge problem. One is an experimental top down approach, by using a charge conditioner to experimentally reduce the number of elementary charges on

large particles before the electrical mobility classification process. The other approach is a numerical bottom up approach, by applying the charging efficiency and charge distribution modeling results calculated from charging theories into the data inversion scheme. More detailed simulation will improve our understanding of the corona-discharge based diffusion charging mechanism via the numerical approach.

Performance evaluation of the Dumbbell DMA: In the Dumbbell EAC design, besides the classified aerosol outlet at the bottom, there is another aerosol outlet near the HV electrode connection port, which is reserved as a monodisperse particle outlet for an optional DMA function. Similar to the Dumbbell EAC evaluation, both experimental and numerical procedures can be used for the Dumbbell DMA classification performance evaluation. If the DMA function performs well, a higher sizing resolution of the next generation EUPS can be further achieved by utilizing this differential electrical mobility classifier.

Variable cutoff size of the miniature size-selective inlet: As a miniature size-selective inlet, the "impaclone" developed in this dissertation is a combination of an impactor and a cyclone, for the sharp cutoff curve and large dust capacity respectively. By switching the impaclone between impactor-only and cyclone-only operations, the device can have a switchable cutoff size for the same operational flowrate. However, theoretically, the impaclone cutoff size can be varied continuously within the size range between impactor-only cutoff size and cyclone-only cutoff size, by carefully tuning the aerosol flowrate ratio between the impactor and cyclone operational flowrates. Besides, although the pressure drop through the whole impaclone unit was reduced by the cyclone

part as compared to a “pure” impactor, an even lower pressure drop is always preferred by the EUPS.

Assembling and evaluation of the second generation EUPS: With designs and evaluations of all hardware components ready, the second generation EUPS can be assembled. If necessary, each individual component will need to be further evaluated according to the flow configuration of the EUPS unit. Based on the updated evaluation results, a data inversion scheme can then be developed, which is expected to be universal for any distribution profile, to provide a fast response to aerosol variation, and to consume low computation effort for the miniaturized sizer unit. Similar to the first generation EUPS, after hardware and software constructions, the new generation EUPS will be experimentally evaluated for its size distribution measurement ability under both laboratory and field conditions.